NATIONAL ADVISORY COMMITTEE FOR AERONAUTICS

WARTIME REPORT

ORIGINALLY ISSUED
February 1943 as
Advance Restricted Report

WIND-TUNNEL INVESTIGATION OF THE CHARACTERISTICS OF BLUNT-NOSE AILERONS ON A TAPERED WING

By Paul E. Purser and Thomas A. Toll

Langley Memorial Aeronautical Laboratory
Langley Field, Va.

NACA

WASHINGTON

NATIONAL ADVISORY COMMITTEE FOR AERONAUTICS

ADVANCE RESTRICTED REPORT

WIND-TUNNEL INVESTIGATION OF THE CHARACTERISTICS OF BLUNT-NOSE AILERONS ON A TAPERED WING

By Paul E. Purser and Thomas A. Toll

SUMMARY

An investigation has been made in the LMAL 7- by 10-foot tunnel of various modifications of a 0.155-chord blunt-nose aileron on a semispan model of the tapered wing of a fighter airplane. The modifications considered included various amounts of overhanging nose balance with various nose radii. The effects of the vertical location of the aileron hinge axis were determined for one balance size and the effects of the gap at the aileron nose were determined for all the modifications. Peak pressures were determined over the nose portions of some of the ailerons.

The stick forces and the rates of roll were estimated for a fighter airplane with plain sealed ailerons and with some of the blunt-nose ailerons.

The results of the tests and computations indicated that, for the arrangement tested, the use of blunt-nose ailerons with 40-percent balance would reduce the high-speed stick forces to a very small value. The adverse effects of a gap at the aileron nose tended to decrease as the chord of the balance was increased. The effects of the vertical location of the hinge for the aileron with 40-percent balance were small. The effects of increasing the nose radii on the blunt-nose ailerons was, in general, to increase the negative slope of the curves of hinge-moment plotted against aileron deflection, to decrease the rolling-moment coefficients at small aileron deflections, to increase the rolling-moment coefficients at large aileron deflections, to increase the effective deflection range of the aileron, and to decrease the magnitude of the peak pressures over the aileron nose.

The magnitude of the peak pressures indicates that severe compressibility effects would probably be encountered if the ailerons were deflected $\pm 15^{\circ}$ while the airplane was flying at a moderately high speed. Accordingly,

it appears that blunt-nose ailerons should be tested at Mach numbers considerably higher than the Mach number of the test data herein presented before being considered for use on high-speed airplanes.

INTRODUCTION

Because of the increased importance of obtaining adequate lateral control with reasonable stick forces for high-speed airplanes under all flight conditions, the NACA has engaged in an extensive program of lateral-control research. The purposes of this program are to determine the characteristics of existing lateral-control devices, to determine the characteristics of modifications to existing devices, and to develop new devices that show promise of being more satisfactory than those now in use.

Investigations in two-dimensional flow (reference 1 to 4) have indicated that use of nose overhang (or balance) offers a powerful means of adjusting control-surface hinge moments. The present tests were made to determine the characteristics of 0.155-chord ailerons with blunt-nose balances on a tapered wing model. The investigation included determination of the effects of balance chord, balance nose radii, nose gaps and seals, and vertical location of the aileron hinge axis on the characteristics of blunt-nose ailerons. The dynamic pressures existing over the nose portions of some of the ailerons at various deflections and angles of attack were also determined.

APPARATUS AND METHODS

Test Installation

A semispan model of a tapered wing was suspended in the LMAL 7- by 10-foot tunnel (reference 5) as shown schematically in figure 1. The root chord of the model was adjacent to one of the vertical walls of the tunnel, which thereby served as a reflection plane. The flow over a semispan wing in this setup is essentially the same as it would be over half a complete symmetrically

loaded wing in a 7- by 20-foot tunnel. No part of the model was fastened to or in contact with the tunnel wall and a small amount of clearance was maintained between the root chord of the model and the tunnel wall. The model was suspended from the balance frame, as shown in figure 1, in such a way that all the forces and moments acting on it could be determined. Provision was made for changing the angle of attack while the tunnel was in operation.

The aileron deflections and hinge moments were determined by means of a calibrated torque rod and linkage system developed especially for this type of setup (fig. 2). The aileron was deflected by turning the hinge-moment dial which, through the torque rod, drove the aileron-deflection drive tube and the link to the aileron horn. When the desired aileron deflection had been attained, the torque rod was clamped in position in order that all wing forces and moments could be determined without any interference from the operator of the hinge-moment unit. The aileron deflection was determined by the reading of the aileron-deflection dial with respect to the pointer attached to the angle-of-attack drive tube. The aileron hinge moments were determined from the twist of the torque rod as indicated by the reading of the hinge-moment dial with respect to the pointer mentioned. The torque rod was calibrated after it was installed in the test setup.

Pressures over the nose portions of some of the ailerons were measured by means of static-pressure tubes located at several chordwise positions for each of two spanwise locations (section A and section B of fig. 3). The tubes were about 0.020-inch outside diameter and were held in position with the tube center line at a distance of about 0.09 inch from the surface of the aileron. The total pressure of the air stream was measured by a total-pressure tube placed about a foot below the model and about 4 inches ahead of the model support-strut fairing.

Models

The tapered-wing model used in these tests was built to the plan form shown in figure 3 and represents the cross-hatched portion of the airplane in figure 4. The basic airfoil sections were of the NACA 230 series tapered in thickness from approximately 15⅛ percent at the root

to 8¼ percent at the tip. The basic chord c_1 of the wing model was increased 0.3 inch to reduce the trailing-edge thickness and the last few stations were refaired to give a smooth contour. Ordinates for the extended and refaired sections are given in table I.

The slotted flap was built to the ordinates given in table II and had a chord of about 20.7 percent of the wing chord. The flap ordinates are given for the root and tip sections although only the portion of the flap extending from the root station to the 52.3-inch station was used for these tests. The slot shapes and flap pivot points are also given in table II.

In figure 5 the details are given for the various 0.155c by 0.405b/2 ailerons, where c is the wing chord at any spanwise station and b is twice the span of the semispan model. Removable aileron-nose blocks and wing-tail blocks were provided in order that the aileron balance, gap, and hinge-axis location could be varied. One nose block was built for each amount of balance. The nose radii were varied by reshaping the nose blocks after the tests of a given set of nose radii had been completed. Provision was made for minimum, 30-percent, and 40-percent balances.

Only one hinge-axis location and nose shape was tested for the minimum-balance (plain) aileron. The hinge axis was located on the aileron mean line, and the aileron nose at any spanwise station was a circular arc tangent to the upper and lower surfaces of the aileron with its center at the hinge axis. The 30-percent-balance nose block was designed in such a manner that the aileron mean line unported above the airfoil surface at all points along the aileron span for very nearly the same aileron deflection. The wing model tapers in percent thickness and therefore it was necessary to vary the percent balance along the aileron span in order to meet the condition just stated. For the aileron with 30-percent balance the balance chord at any spanwise station was fixed by the condition that has been specified and by the additional condition that the balance root-mean-square chord $\overline{c}_b$ must equal 30 percent of the aileron root-mean-square chord $\overline{c}_a$. The aileron with 30-percent balance will be called the $0.30\overline{c}_a$-balance aileron. The aileron with 40-percent balance was designed in a similar manner and will be called the $0.40\overline{c}_a$-balance aileron.

The three nose radii tested on the $0.30\bar{c}_a$- and the $0.40\bar{c}_a$-balance ailerons were selected in the following manner: When the center of curvature was located on the aileron mean line, the radii that would describe continuous circular arcs tangent to the upper and lower surfaces of the aileron were designated medium radii. Small radii were taken as one-half the medium radii and large radii were taken as one and one-half times the medium radii.

Provision was made for two hinge-axis locations and two gaps for the $0.40\bar{c}_a$-balance aileron. A separate wing-tail block was constructed for each gap and for each position of the hinge axis. The two positions of the hinge axis were at the mean line and at a location 80 percent of the aileron semithickness t below the mean line.

Test Conditions

All the tests were made at a dynamic pressure of 9.21 pounds per square foot, which corresponds to a velocity of about 60 miles per hour and to a test Reynolds number of about 1,540,000 based on a mean aerodynamic chord of 33.66 inches of the model wing. The effective Reynolds number of the tests was about 2,460,000 based on a turbulence factor of 1.6 for the LMAL 7- by 10-foot tunnel. The present tests were made at low scale, low velocity, and high turbulence relative to the flight conditions to which the results are applied. The effects of these variables were not determined or estimated.

RESULTS AND DISCUSSION

Coefficients and Corrections

The symbols used in the presentation of the results are

C_L lift coefficient (L/q_0S)

C_D uncorrected drag coefficient (D/q_0S)

C_m pitching-moment coefficient (M/q_0Sc')

C_l' rolling-moment coefficient (L'/q_0Sb)

$C_{l'_m}$	uncorrected model rolling-moment coefficient (L'_m/q_oSb)
$C_{n'}$	yawing-moment coefficient (N'/q_oSb)
C_h	aileron hinge-moment coefficient $(H/q_ob_a\bar{c}_a^2)$
ΔC_h	C_h of up aileron minus C_h of down aileron
c	actual wing chord at any spanwise location
c_l	chord of basic airfoil section at any spanwise location
$\bar{c}$	mean aerodynamic chord
c_a	aileron chord measured along airfoil chord line from hinge axis of aileron to trailing edge of airfoil
$\bar{c}_a$	root-mean-square chord of aileron
c_b	aileron balance chord measured along airfoil chord line from balance nose to aileron hinge axis
$\bar{c}_b$	root-mean-square chord of aileron balance
$\bar{c}_b/\bar{c}_a$	aileron-balance ratio
b	twice span of semispan model
b_a	aileron span
S	twice area of semispan model
t	semithickness of aileron at hinge axis
L	twice lift on semispan model
D	twice drag on semispan model
H	twice pitching moment of semispan model about support axis

L' rolling-moment, due to aileron deflection, about wind axis in plane of symmetry

L'_m uncorrected rolling moment, due to aileron deflection, about wind axis in plane of symmetry

N' yawing moment, due to aileron deflection, about wind axis in plane of symmetry

H aileron hinge moment

q local dynamic pressure $\left(\frac{1}{2}\rho V^2\right)$

q_o dynamic pressure of air stream, uncorrected for blocking $\left(\frac{1}{2}\rho V_o^2\right)$

q_{max} maximum local dynamic pressure

V local velocity

V_o free-stream velocity

V_i indicated velocity

α angle of attack

δ_a aileron deflection relative to wing, positive when trailing edge is down

δ_f slotted flap deflection relative to wing, positive when trailing edge is down

θ_s control-stick deflection

$C_{l'_p}$ rate of change of rolling-moment coefficient $C_{l'}$ with helix angle $pb/2V$

p rate of roll

F_s stick force

A positive value of L' or $C_{l'}$ corresponds to an increase in lift of the model and a positive value of N'

or $C_{n'}$ corresponds to a decrease in drag of the model. Twice the actual lift, drag, pitching moment, area, and span of the model were used in the reduction of the results because the model represented half a complete wing.

The angle of attack, the drag coefficient, the rolling-moment coefficient, and the yawing-moment coefficient have been corrected for the effect of the tunnel walls in accordance with the theory of trailing-vortex images. The corrections applied to the rolling- and yawing-moment coefficients account for the fact that the spanwise loading induced by aileron deflection on a semispan wing with a reflection plane at the plane of symmetry is somewhat different from the loading that would be induced over a complete wing with no reflection plane. This statement is made in an attempt to clarify statements in previous reports as to the corrections applied to lateral-control data from tests of the tapered-wing model used and should not be construed to mean that the corrections applied to the data presented herein differ from those applied in previous lateral-control tests of 0.155c by 0.405b/2 ailerons on this wing model. No corrections have been applied to the lift, the pitching-moment, and the hinge-moment coefficients, but computations indicate that these corrections would be very small. No corrections have been applied to any of the results for blocking, for misalinement of the air stream, for the effects of the support strut, or for the treatment of the inboard end of the wing, that is, the small gap between the root section of the wing and the wall, the leakage through the wall around the support tube, and the boundary layer at the wall. These effects are probably of second-order importance for the rolling- and yawing-moment coefficients (which are basically incremental data) but may be more important for the other forces and moments, particularly for the drag coefficients. It is for this reason that the drag coefficients are referred to as uncorrected.

The corrections that were applied (by addition) to the angle of attack (in deg), the drag coefficient, the rolling-moment coefficient, and the yawing-moment coefficient were

$$\Delta\alpha = 1.30\ C_L$$

$$\Delta C_D = 0.023\ C_L^2$$

$$\Delta C_l' = -0.15\, C_l'_m$$

$$\Delta C_n' = -0.03\, C_L\, C_l'_m$$

Characteristics with Ailerons Neutral

A comparison of the lift, drag, and pitching-moment characteristics of the tapered-wing model equipped with plain ailerons and blunt-nose balance ailerons fixed at neutral is shown in figure 6. In order to make the comparison for the case in which the greatest possible deviation might be expected to occur, the $0.40c_a$-balance blunt-nose aileron with large nose radii was selected. It is seen from this figure that these characteristics agree reasonably well for the various aileron installations; for this reason, it was not considered necessary to present data of this type for each of the modifications tested in this investigation.

Plain Aileron

The characteristics of the plain aileron, shown in figure 7, are presented primarily to provide a base with which the blunt-nose-balance ailerons might be compared. The most significant points to be noted from figure 7 are the high negative slopes of the hinge-moment curves $\partial C_h/\partial \delta_a$ for both sealed and unsealed ailerons and the marked loss in rolling-moment coefficient caused by an open gap at the aileron nose.

Effect of Type of Seal

Although the grease seal seemed to be satisfactory during the tests of the plain aileron, great difficulty was experienced in measuring the hinge moments of the balanced ailerons when this type of seal was used. It was found during the course of the investigation that consistent results could be obtained more easily by replacing the grease seal with a thin strip of rubber dam, cemented at the mean line to the nose of the aileron balance and to the wing tail block. The longitudinal gaps, 0.002c wide, between the wing and the ends of the balance were left open for all tests. The tests that had already been made with the grease seal were not repeated with the rubber

seal, with the exception of a single test of a $0.40\bar{c}_a$-balance aileron with medium nose radii at an angle of attack of 13.3°. A comparison of the characteristics of the aileron with the two types of seal is presented in figure 8. The principal differences to be noted are that the negative slope of the hinge-moment curve is smaller and the effectiveness at positive aileron deflections is slightly larger for the grease seal. These differences are probably caused by the fact that the grease, in addition to sealing the gap, filled the space between the wing and the aileron nose, which may have prevented lateral flow along the leading edge of the aileron, and also gave a less abrupt change in contour at that point. The less abrupt change in contour should cause a smoother flow over the aileron nose and thereby cause both the aileron and the balance to be more effective. The increase in balance effectiveness is especially noticeable at large negative aileron deflections; at $\delta_a = -20°$ the hinge-moment coefficients for the two types of seal are approximately equal but opposite in sign, with the grease-seal results indicating the larger balance effectiveness.

$0.30\bar{c}_a$-Balance Ailerons

The characteristics of some of the modifications of the $0.30\bar{c}_a$-balance aileron are given in figures 9 to 11. The characteristics of some additional modifications are presented in figures 12 to 14, which show the effect of nose radius.

At an angle of attack of 1.5° the presence of the seal on the aileron with small nose radii decreased the negative slope of the hinge-moment curve $\partial C_h/\partial \delta_a$ at small deflections by about 0.001 and increased the effectiveness for $\delta_a = \pm 15°$ by about 14 percent. (See fig. 9.) At an angle of attack of 14.8°, however, the seal had little effect on the slope of the hinge-moment curve at small deflections and the unsealed aileron was slightly more effective than the sealed aileron.

Neither nose radius nor gap had much effect on the variation of the hinge-moment coefficient with angle of attack. (See fig. 12.) For all the modifications $\partial C_h/\partial \alpha$ is very nearly zero within the range of $\alpha = -4°$ to $\alpha = 4°$ but assumes a gradually increasing negative value

as the angle of attack is increased above 4°. The value of $\partial C_h/\partial\alpha$ at $\alpha = 16°$ is about −0.005.

The negative slope of the hinge-moment curve $\partial C_h/\partial\delta_\alpha$ increases as the nose radii are increased (figs. 13 and 14) for both open and sealed gaps. Increasing the nose radii decreased the aileron effectiveness at small aileron deflections for the open gap but the effect was negligible for the sealed gap. The ailerons with the large nose radii maintain their effectiveness over a greater deflection range and therefore are usually the most effective and have the lowest hinge moments for values of δ_a greater than 15° or 20°.

0.40$\overline{c}_a$-Balance Ailerons with Mean Hinge Axes

The characteristics of some of the 0.40$\overline{c}_a$-balance ailerons having the hinge axis on the mean line are presented in figures 15 to 17. The characteristics of some additional modifications are presented in figures 18 to 20, which show the effect of nose radius.

As in the case of the 0.30$\overline{c}_a$-balance ailerons, the variation of the hinge-moment coefficient with angle of attack does not seem to be appreciably affected by the nose radius (fig. 18). With a gap of 0.005c, however, $\partial C_h/\partial\alpha$ is slightly positive for angles of attack less than 2°; whereas, with the gap sealed, $\partial C_h/\partial\alpha$ is about zero over the same range. At $\alpha = 16°$, $\partial C_h/\partial\alpha$ is about −0.004 for all modifications.

The tendency of the larger nose radii to cause higher negative slopes of the hinge-moment curves at $\delta_a = 0°$ is also apparent for the 0.40$\overline{c}_a$-balance ailerons, and again the effect of increasing the nose radii was to decrease the rolling-moment coefficients at small deflections when the gap was open. With small nose radii and 0.005c gap, the aileron was overbalanced at an angle of attack of 0.1°. (See fig. 19(a).) At aileron deflections of −15° and 8° both the hinge-moment-coefficient and rolling-moment-coefficient curves break away quite rapidly when the small radii are used, and high hinge moments and low effectiveness can be expected beyond these limits.

Effect of gap.- The $0.40\overline{c}_a$-balance aileron having medium nose radii was tested with a gap of 0.0025c as well as the usual 0.005c and sealed gaps. Figure 21 shows that the characteristics of the aileron with the intermediate gap are not unusual and lie about halfway between the characteristics with 0.005c gap and those with sealed gap.

The principal effects of gap on hinge- and rolling-moment parameters for the $0.40\overline{c}_a$-balance aileron with medium nose radii may be judged from figure 21 and from the following table:

Gap	α	$\frac{\partial C_h}{\partial \delta_a}$ for $\delta_a = 0^\circ$	$\Delta C_l'$ for $\delta_a = \pm 15^\circ$
Sealed	0.1	-0.0017	0.0428
.0025c		-.0012	.0407
.005c		-.0008	.0392
Sealed	13.3	-0.0047	0.0405
.0025c		-.0034	.0404
.005c		-.0033	.0409

Doubling the width of the gap very nearly doubles its effect on the slope of the hinge-moment curve at either angle of attack. The increment of rolling-moment coefficient produced by aileron deflections of $\pm 15^\circ$ is quite noticeably decreased with increasing gap at the low angle of attack but shows practically no change at the high angle of attack. At the low angle of attack the effect of the gap in decreasing the rolling-moment coefficient appears to be almost entirely on the up aileron; at the high angle of attack, however, the reduction in effectiveness on the up aileron is counteracted by a corresponding increase in effectiveness on the down aileron.

$0.40\overline{c}_a$-Balance Aileron with Low Hinge Axes

The characteristics of two $0.40\overline{c}_a$-balance ailerons having low hinge axes are shown in figures 22 and 23.

The characteristics of some additional modifications are included in figures 24 to 29, which show the effect of hinge-axis location.

The hinge-axis location had very little effect on the variation of hinge-moment coefficient with angle of attack when the flap was retracted (fig. 24) but, with the flap deflected 50° (fig. 25), the ailerons with low hinge axes showed a greater tendency toward positive values of $\partial C_h/\partial \alpha$ for angles of attack below 3°. In general, it can be said that the change in vertical position of the hinge axis had little effect on any of the characteristics. For most of the nose modifications the ailerons with low hinge axes seemed to retain their effectiveness to slightly higher positive deflections and to lose their effectiveness at slightly lower negative deflections. There was a corresponding shift in the values of δ_a at which the breaks in the hinge-moment curves occurred. At high angles of attack the aileron with a gap of 0.005c, medium nose radii, and low hinge axis (figs. 26 and 27) gave considerably higher effectiveness for negative deflections and only slightly less effectiveness for positive deflections than the same aileron with a mean hinge axis, but this tendency was not evident for the ailerons with sealed or 0.005c gap and with large nose radii. (See figs. 28 and 29.)

Effect of Balance Chord

The effect of the balance chord $\bar{c}_b$ on the characteristics of the blunt-nose ailerons with medium nose radii and mean hinge axes are shown in figure 30. Some of the more important effects of balance are summarized for several of the ailerons in figure 31. Increasing the balance chord was more effective in decreasing the slope of the hinge-moment curve for ailerons with 0.005c gaps than for ailerons with sealed gaps. The increment of rolling-moment coefficient produced by aileron deflections of ±15° was increased as the balance chord was increased for both medium and large nose radii and 0.005c and sealed gaps. The effectiveness of the ailerons with 0.005c gaps increased more rapidly with balance chord than did the effectiveness of the ailerons with sealed gaps.

Peak Pressures

Local dynamic pressures were determined at various positions over the noses of some of the ailerons, and the results are presented in figures 32 to 35 in terms of the ratio of the local dynamic pressure to the free-stream dynamic pressure. In each case an attempt was made to select positions as near as possible to the point at which the peak pressure could be expected to occur. The peak pressure for a given spanwise position on a given aileron seemed to depend principally on the aileron deflection, being practically independent of angle of attack until the occurrence of local stalling over the aileron nose. The peak pressures at the inboard and outboard sections were very nearly the same for a given aileron deflection except during a condition of partial aileron-nose stall, as in figures 33(c) and 33(d). The pressures on the lower surface of each of the ailerons were generally somewhat lower than the pressures on the upper surface. Sealing the gap seemed to have little effect on the peak pressure on either surface.

The ratio of the peak dynamic pressure to the free-stream dynamic pressure q_{max}/q_o is plotted against aileron deflection for the three nose-radius modifications in figure 36. At aileron deflections of 15° the ratio q_{max}/q_o at the inboard section ranges from 2.65 for the large nose radii to 3.03 for the small nose radii; these values correspond, respectively, to local velocities of 1.63 and 1.74 times the velocity of the free stream. The peak pressures over the nose of the aileron with medium nose radii are only slightly higher than the peak pressures over the aileron with large nose radii.

Because the peak pressures were relatively high for all the modifications tested, it is probable that the effects of compressibility will be severe at high speeds. It is recommended that blunt-nose ailerons be tested at Mach numbers considerably higher than the Mach number of the test data herein presented before they are considered for use on high-speed airplanes.

Estimated Rates of Roll and Stick Forces

The rates of roll and the stick forces during steady rolling of the airplane, shown in figure 4, have been

estimated from the data of figures 7, 10, 11, 16, 17, 22, and 23. The rates of roll were estimated by means of the relationship

$$\frac{pb}{2V} = \frac{C_l'}{C_{l'_p}} \qquad (1)$$

where the coefficient of damping in roll $C_{l'_p}$ was taken as 0.46 from the data of reference 6. It has been assumed that the rudder will be used to counteract the yawing moment, that the aileron-operating mechanism is nonelastic, and that the wing will not twist. The stick forces were estimated from the relationship

$$F_s = \frac{90.3}{C_L} \Delta C_h \frac{d\delta_a}{d\theta_s} \qquad (2)$$

which may be derived from the aileron dimensions and the following airplane characteristics:

Wing area, square feet	260
Span, feet	38
Taper ratio	1.67:1
Airfoil section (basic)	NACA 230 series
Mean aerodynamic chord, inches	84.14
Weight, pounds	7063
Wing loading, pounds per square foot	27.2
Stick length, feet	.2
Maximum stick deflection, θ_s, degrees	±21

The value of the constant in equation (2) is dependent upon the wing loading, the size of the ailerons, and the length of the stick. The values of $d\delta_a/d\theta_s$ in equation (2) may be determined from the maximum stick deflection of ±21° and from the maximum aileron deflections noted on the figures showing the computed results; for a given aileron $d\delta_a/d\theta_s$ is assumed constant. The values of C_l' and ΔC_h used in equations (1) and (2) are the values computed for the condition of steady roll; the difference in angle of attack of the two ailerons due to rolling has been taken into account. All the ailerons were assumed to deflect equally up and down with maximum deflections

sufficient to produce $pb/2V = 0.09$ at high speed, which would allow for a 20-percent loss due to cable stretch and wing twist for the nonrigid airplane and still provide $pb/2V = 0.07$ (the minimum requirement stated in reference 6).

Stick-force characteristics of the $0.30\bar{c}_a$-balance aileron with 0.005c gap and medium and large nose radii are presented in figure 37. Stick-force characteristics for the $0.40\bar{c}_a$-balance aileron with 0.005c gap and medium and large nose radii are presented in figure 38 for the mean hinge-axis location and in figure 39 for the low hinge-axis location. No computations were made for the ailerons with small nose radii because the aileron nose was nearly stalled at the deflections required for the small aileron used in these tests. For all cases shown in figures 37 to 39 increasing the nose radii increased the stick forces and the aileron deflection required to attain a given $pb/2V$. In general deflecting the flap increased the aileron effectiveness. With the $0.40\bar{c}_a$-balance aileron, lowering the hinge axis decreased the high-speed stick forces for the medium nose radii and increased the high-speed stick forces for the large nose radii.

A comparison of the stick-force characteristics of the plain sealed aileron and the three balanced ailerons with 0.005c gaps and medium nose radii is given in figure 40. As shown by the curves of figure 40, the use of $0.40\bar{c}_a$-balance blunt-nose ailerons will reduce the maximum high-speed stick forces to about 15 percent of those experienced in the use of plain sealed ailerons. There was no indication that the use of blunt-nose ailerons would cause overbalance at low speeds. The small reduction in stick force produced by the $0.30\bar{c}_a$ balance as compared with the reduction caused by the $0.40\bar{c}_a$ balance may be attributed to the larger rate of change of $\partial C_h/\partial \delta_a$ with balance chord for the larger balance and also to the fact that the $0.30\bar{c}_a$-balance aileron with 0.005c gap was less effective than both the plain sealed aileron and the $0.40\bar{c}_a$-balance aileron with 0.005c gap. Had all three ailerons been sealed, the difference in balance effectiveness would have been smaller.

CONCLUSIONS

From the results of the tests and computations herein reported, in which the effects of compressibility, turbulence, and scale have been neglected, the following conclusions may be drawn:

1. For the arrangement tested, the use of blunt-nose ailerons with 40-percent balance and medium nose radii would reduce the high-speed stick forces to about 15 percent of those experienced in the use of plain sealed ailerons.

2. Increasing the balance chord increased the aileron effectiveness slightly and reduced the adverse effects of a gap at the aileron nose.

3. Increasing the nose radii decreased the aileron effectiveness for small deflections but increased the effectiveness at large deflections and extended the deflection range over which the ailerons maintained their effectiveness.

4. Increasing the nose radii increased the negative slope of the curves of hinge-moment coefficient plotted against aileron deflection but, at the same time, extended the deflection range over which the slope was relatively small.

5. Changing the position of the hinge axis from the aileron mean line to a position near the lower surface of the aileron had comparatively little effect on the aileron characteristics.

6. The peak pressures over the noses of the blunt-nose ailerons were relatively high at moderate deflections.

Langley Memorial Aeronautical Laboratory,
National Advisory Committee for Aeronautics,
Langley Field, Va.

REFERENCES

1. Sears, Richard I., and Hoggard, H. Page, Jr.: Wind-Tunnel Investigation of Control-Surface Characteristics. II - A Large Aerodynamic Balance of Various Nose Shapes with a 30-Percent-Chord Flap on an NACA 0009 Airfoil. NACA A.R.R., Aug. 1941.

2. Ames, Milton B., Jr., and Eastman, Donald R., Jr.: Wind-Tunnel Investigation of Control-Surface Characteristics. IV - A Medium Aerodynamic Balance of Various Nose Shapes Used with a 30-Percent-Chord Flap on an NACA 0009 Airfoil. NACA A.R.R., Sept. 1941.

3. Sears, Richard I., and Hoggard, H. Page, Jr.: Wind-Tunnel Investigation of Control-Surface Characteristics. VII - A Medium Aerodynamic Balance of Two Nose Shapes Used with a 30-Percent-Chord Flap on an NACA 0015 Airfoil. NACA A.R.R., July 1942.

4. Sears, Richard I., and Gillis, Clarence L.: Wind-Tunnel Investigation of Control-Surface Characteristics. VIII - A Large Aerodynamic Balance of Two Nose Shapes Used with a 30-Percent-Chord Flap on an NACA 0015 Airfoil. NACA A.R.R., July 1942.

5. Wenzinger, Carl J., and Harris, Thomas A.: Wind-Tunnel Investigation of an N.A.C.A. 23012 Airfoil with Various Arrangements of Slotted Flaps. Rep. No. 664, NACA, 1939.

6. Gilruth, R. R., and Turner, W. N.: Lateral Control Required for Satisfactory Flying Qualities Based on Flight Tests of Numerous Airplanes. Rep. No. 715, NACA, 1941.

TABLE I

ORDINATES FOR AIRFOIL

[Spanwise stations in inches from root section. Chord stations and ordinates in percent of basic wing chord c_1]

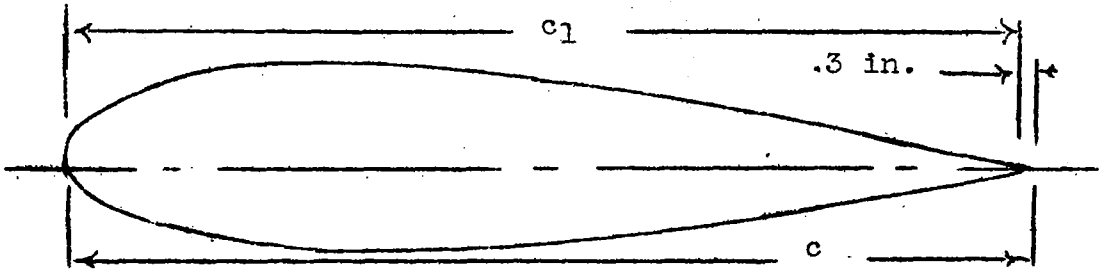

Model wing station 0		
Station	Upper surface	Lower surface
0	0	0
1.25	3.48	-1.60
2.5	4.61	-2.36
5	6.10	-3.21
7.5	7.14	-3.82
10	7.89	-4.33
15	8.80	-5.12
20	9.22	-5.71
25	9.40	-6.10
30	9.37	-6.28
40	8.90	-6.23
50	8.02	-5.78
60	6.85	-5.05
70	5.44	-4.10
80	3.87	-2.97
90	2.12	-1.67
95	1.16	-.94
100	.18	-.16
100.73	.03	-.03
L.E. radius: 2.65. Slope of radius through end of chord: 0.305		

Model wing station 88.8		
Station	Upper surface	Lower surface
0	0	0
1.25	1.89	-.84
2.5	2.65	-1.07
5	3.70	-1.26
7.5	4.45	-1.40
10	4.98	-1.52
15	5.54	-1.86
20	5.73	-2.22
25	5.77	-2.46
30	5.71	-2.62
40	5.36	-2.70
50	4.78	-2.56
60	4.06	-2.27
70	3.21	-1.87
80	2.26	-1.36
90	1.22	-.78
95	.70	-.46
100	.18	-.14
101.2	.05	-.05
L.E. radius: 0.70. Slope of radius through end of chord: 0.305		

TABLE II

ORDINATES FOR FLAP AND SLOT SHAPES

[Spanwise stations in inches from root section. Chord stations and ordinates in percent of basic wing chord c_1]

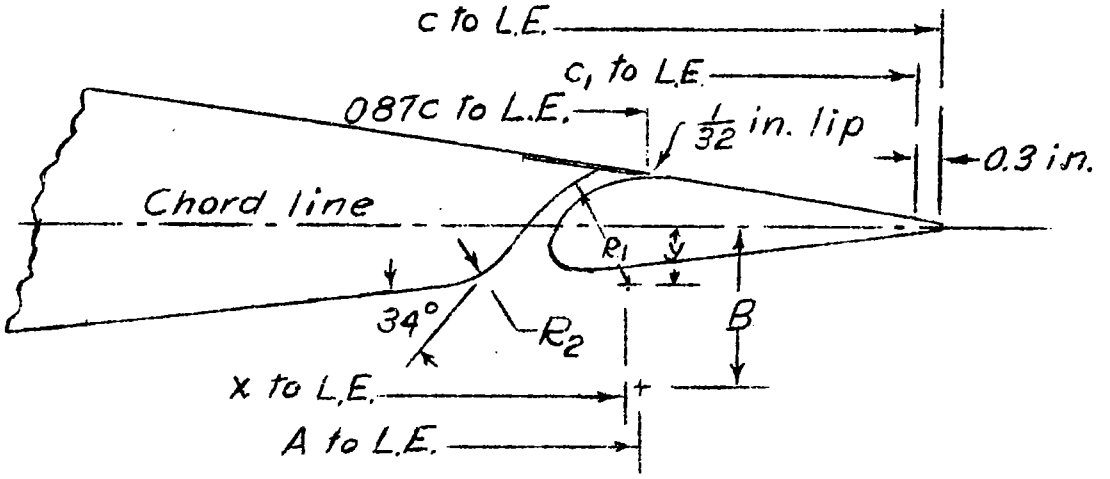

Flap Stations

Model wing station 0			Model wing station 88.8		
Station	Upper surface	Lower surface	Station	Upper surface	Lower surface
0	-1.29	-1.29	0	-0.76	-0.76
.52	-.08	-2.30	.53	.01	-1.16
1.04	.48	-2.50	1.06	.36	-1.23
2.07	1.29	-2.60	2.12	.80	-1.22
4.15	2.17	-2.44	4.24	1.30	-1.10
6.22	2.53	-2.18	6.36	1.42	-.99
8.29	2.40	-1.91	8.48	1.35	-.87
12.44	1.65	-1.32	12.72	.93	-.62
16.58	.85	-.69	16.96	.51	-.32
20.72	.03	-.03	21.20	.05	-.05
L.E. radius: 1.19			L.E. radius: 0.32		

Slot Shape

	Station 0	Station 88.8
R_1	5.3	5.1
R_2	2	2
x	85	83.3
y	2.5	3.3

Flap Pivot Point

	Station 0	Station 88.8
A	85.8	84
B	7.7	8

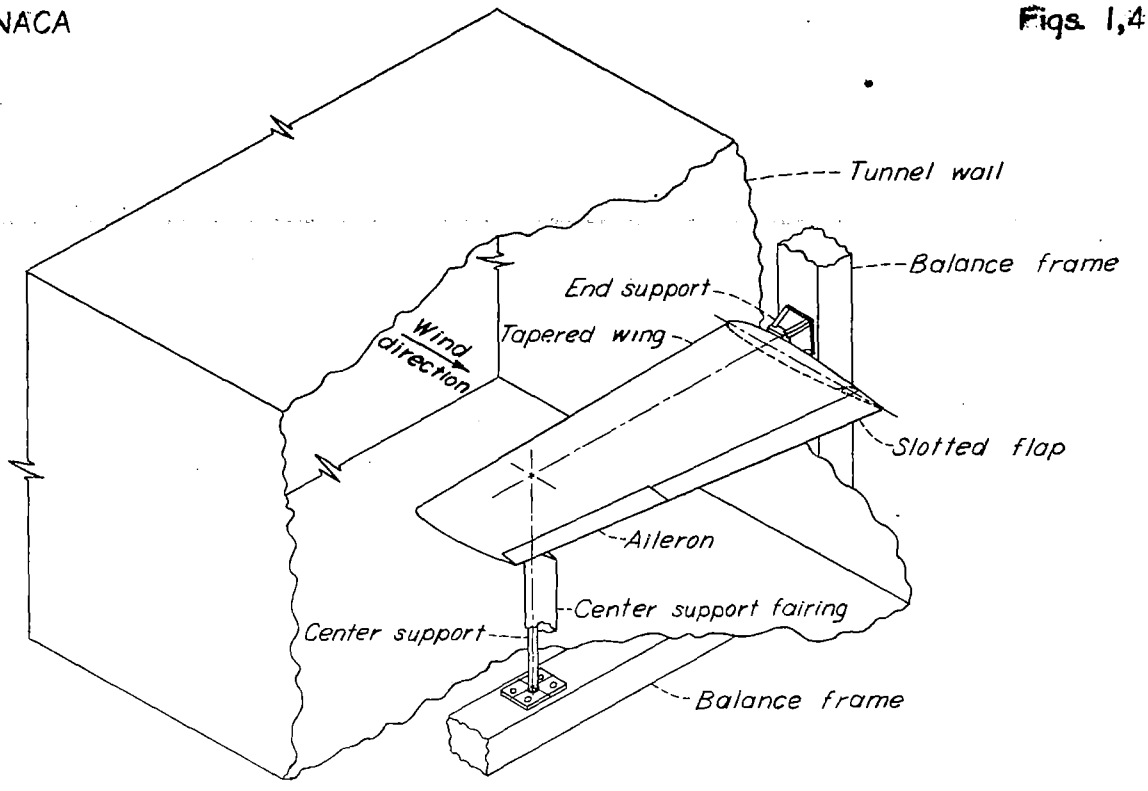

Figure 1.- Schematic diagram of test installation.

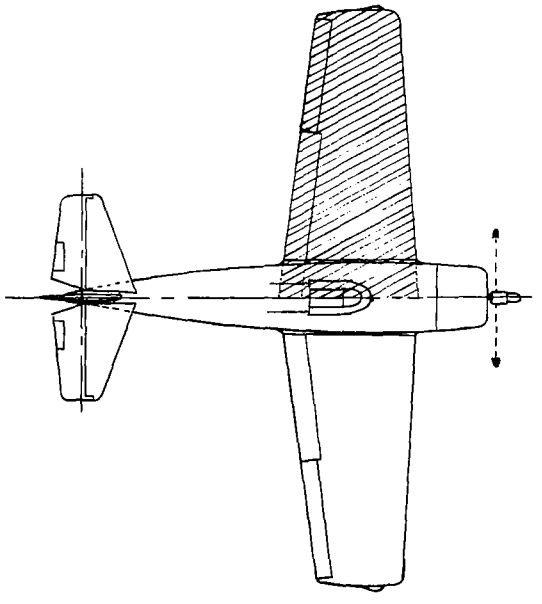

Figure 4.- Portion of airplane simulated by model.

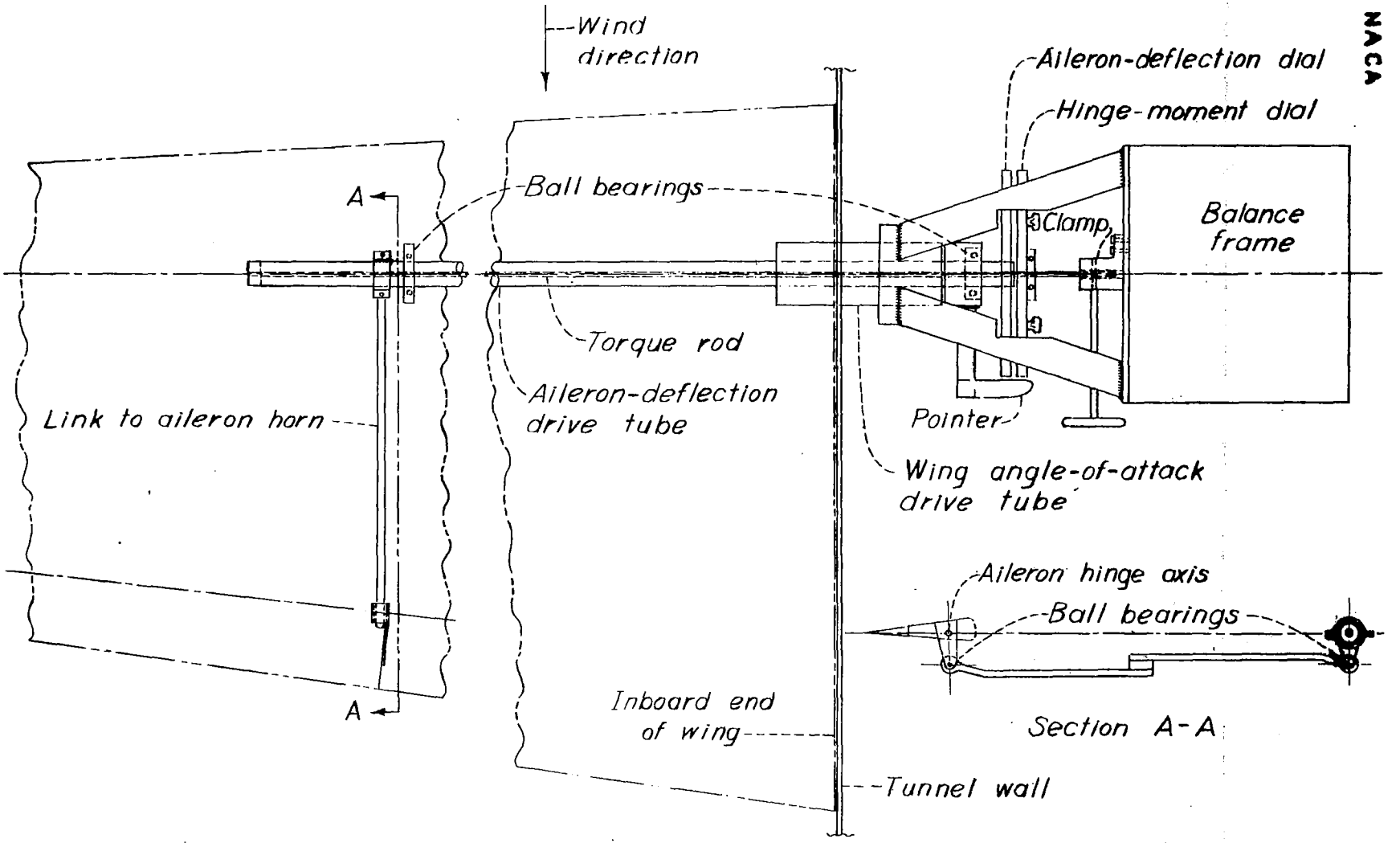

Figure 2. - Schematic diagram of the torque-rod assembly for measuring aileron hinge moments.

NACA

Fig. 2

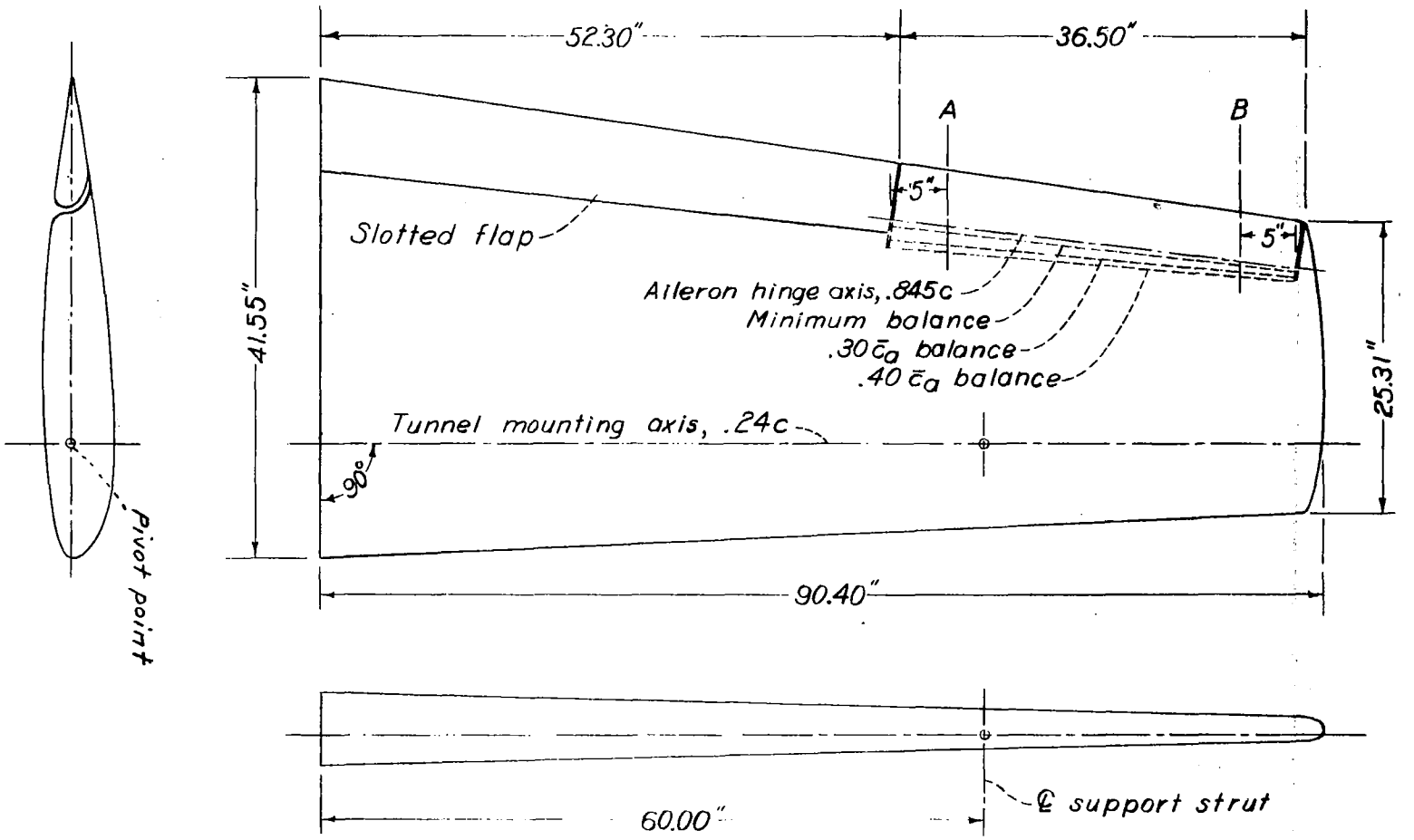

Figure 3.- Semispan model of tapered wing.

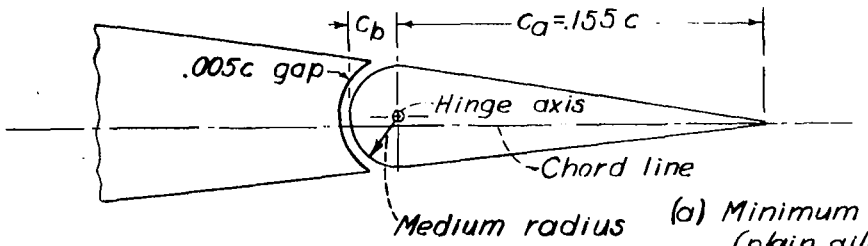

(a) Minimum balance, 0.113 $\bar{c}_a$ (plain aileron)

	Inboard end c = 31.986" c_a = 4.942"	Outboard end c = 25.314" c_a = 3.965"
c_b	0.1315 c_a	0.0878 c_a
Medium radius	.1315 c_a	.0878 c_a

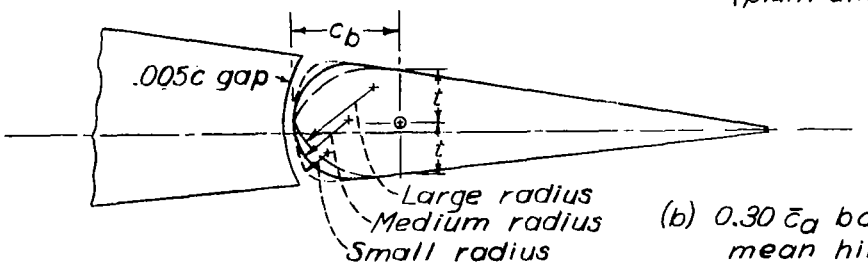

(b) 0.30 $\bar{c}_a$ balance; mean hinge axis

c_b	.3570 c_a	.2175 c_a
Small radius	.0782 c_a	.0492 c_a
Medium radius	.1564 c_a	.0984 c_a
Large radius	.2346 c_a	.1476 c_a

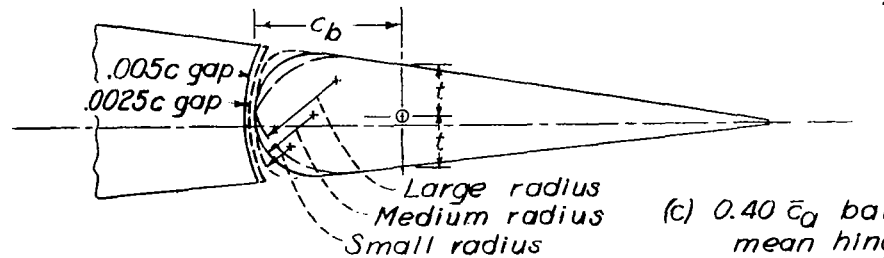

(c) 0.40 $\bar{c}_a$ balance; mean hinge axis

c_b	.4758 c_a	.2896 c_a
Small radius	.0840 c_a	.0517 c_a
Medium radius	.1681 c_a	.1034 c_a
Large radius	.2521 c_a	.1551 c_a

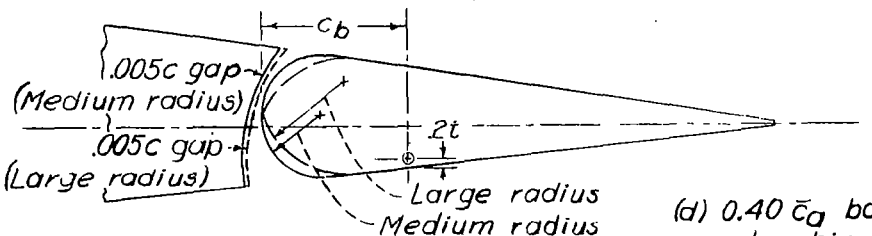

(d) 0.40 $\bar{c}_a$ balance; low hinge axis

c_b	.4758 c_a	.2896 c_a
Medium radius	.1681 c_a	.1034 c_a
Large radius	.2521 c_a	.1551 c_a

Figure 5.- The various 0.155 c by 0.405 b/2 ailerons tested on the tapered-wing model.

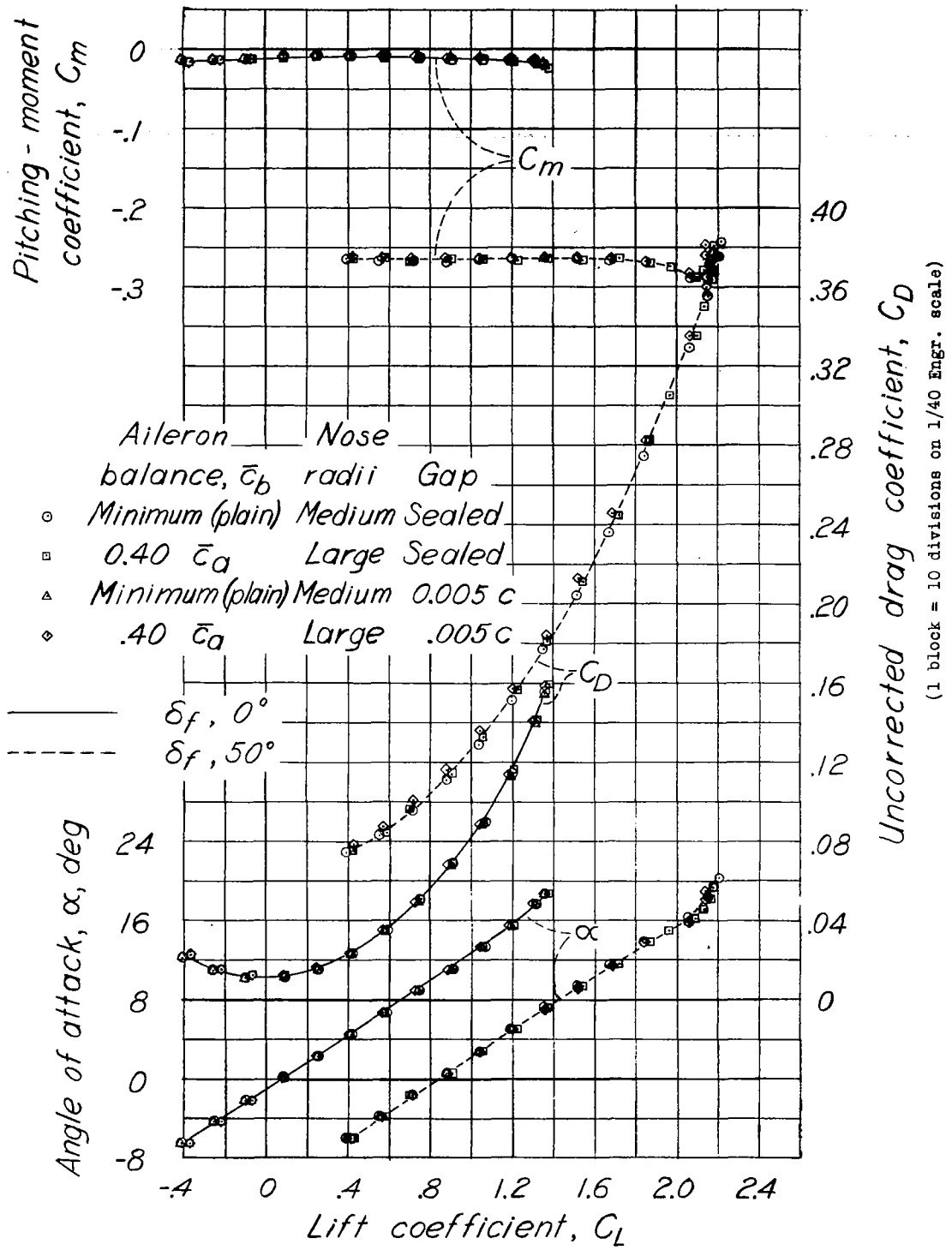

Figure 6.- Comparison of the lift, drag, and pitching-moment characteristics of the tapered-wing model with plain ailerons and with 0.40 $\bar{c}_a$ - balance ailerons having large nose radii and mean hinge-axis locations. δ_a, 0°.

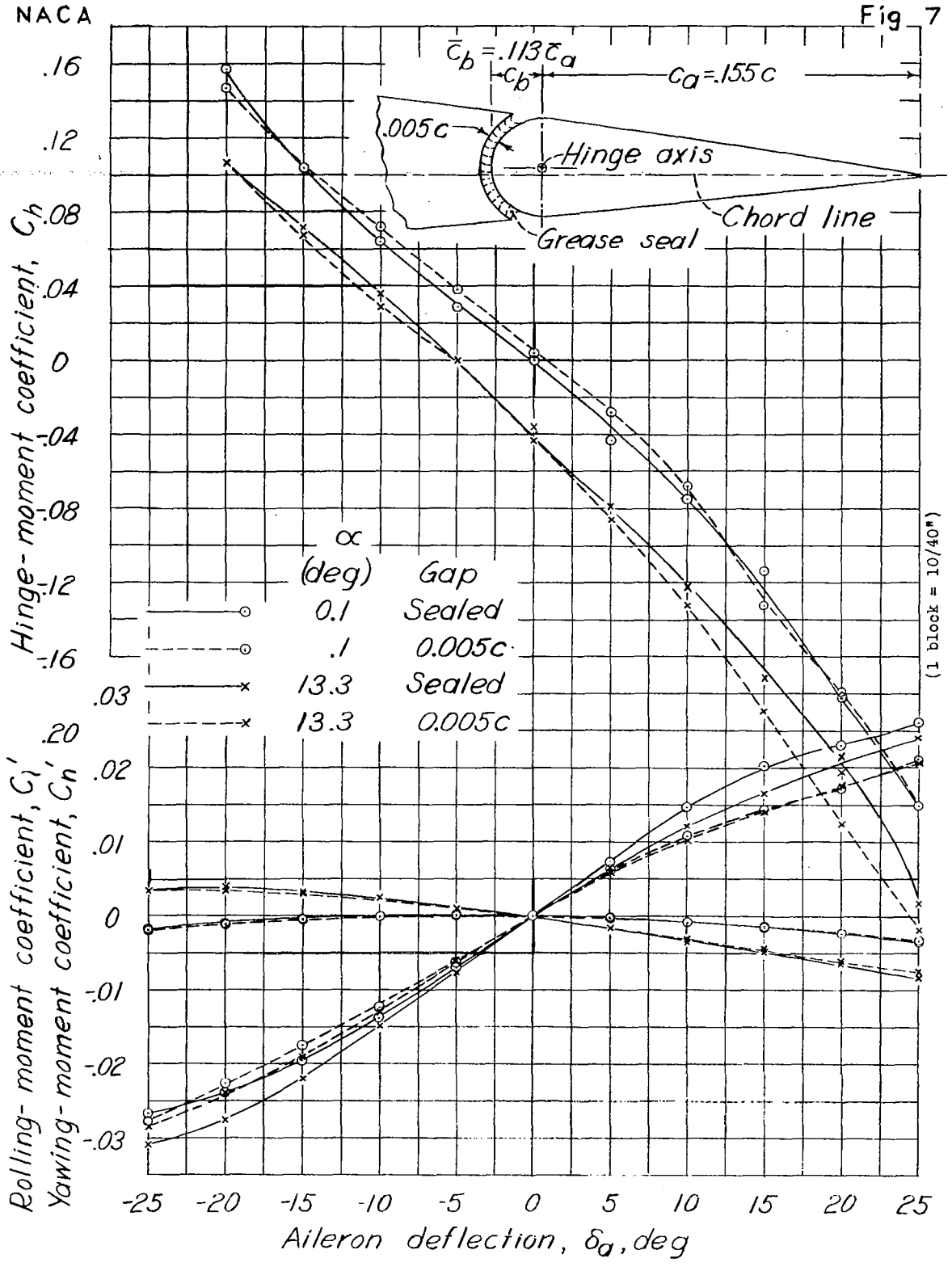

Figure 7.-Characteristics of the plain aileron on the tapered-wing model. δ_f, 0°.

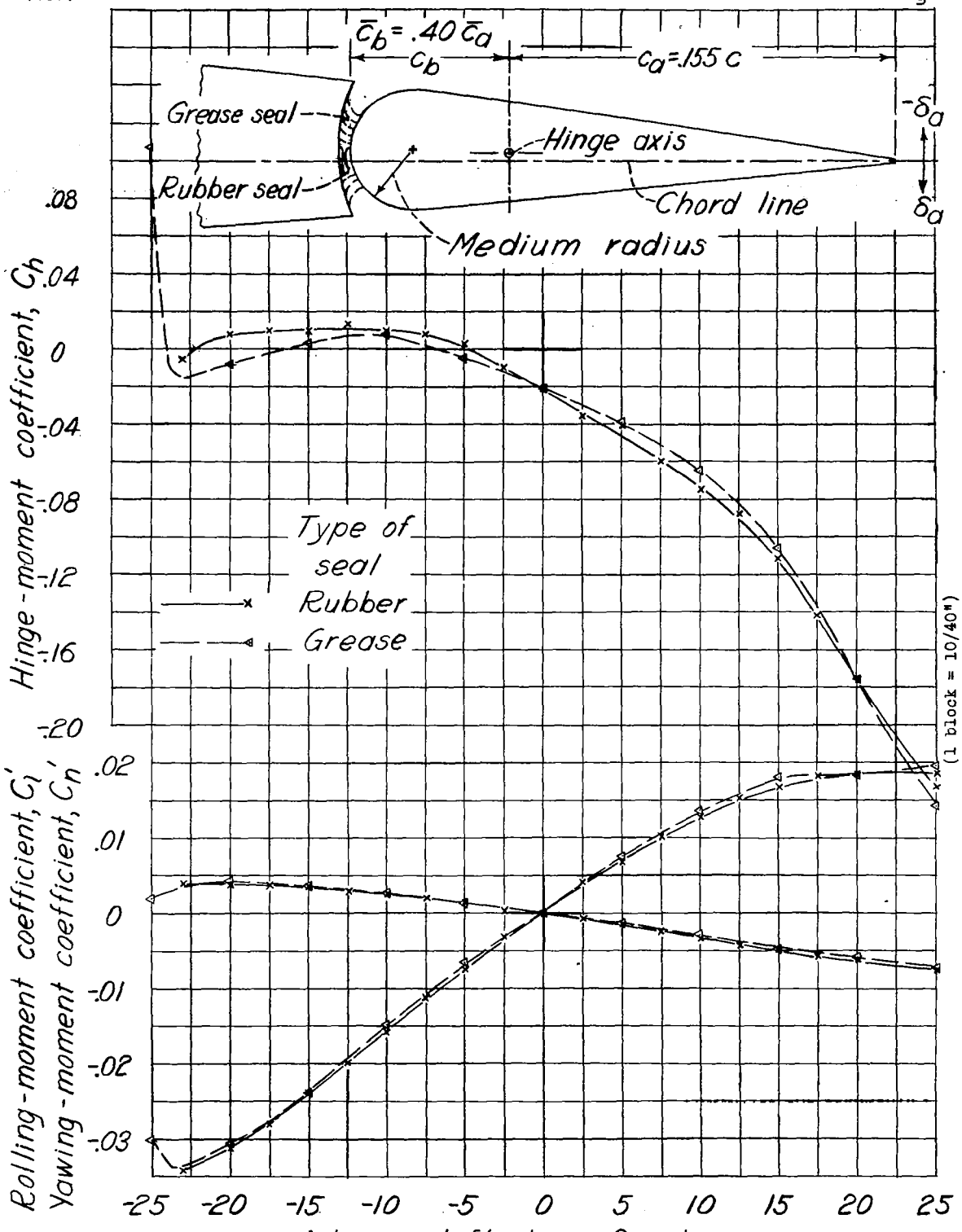

nose radii, medium; δ_f, 0°; α, 13.3°.

Figure 8.- Effect of type of seal on the characteristics of a 0.40 $\bar{c}_a$-balance blunt-nose aileron on the tapered-wing model. Hinge-axis location, mean.

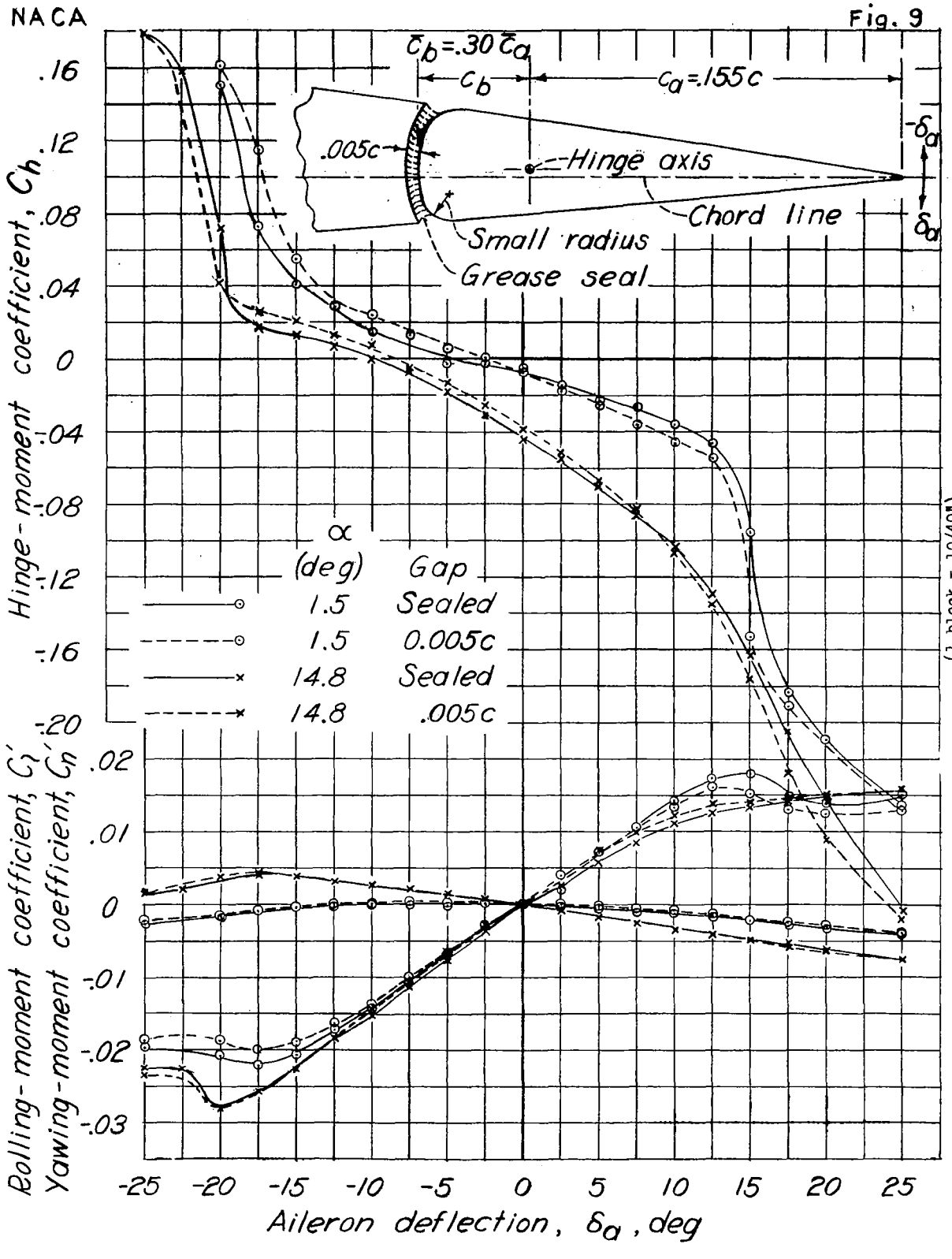

Figure 9.- Characteristics of a $0.30\,\bar{c}_a$-balance blunt-nose aileron on the tapered-wing model. Nose radii, small; δ_f, 0°.

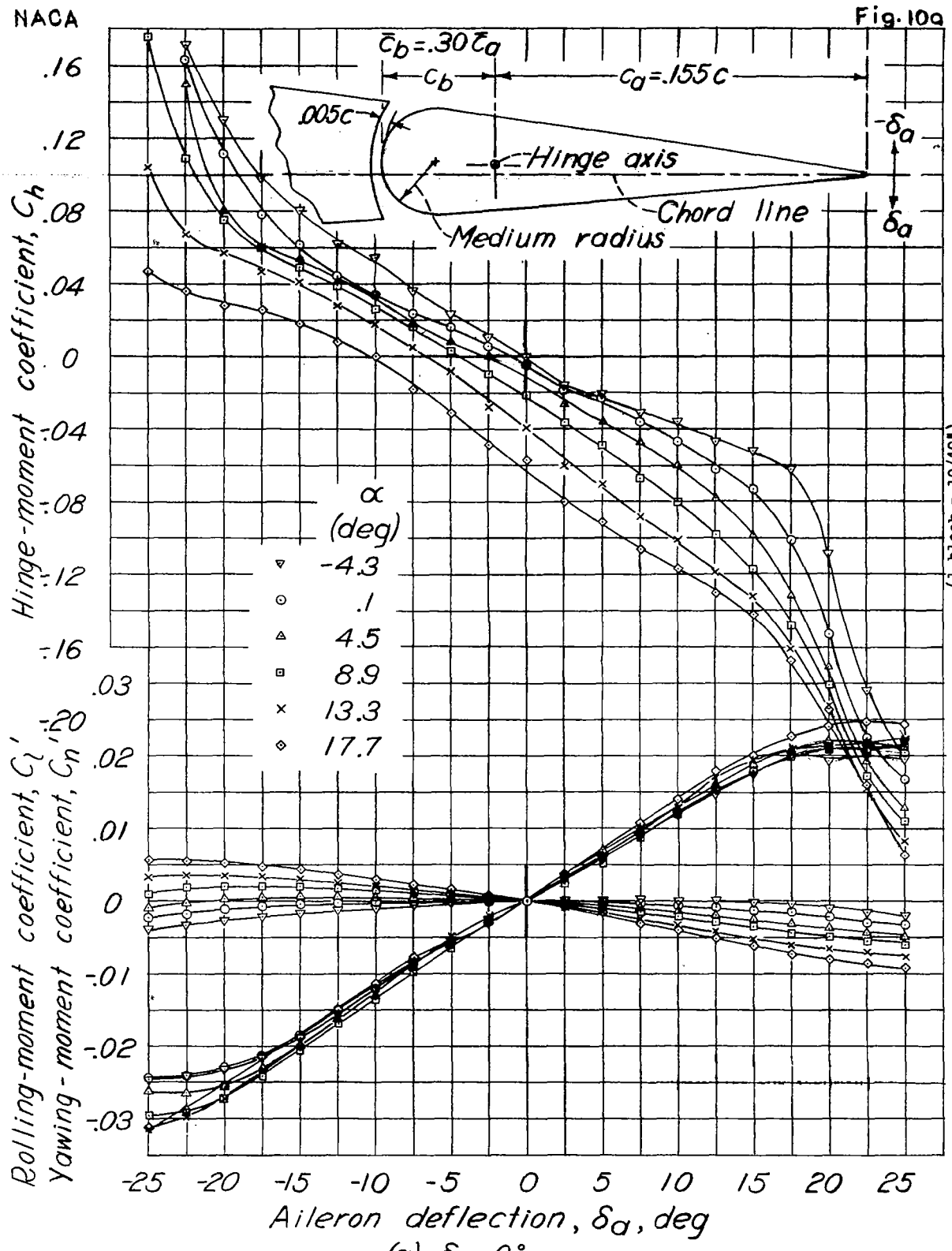

(a) $\delta_f = 0°$.

Figure 10.- Characteristics of a 0.30 $\bar{c}_a$-balance blunt-nose aileron on the tapered-wing model. Nose radii, medium; gap, 0.005c.

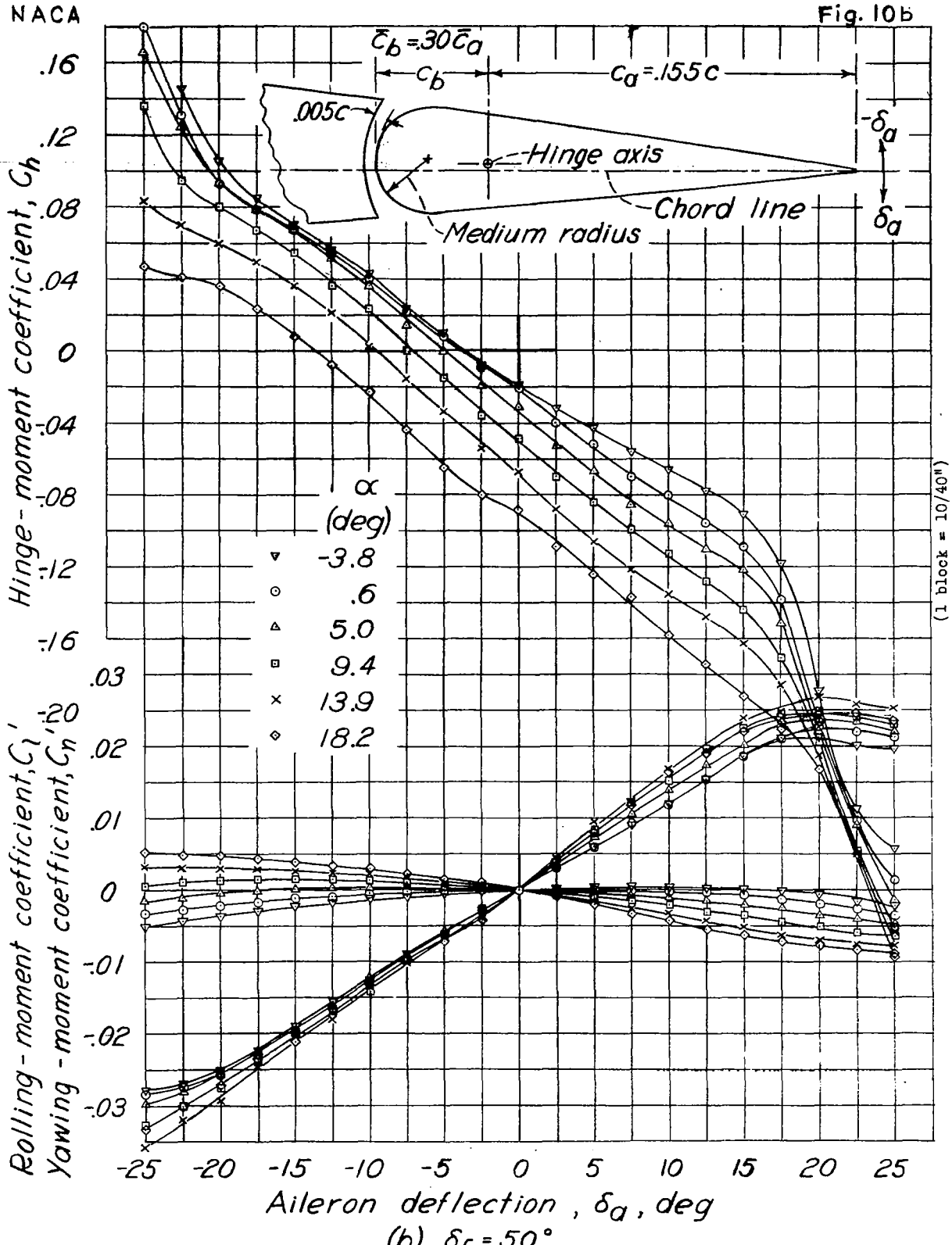

(b) $\delta_f = 50°$.

Figure 10.- Concluded.

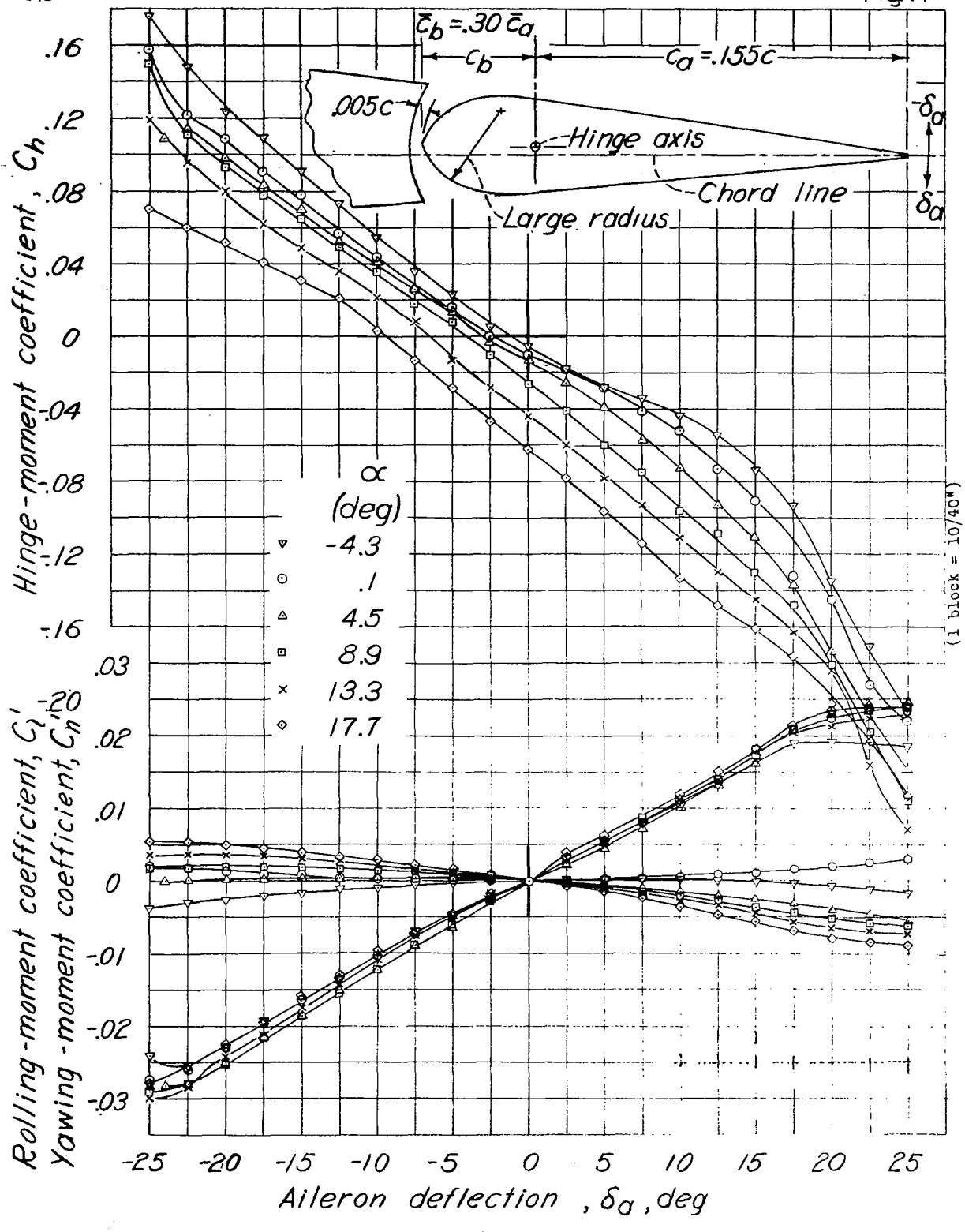

Figure 11.- Characteristics of a $0.30\bar{c}_a$-balance blunt-nose aileron on the tapered-wing model. Nose radii, large; gap, 0.005c; δ_f, 0°.

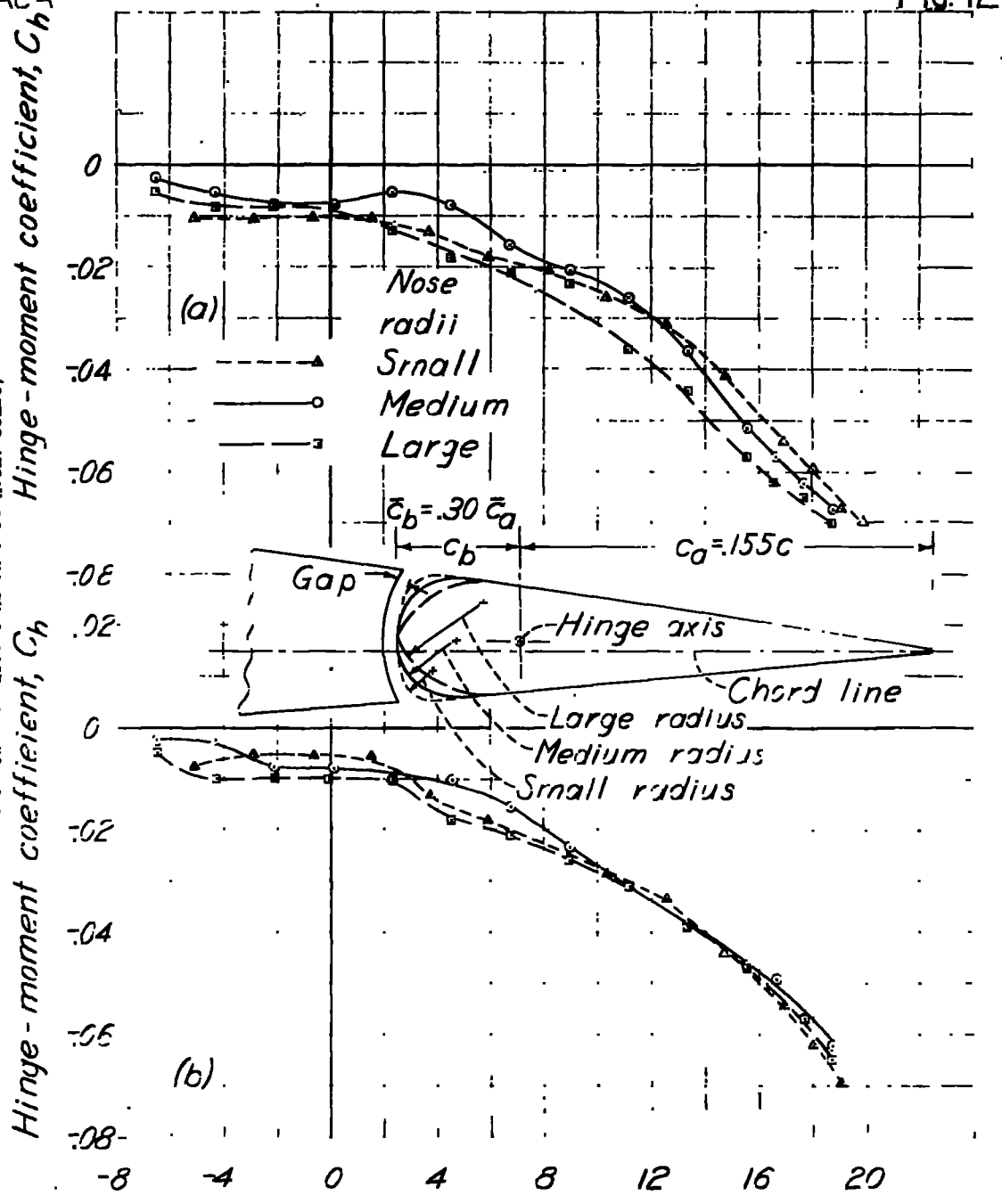

(a) Gap, 0.005c.
(b) Gap, sealed.

Figure 12.- Effect of nose radius on the variation of hinge-moment coefficient with angle of attack for a 0.30 $\bar{c}_a$ - balance blunt-nose aileron on the tapered-wing model. δ_f, 0°; δ_a, 0°.

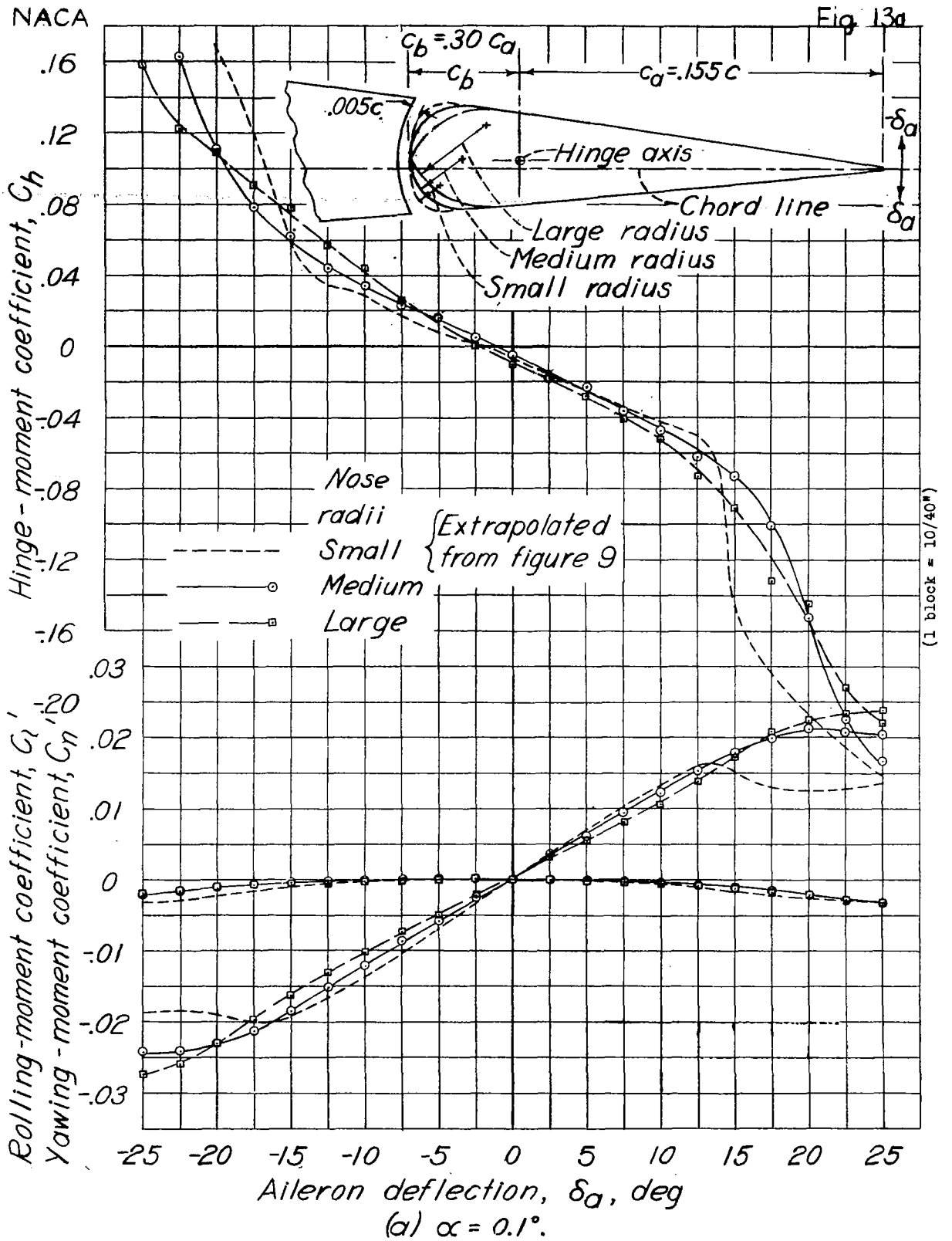

Figure 13.- Effect of nose radius on the characteristics of a $0.30\bar{c}_a$-balance blunt-nose aileron on the tapered-wing model. Gap, 0.005c; δ_f, 0°.

NACA

Fig. 13b

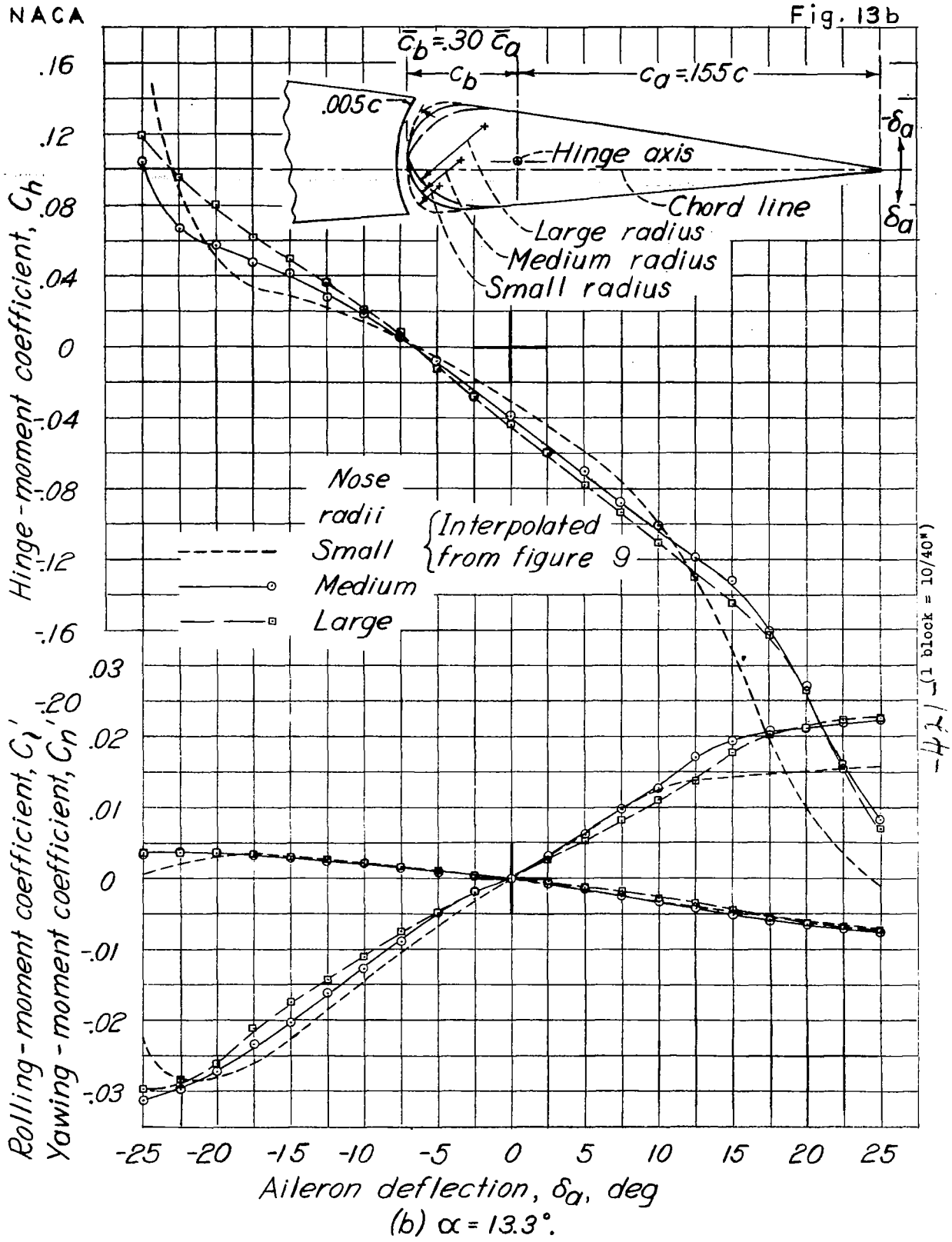

(b) $\alpha = 13.3°$.

Figure 13.- Concluded.

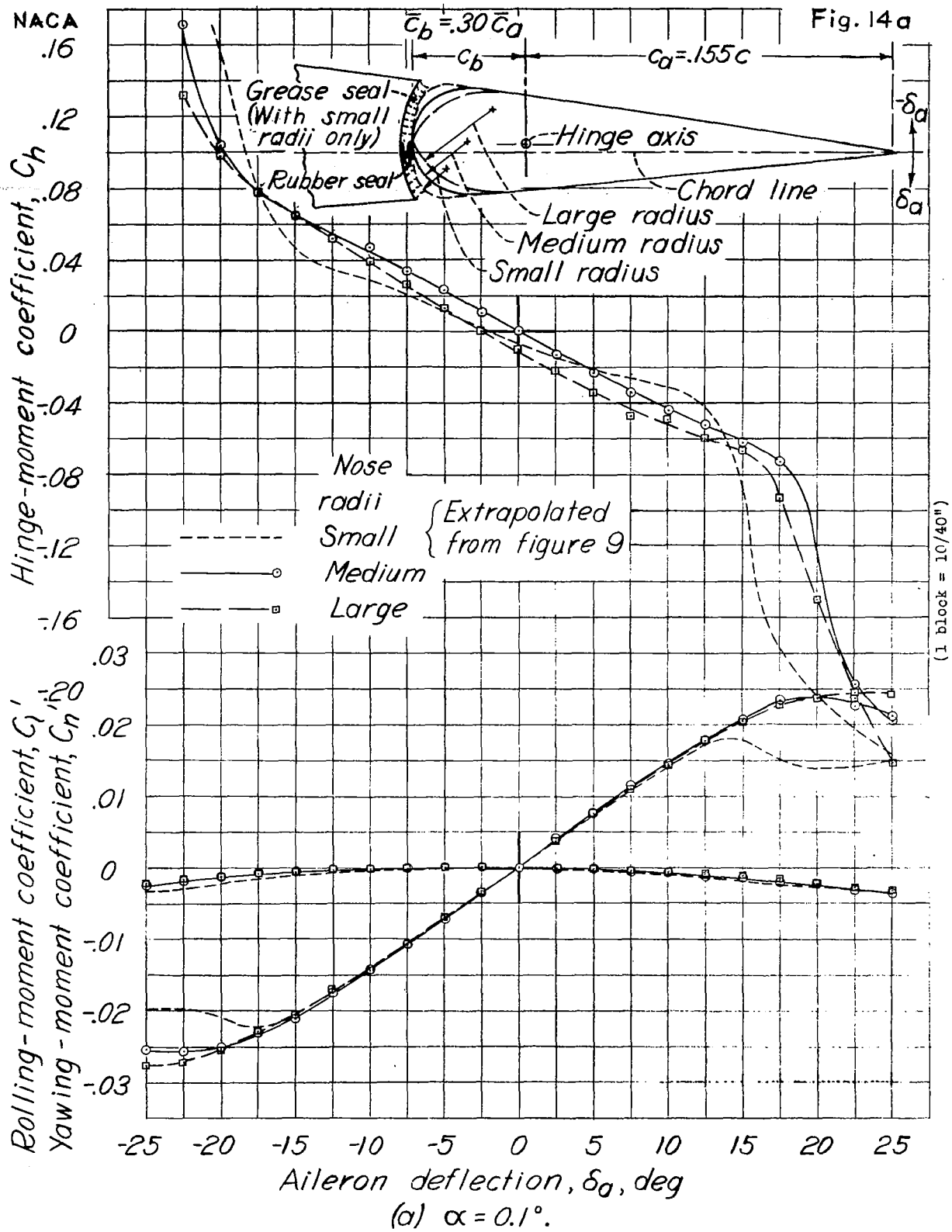

(a) $\alpha = 0.1°$.

Figure 14.- Effect of nose radius on the characteristics of a 0.30 $\bar{c}_a$ - balance blunt-nose aileron on the tapered-wing model. Gap, sealed; δ_f, 0°.

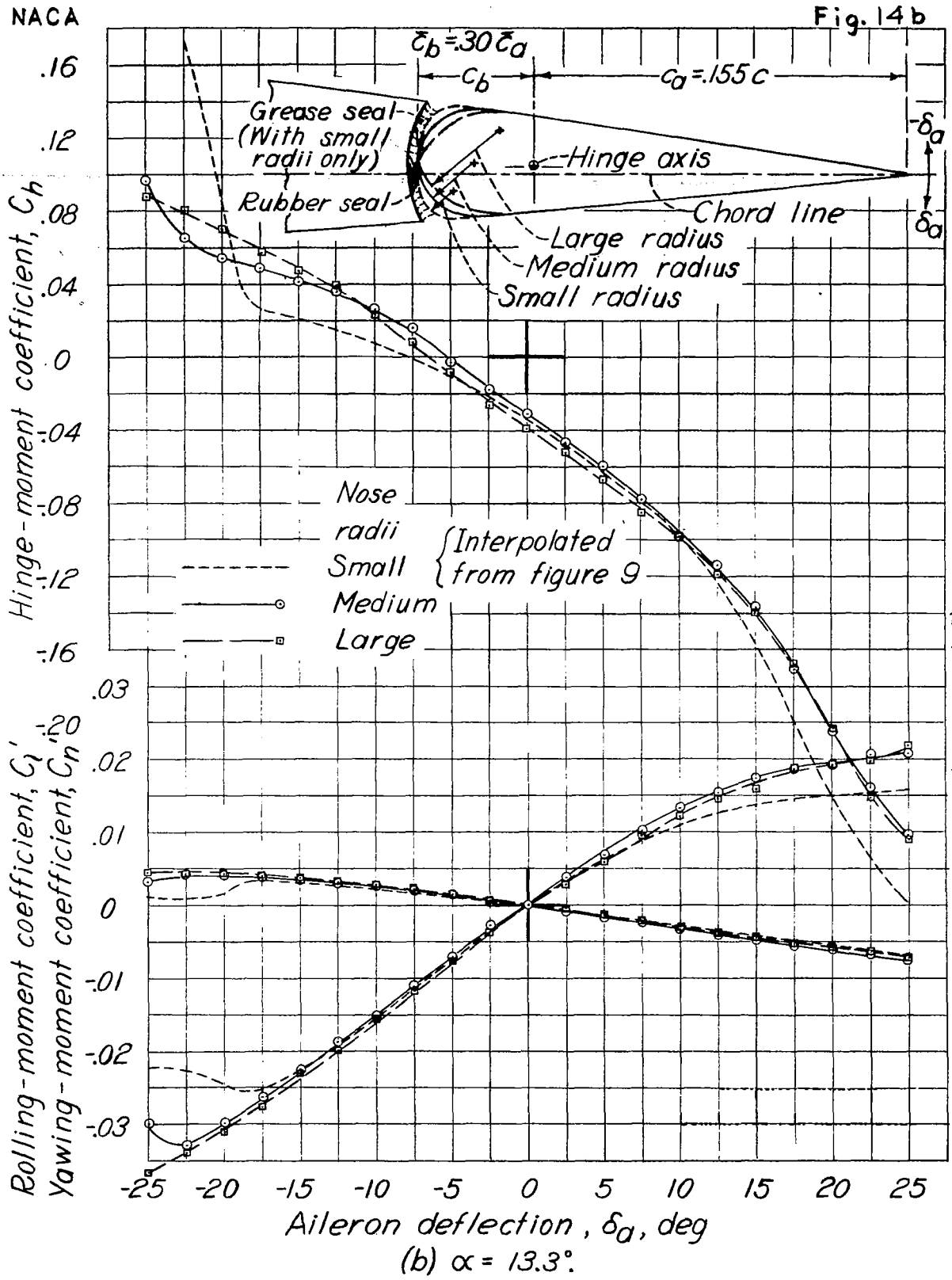

(b) $\alpha = 13.3°$.

Figure 14.- Concluded.

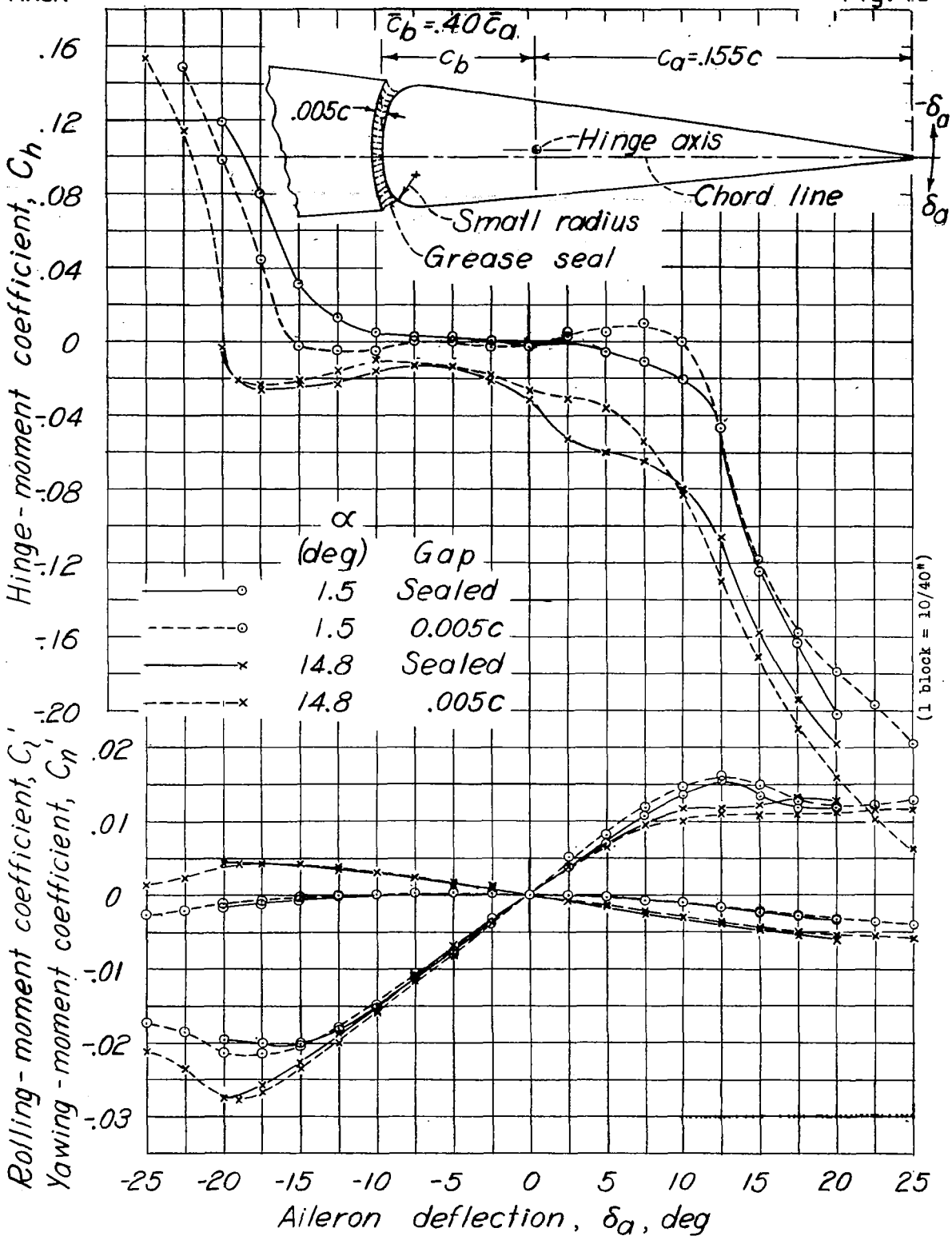

Figure 15.- Characteristics of a $0.40\bar{c}_a$-balance blunt-nose aileron on the the tapered-wing model. Hinge-axis location, mean; nose radii, small; δ_f, 0°.

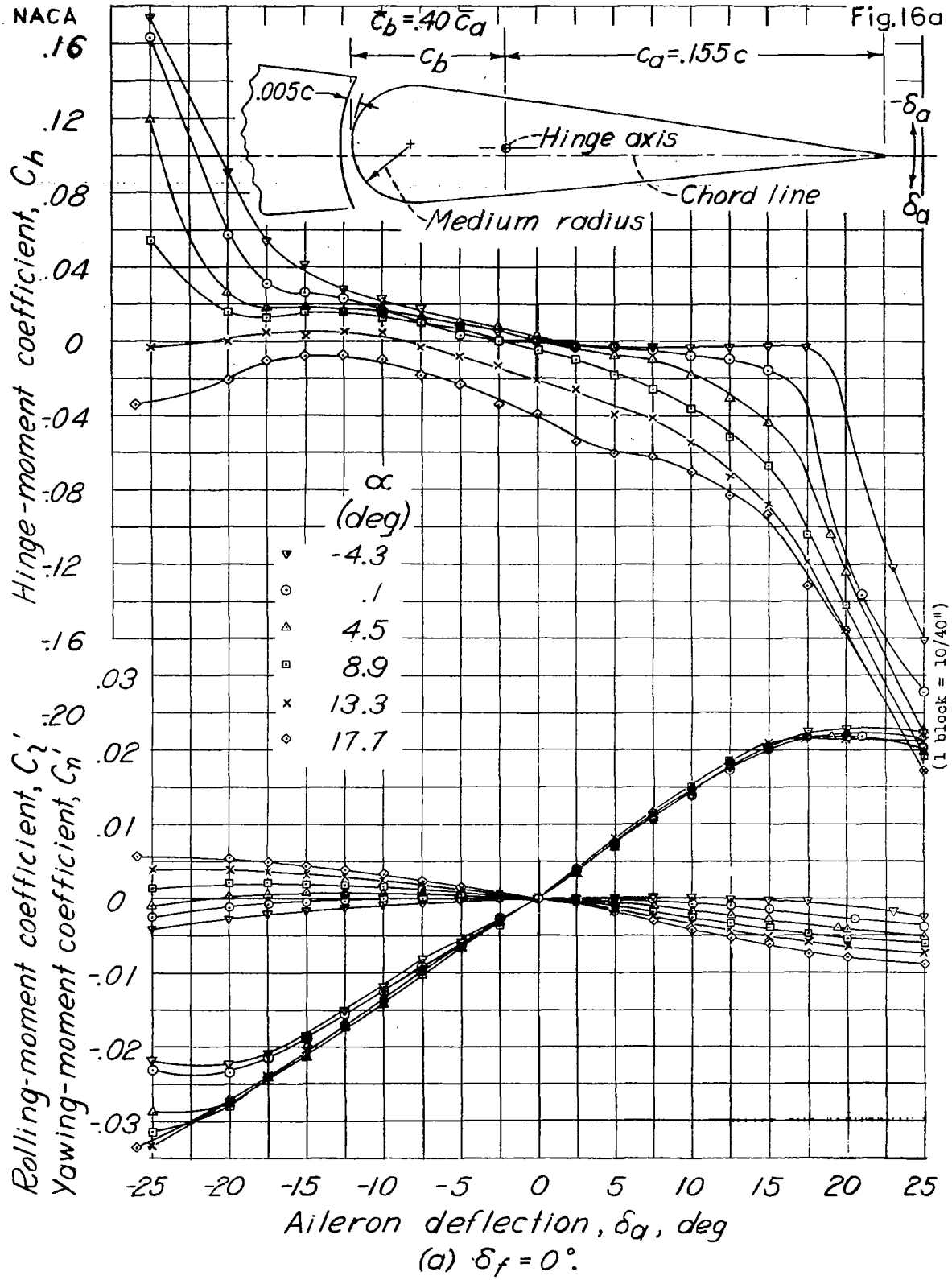

(a) $\delta_f = 0°$.

Figure 16.- Characteristics of a 0.40 $\bar{c}_a$-balance blunt-nose aileron on the tapered-wing model. Hinge-axis location, mean; nose radii, medium; gap, 0.005c.

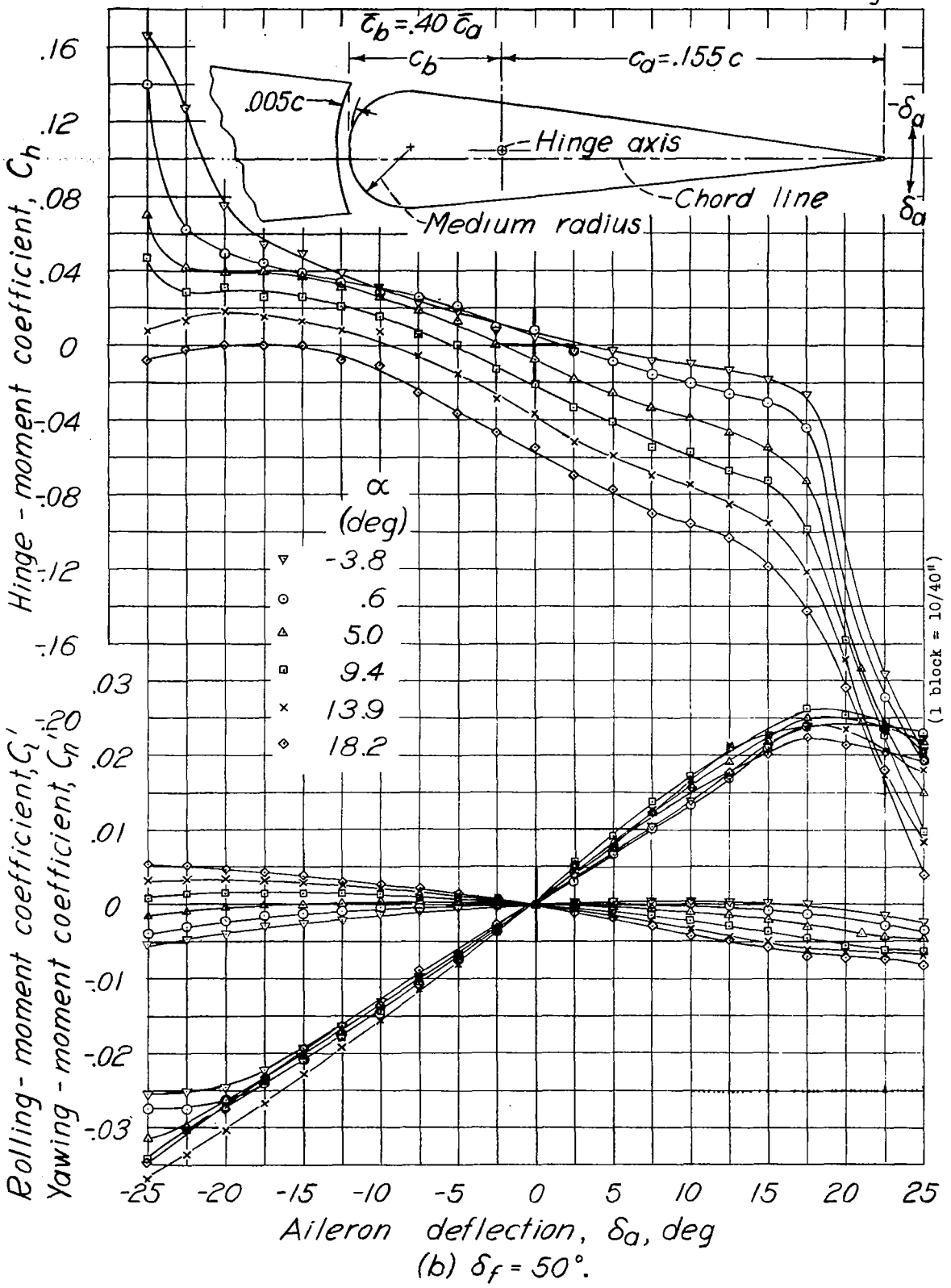

(b) $\delta_f = 50°$.

Figure 16.- Concluded.

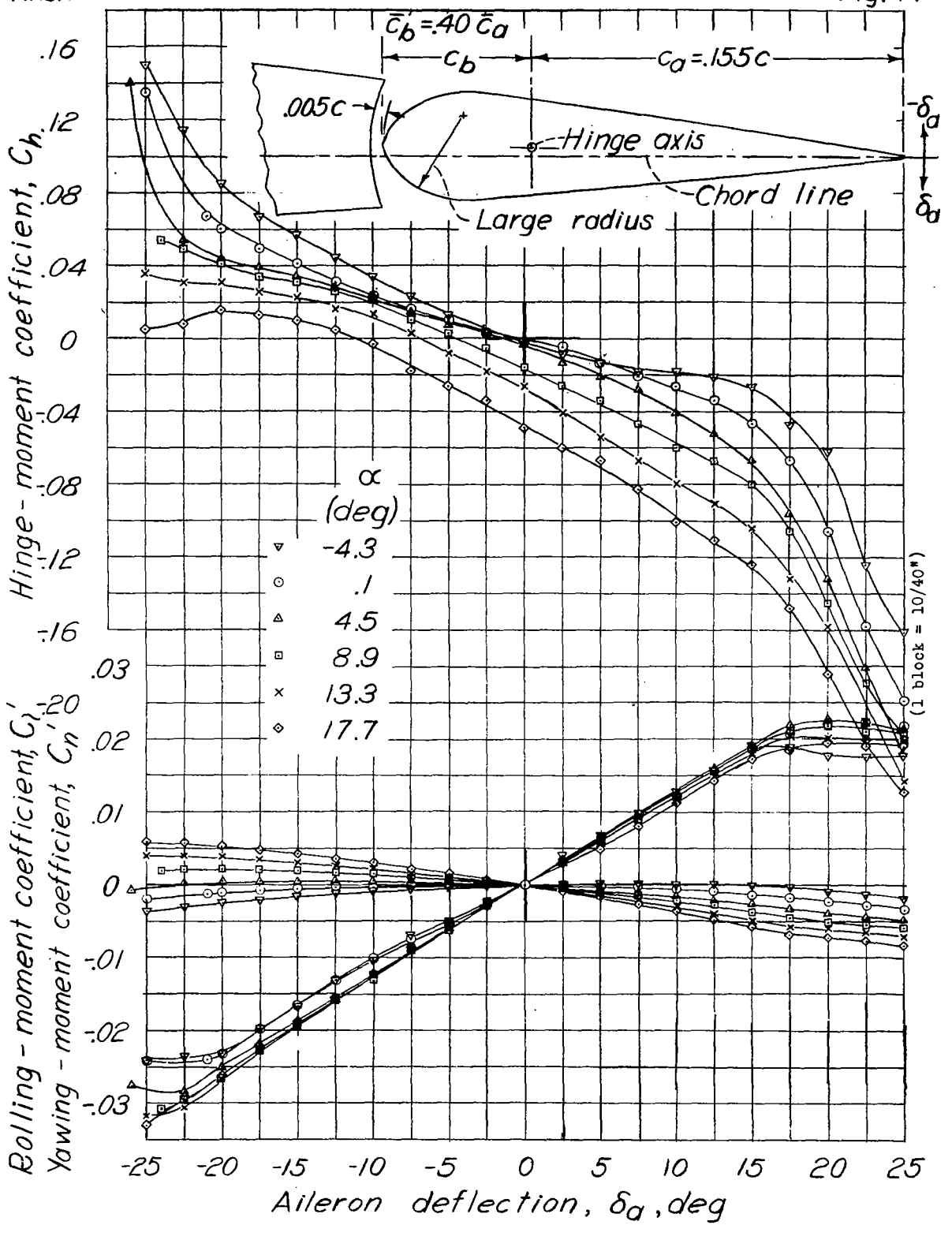

Figure 17.- Characteristics of a $0.40\bar{c}_a$-balance blunt-nose aileron on the tapered-wing model. Hinge-axis location, mean; nose radii, large; gap, 0.005c; δ_f, 0°.

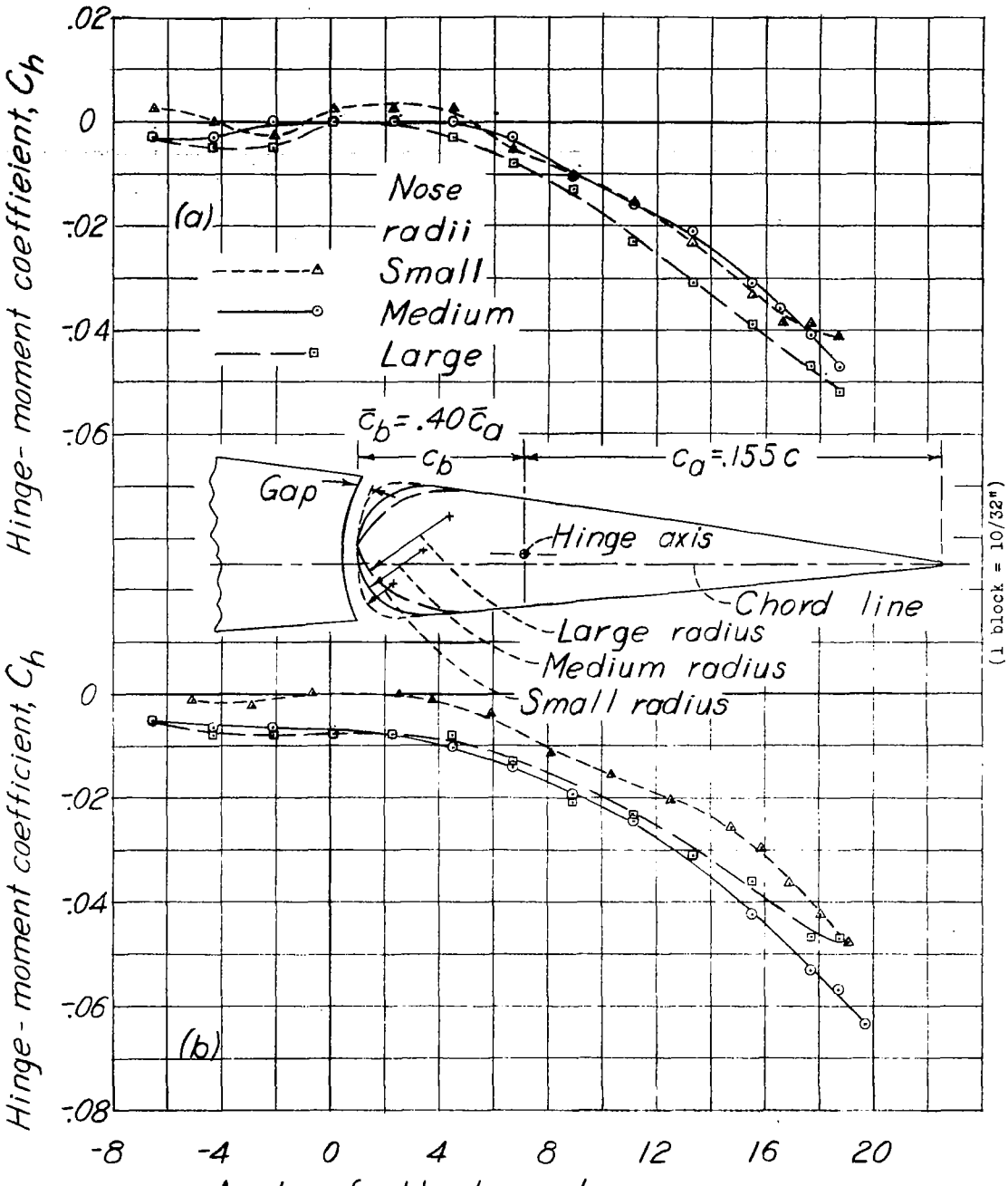

(a) Gap, 0.005c.
(b) Gap, sealed.

Figure 18.- Effect of nose radius on the variation of hinge-moment coefficient with angle of attack for a $0.40\bar{c}_a$ balance blunt-nose aileron on the tapered-wing model. Hinge-axis location, mean; δ_f, 0°; δ_a, 0°.

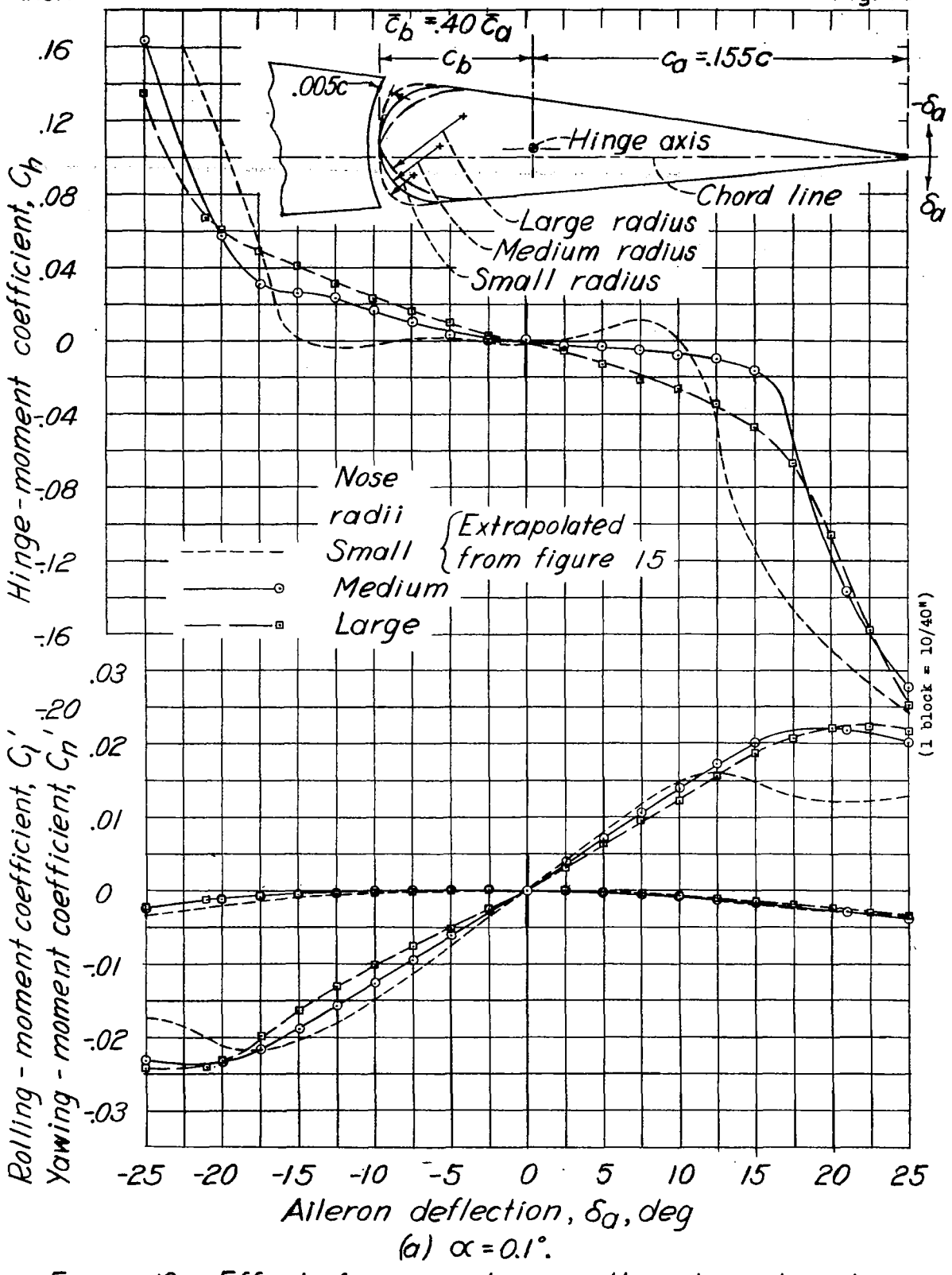

(a) $\alpha = 0.1°$.

Figure 19.- Effect of nose radius on the characteristics of a $0.40\,\bar{c}_a$-balance blunt-nose aileron on the tapered-wing model. Hinge-axis location, mean; gap, 0.005c; δ_f, 0°.

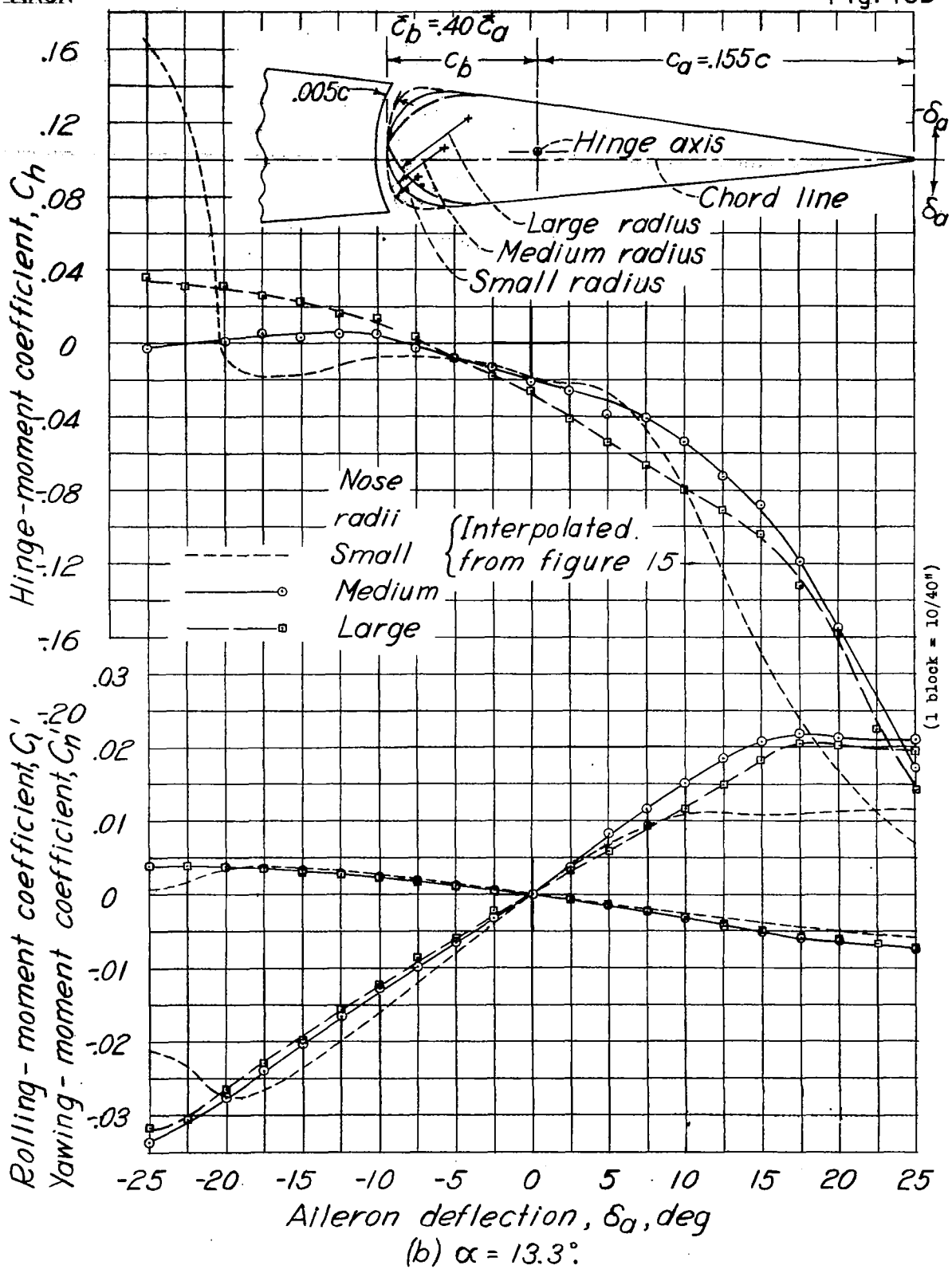

(b) $\alpha = 13.3°$.

Figure 19.- Concluded.

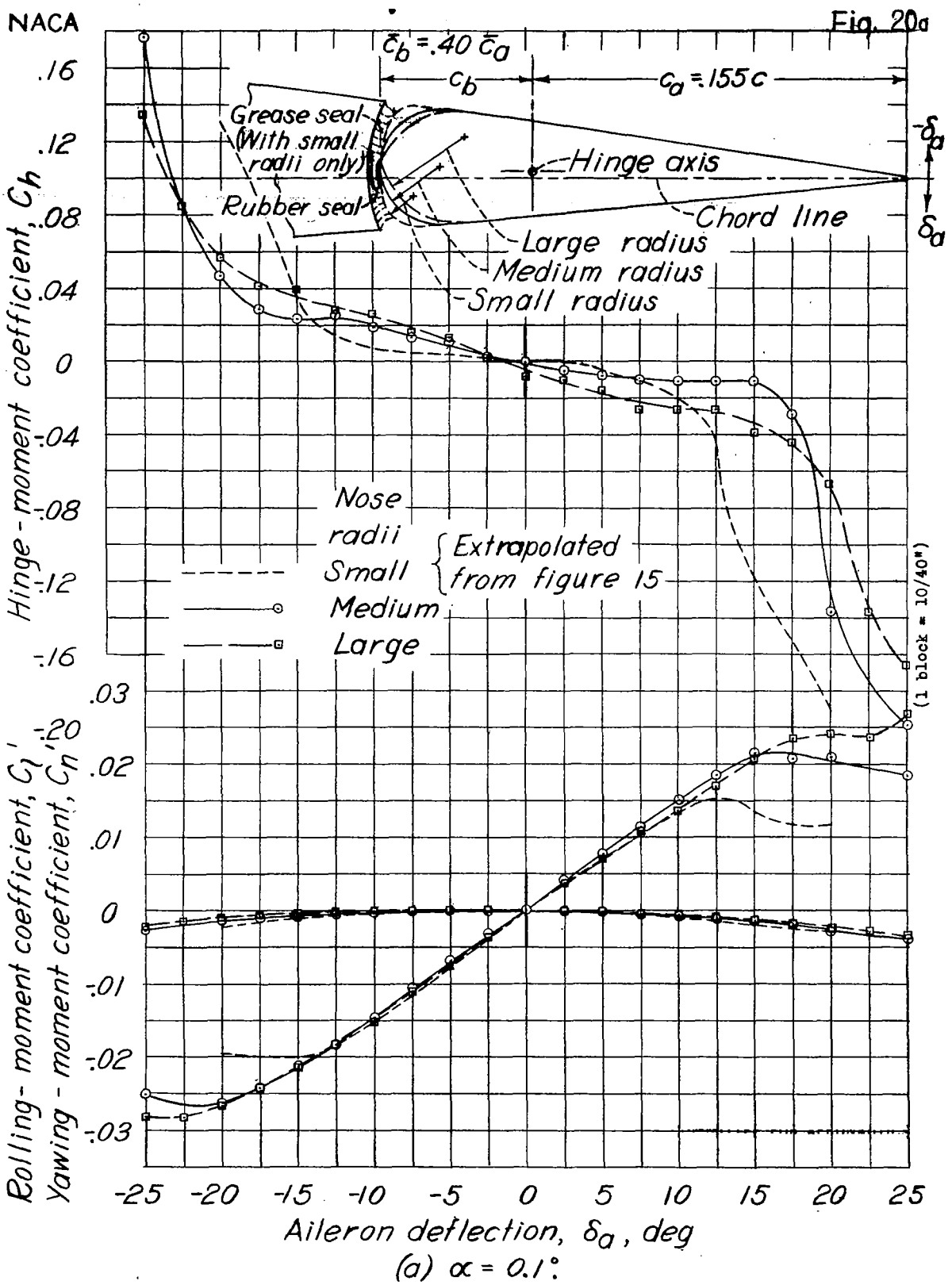

(a) $\alpha = 0.1°$.

Figure 20.- Effect of nose radius on the characteristics of a $0.40\,\bar{c}_a$-balance blunt-nose aileron on the tapered-wing model. Hinge-axis location, mean; gap, sealed; δ_f, 0°.

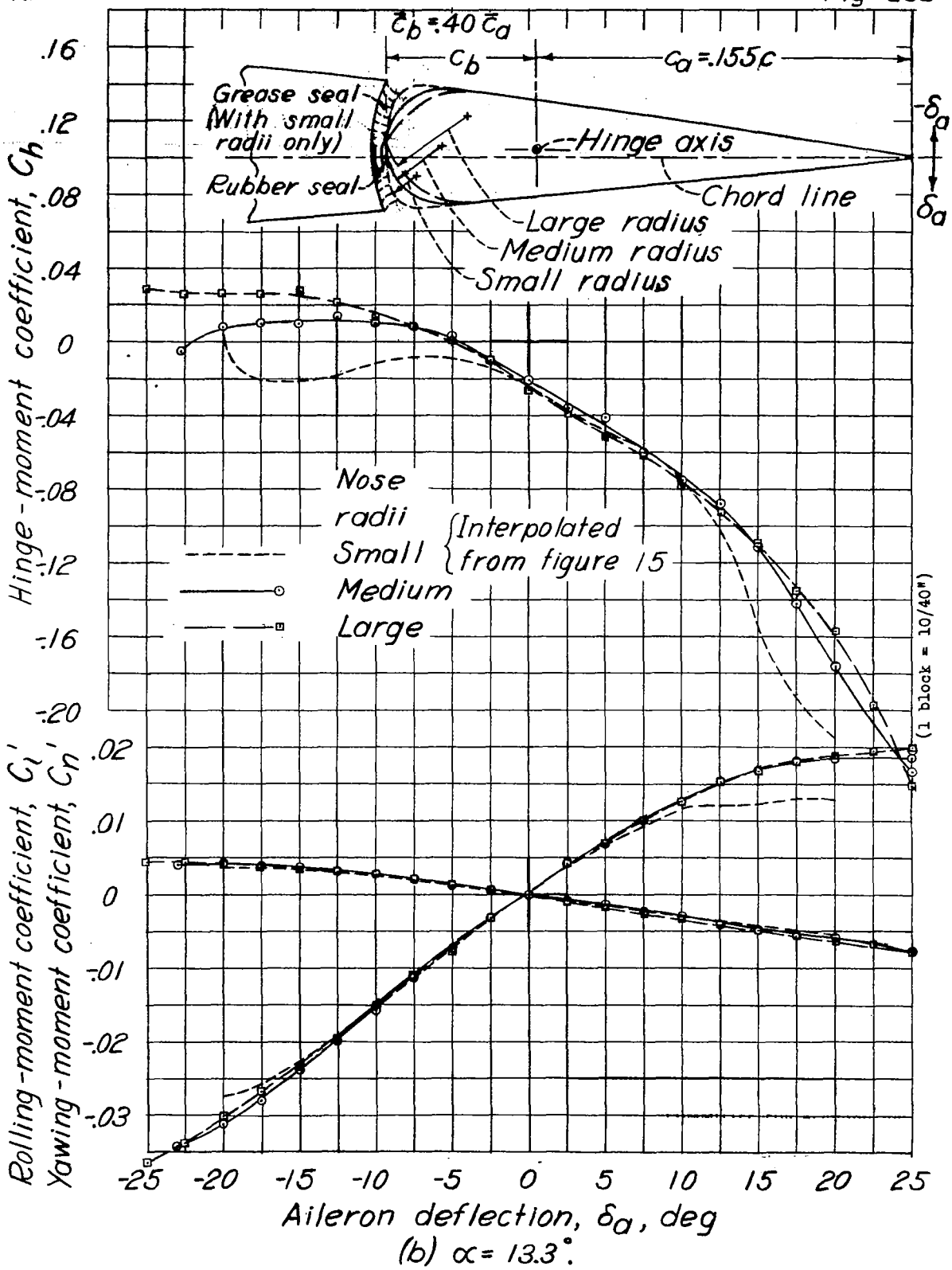

(b) $\alpha = 13.3°$.

Figure 20.- Concluded.

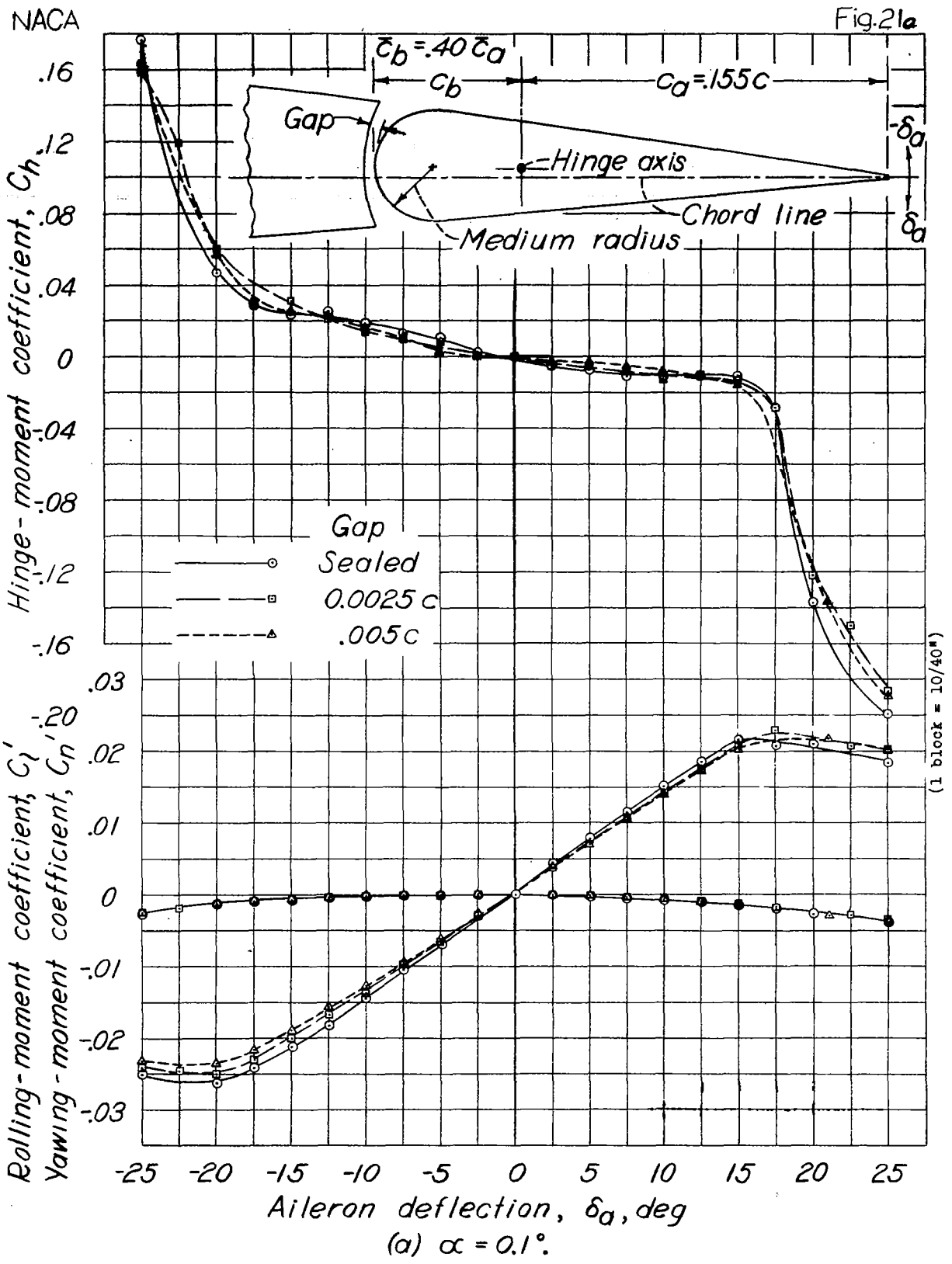

(a) $\alpha = 0.1°$.

Figure 21.- Effect of gap on the characteristics of a $0.40\,\bar{c}_a$ - balance blunt-nose aileron on the tapered- wing model. Hinge- axis location, mean; nose radii, medium; δ_f, 0°.

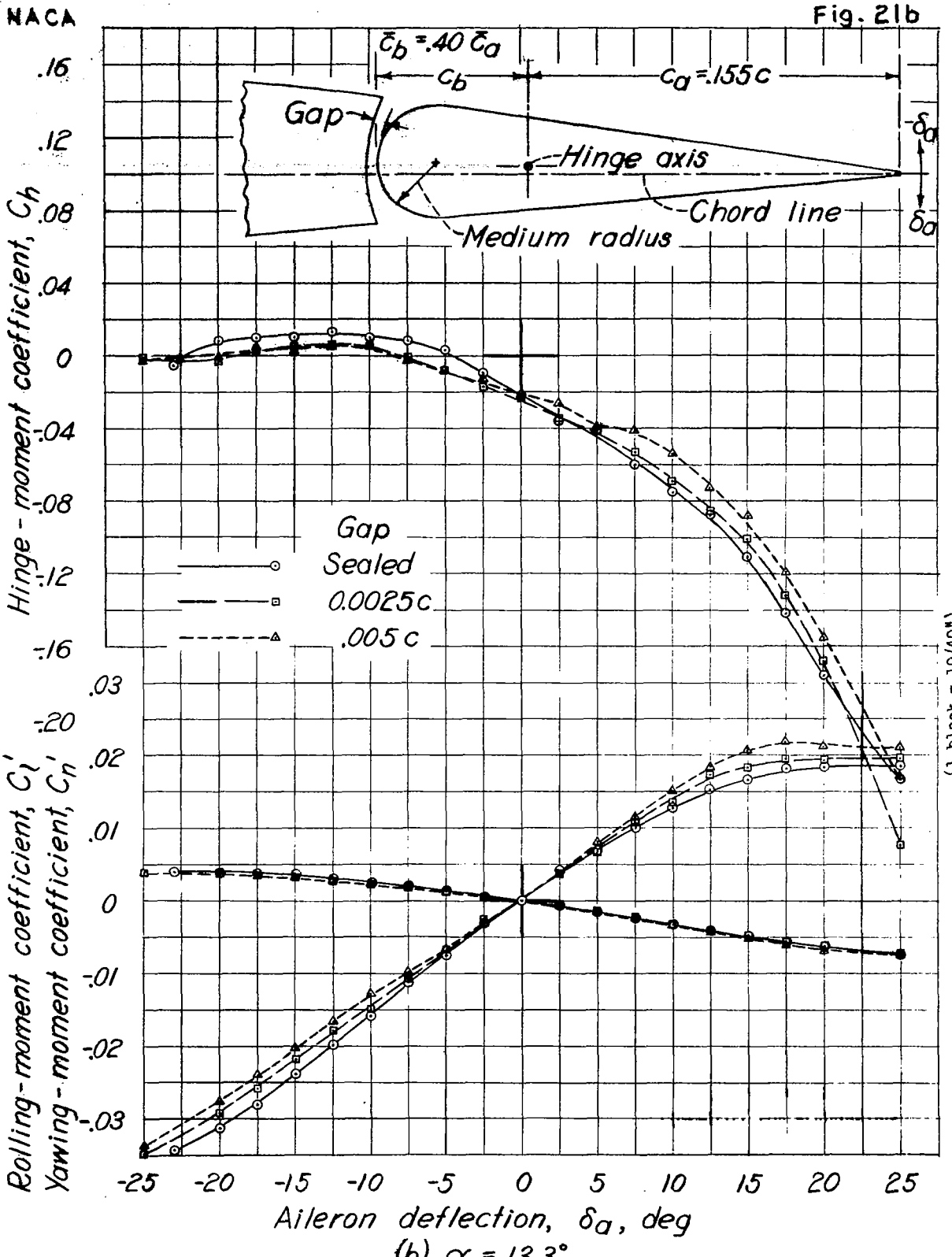

(b) $\alpha = 13.3°$.

Figure 21.- Concluded.

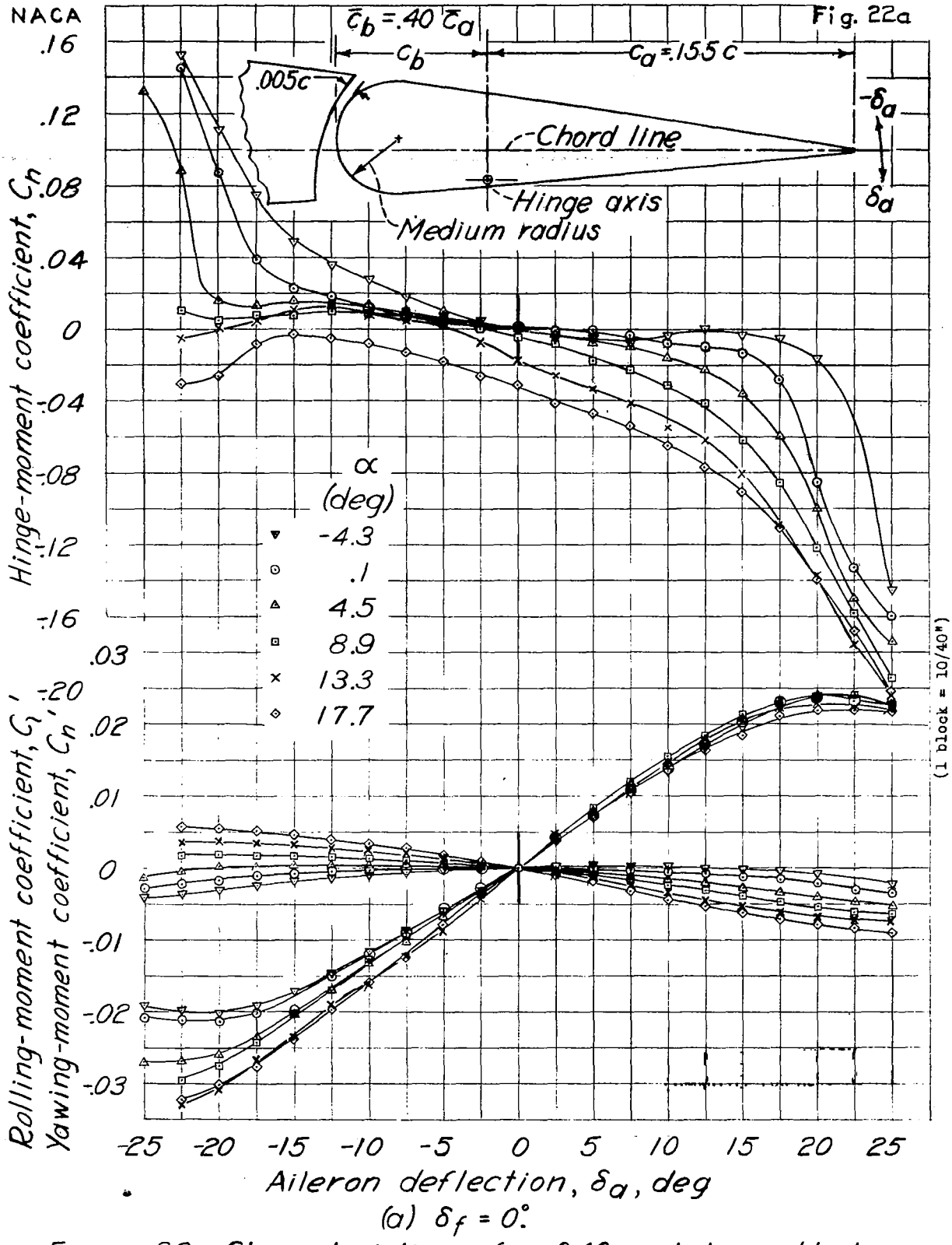

Figure 22.- Characteristics of a $0.40\,\bar{c}_a$ - balance blunt-nose aileron on the tapered-wing model. Hinge-axis location, low; nose radii, medium; gap, 0.005c.

NACA

Fig. 22b

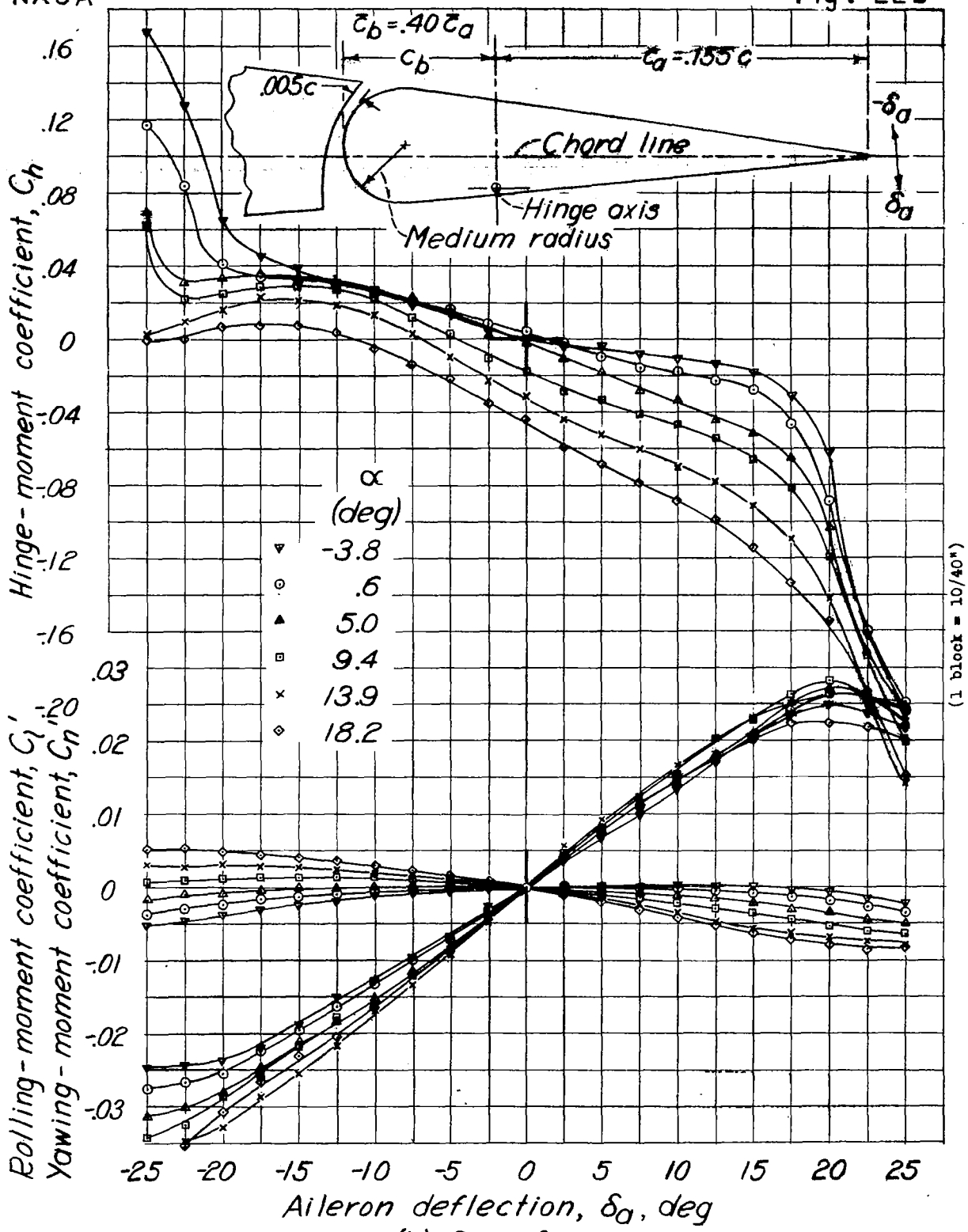

(b) $\delta_f = 50°$.

Figure 22.- Concluded.

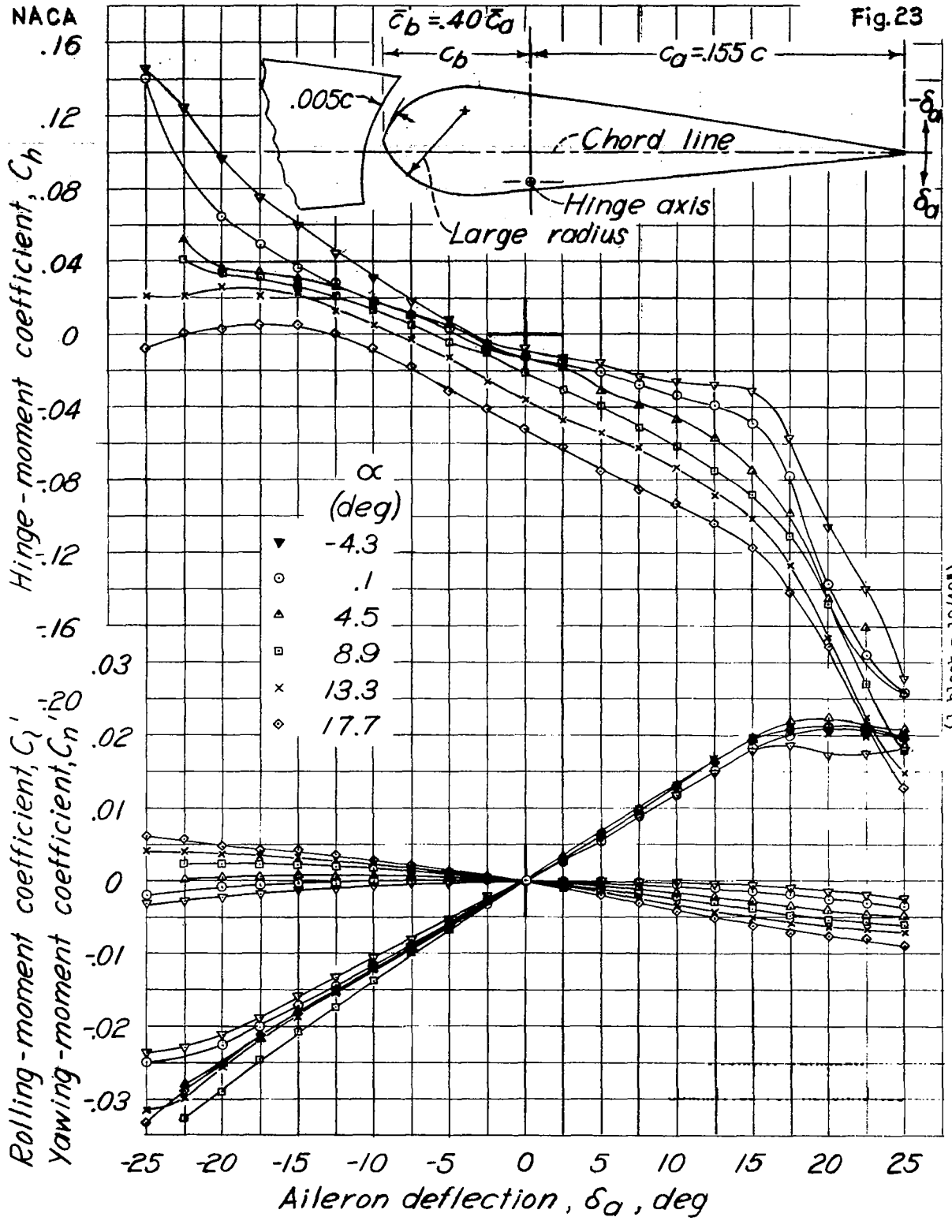

Figure 23.- Characteristics of a 0.40 $\bar{c}_a$-balance blunt-nose aileron on the tapered-wing model. Hinge-axis location, low; nose radii, large; gap, 0.005 c; δ_f, 0°.

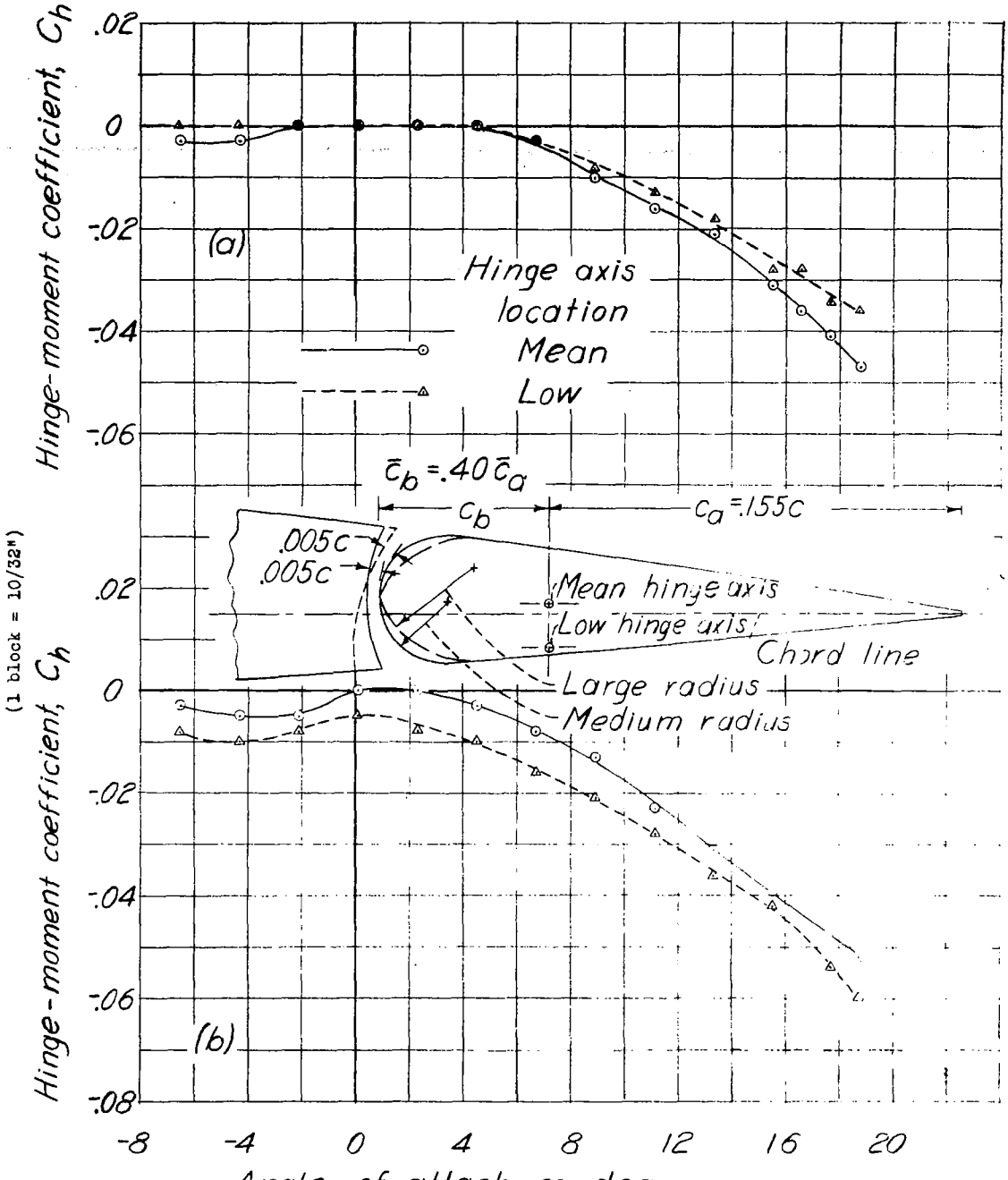

(a) Nose radii, medium.
(b) Nose radii, large.

Figure 24.- Effect of hinge-axis location on the variation of hinge-moment coefficient with angle of attack for a $0.40\bar{c}_a$-balance blunt-nose aileron on the tapered-wing model. Gap, 0.005c; δ_f, 0°; δ_a, 0°.

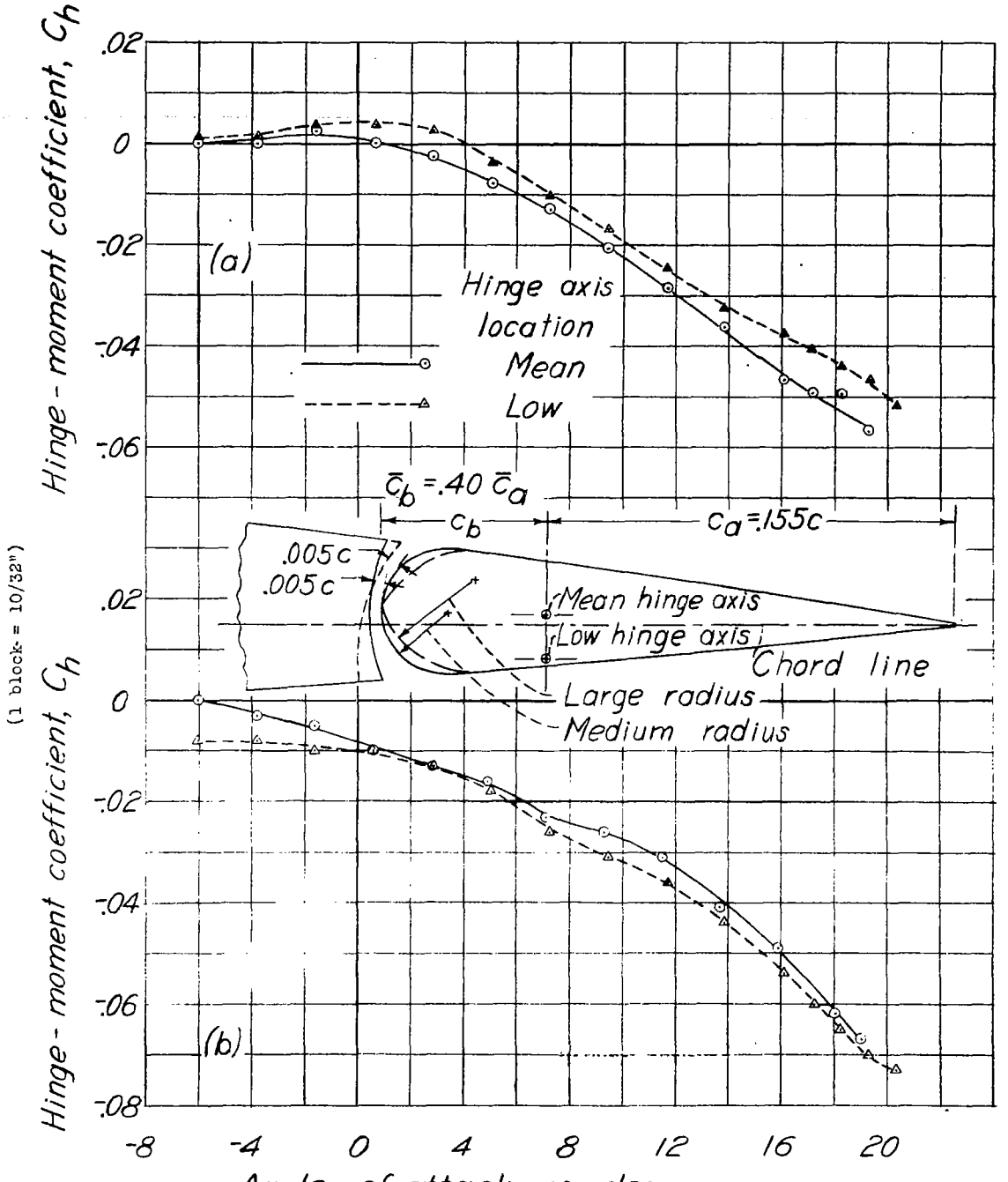

(a) Nose radii, medium.
(b) Nose radii, large.

Figure 25.- Effect of hinge-axis location on the variation of hinge-moment coefficient with angle of attack for a $0.40\bar{c}_a$-balance blunt-nose aileron on the tapered-wing model. Gap, 0.005c; δ_f, 50°; δ_a, 0°.

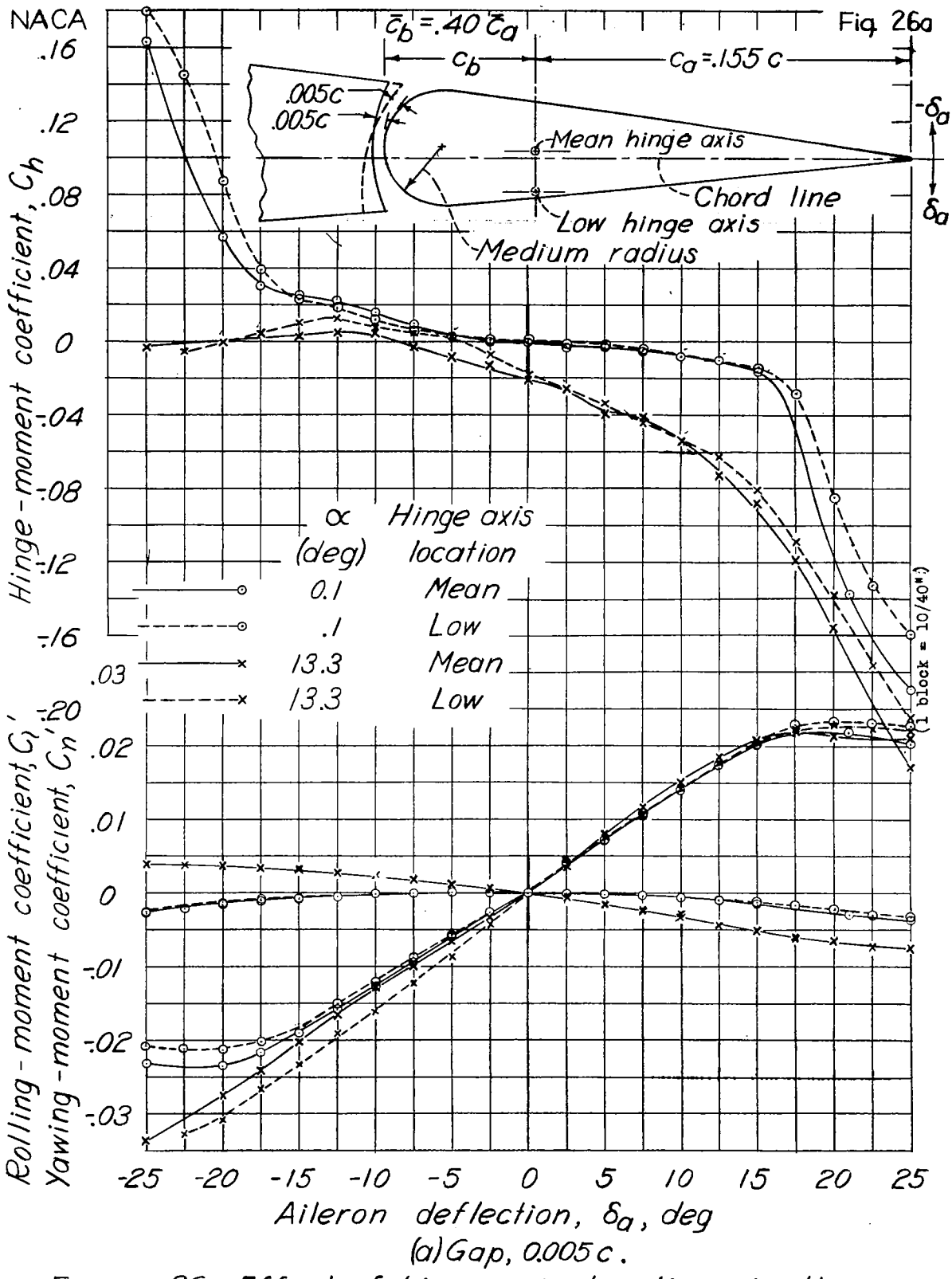

(a) Gap, 0.005 c.

Figure 26.- Effect of hinge-axis location on the characteristics of a 0.40 $\bar{c}_a$-balance blunt-nose aileron on the tapered-wing model. Nose radii, medium; δ_f, 0°.

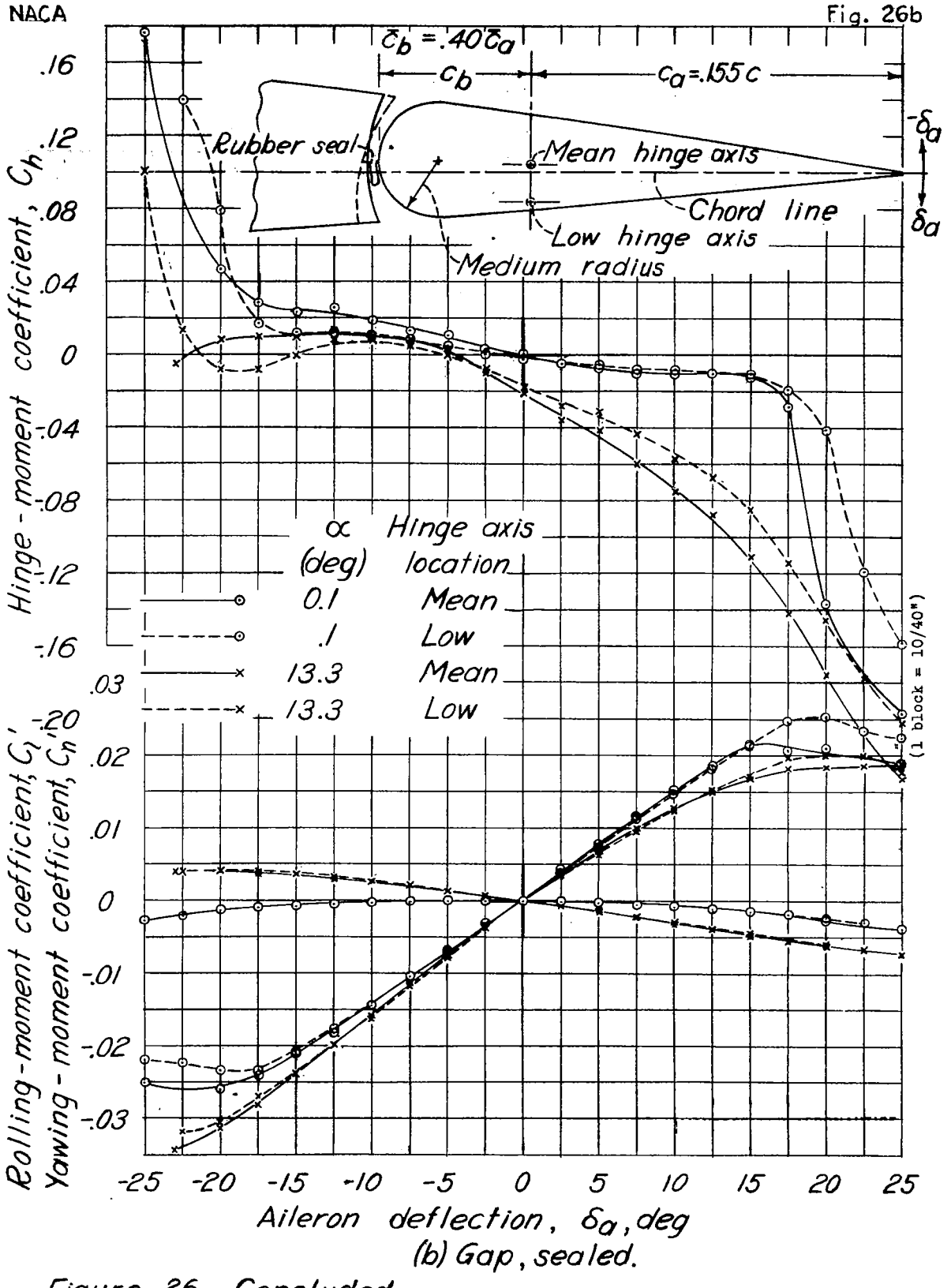

(b) Gap, sealed.

Figure 26.- Concluded.

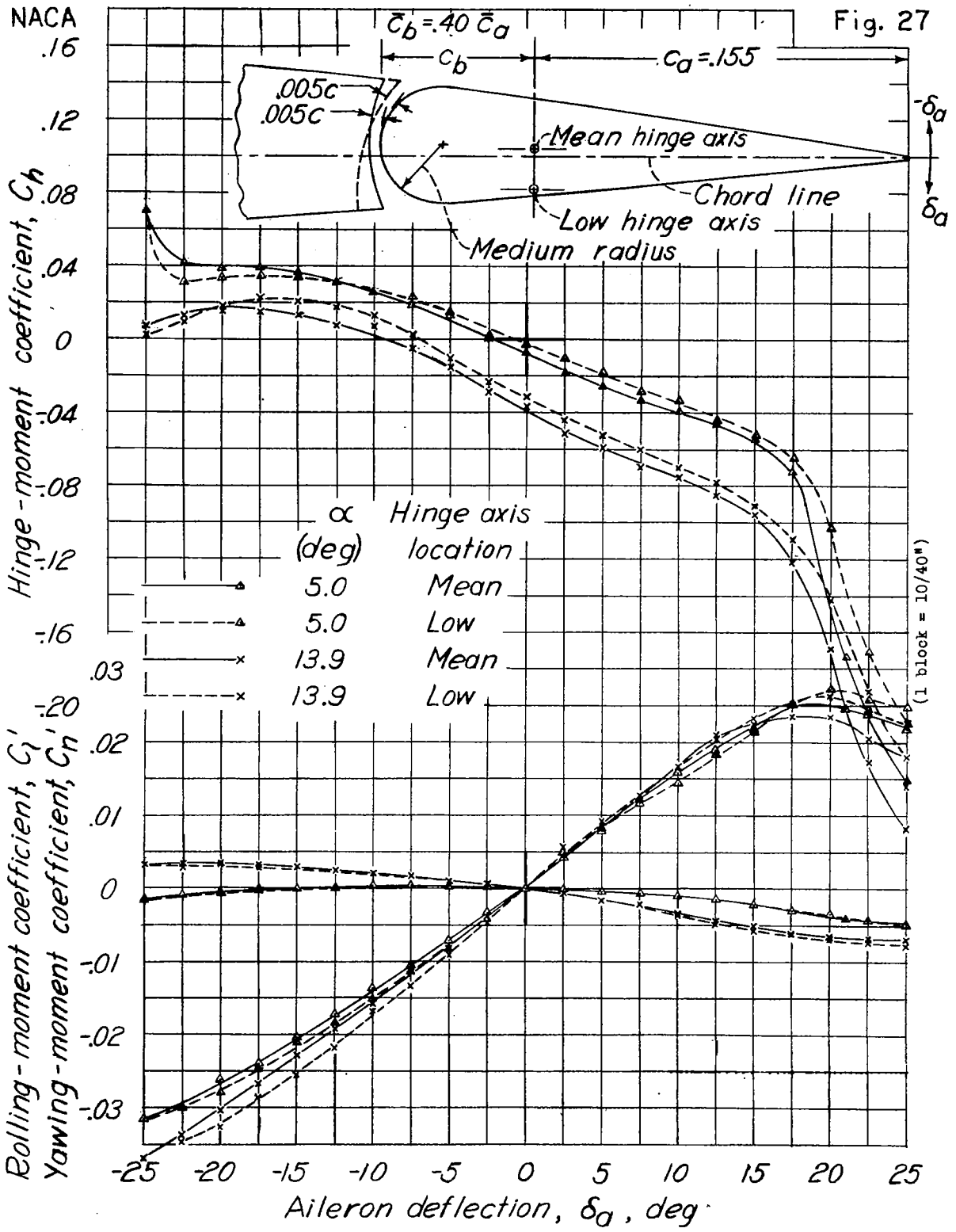

Figure 27.- Effect of hinge-axis location on the characteristics of a $0.40\bar{c}_a$-balance blunt-nose aileron on the tapered-wing model. Nose-radii, medium; gap, 0.005c; δ_f, 50°.

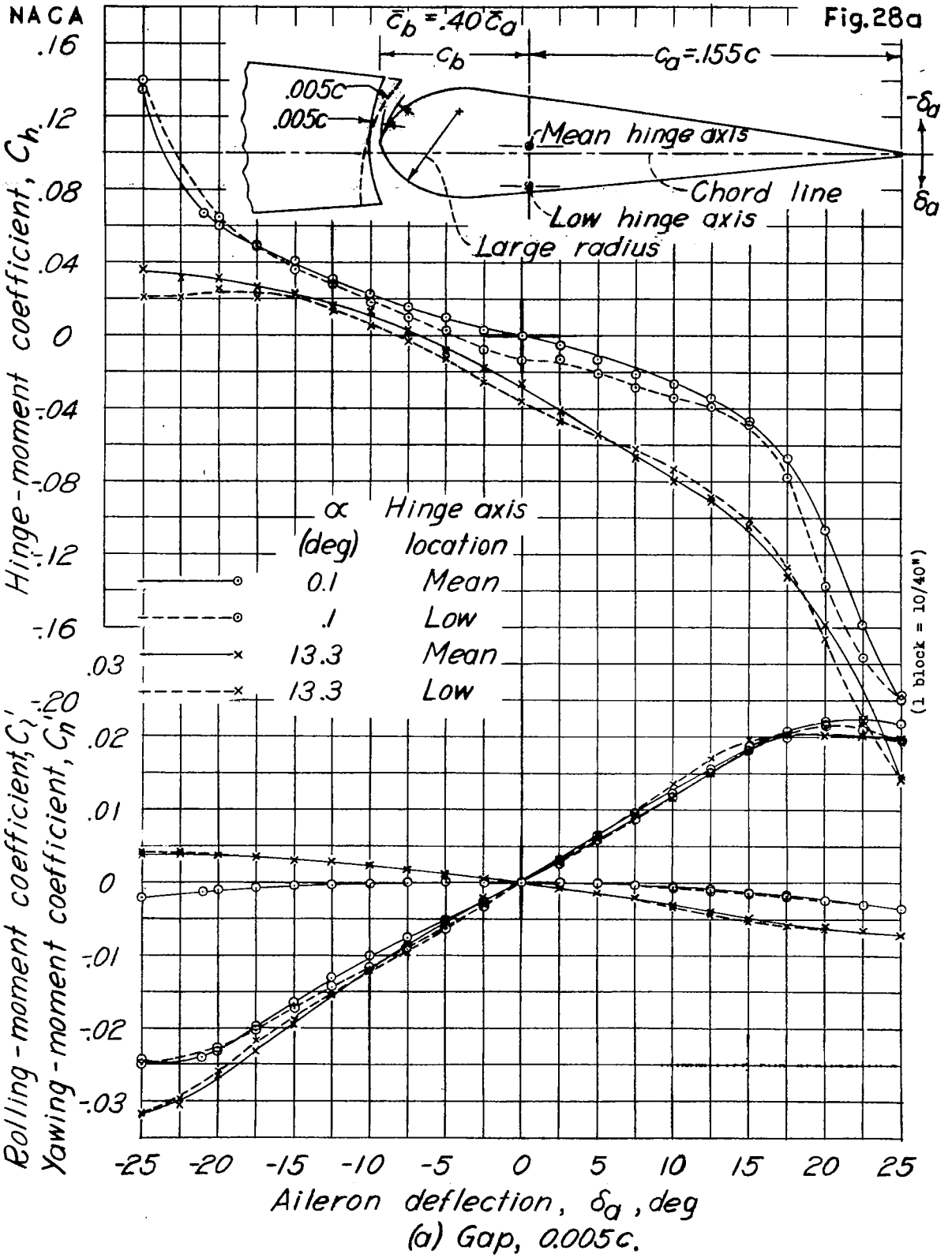

Figure 28.- Effect of hinge-axis location on the characteristics of a 0.40 $\bar{c}_a$-balance blunt-nose aileron on the tapered-wing model. Nose radii, large; δ_f, 0°.

NACA

Fig. 28b

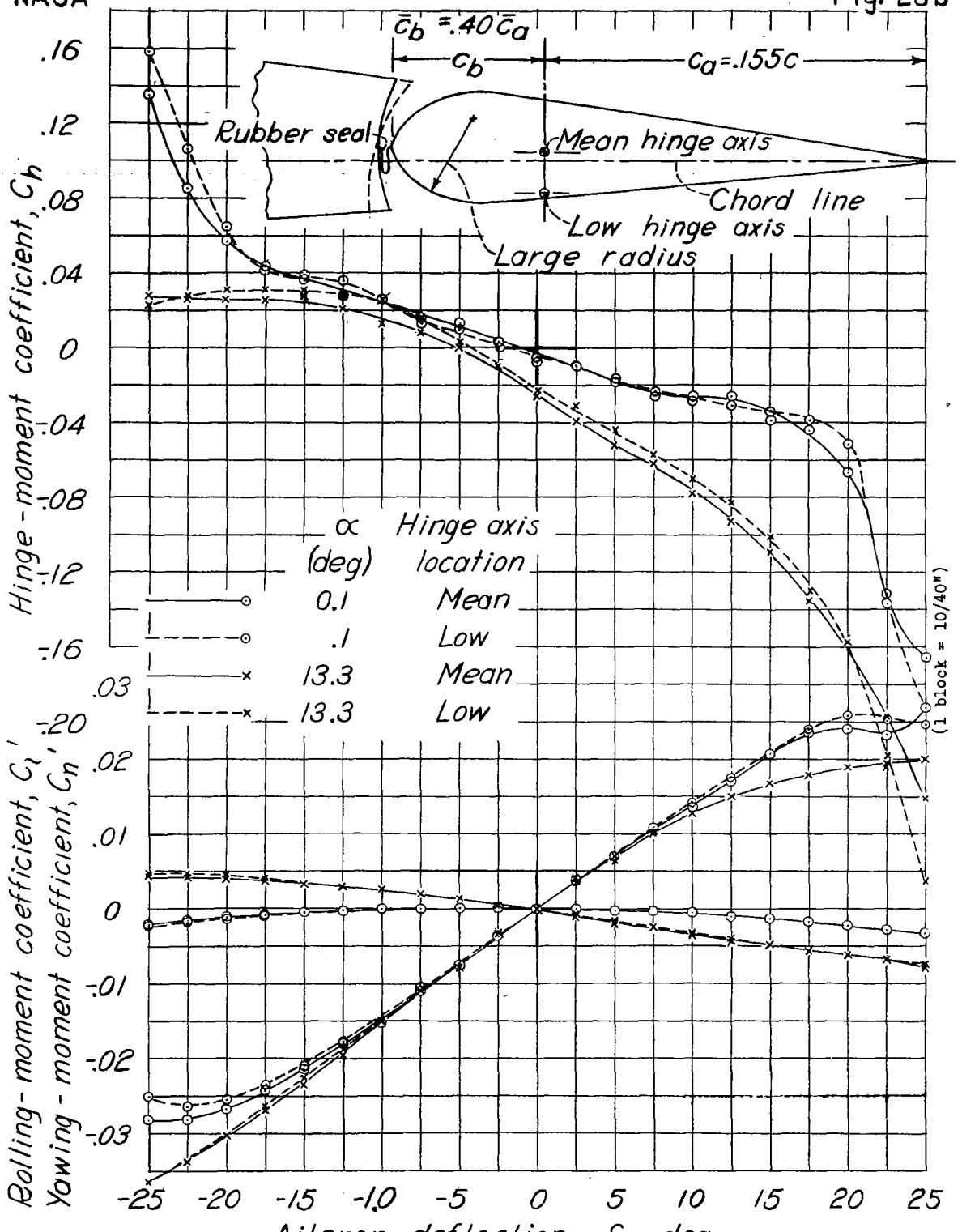

(b) Gap, sealed.

Figure 28.- Concluded.

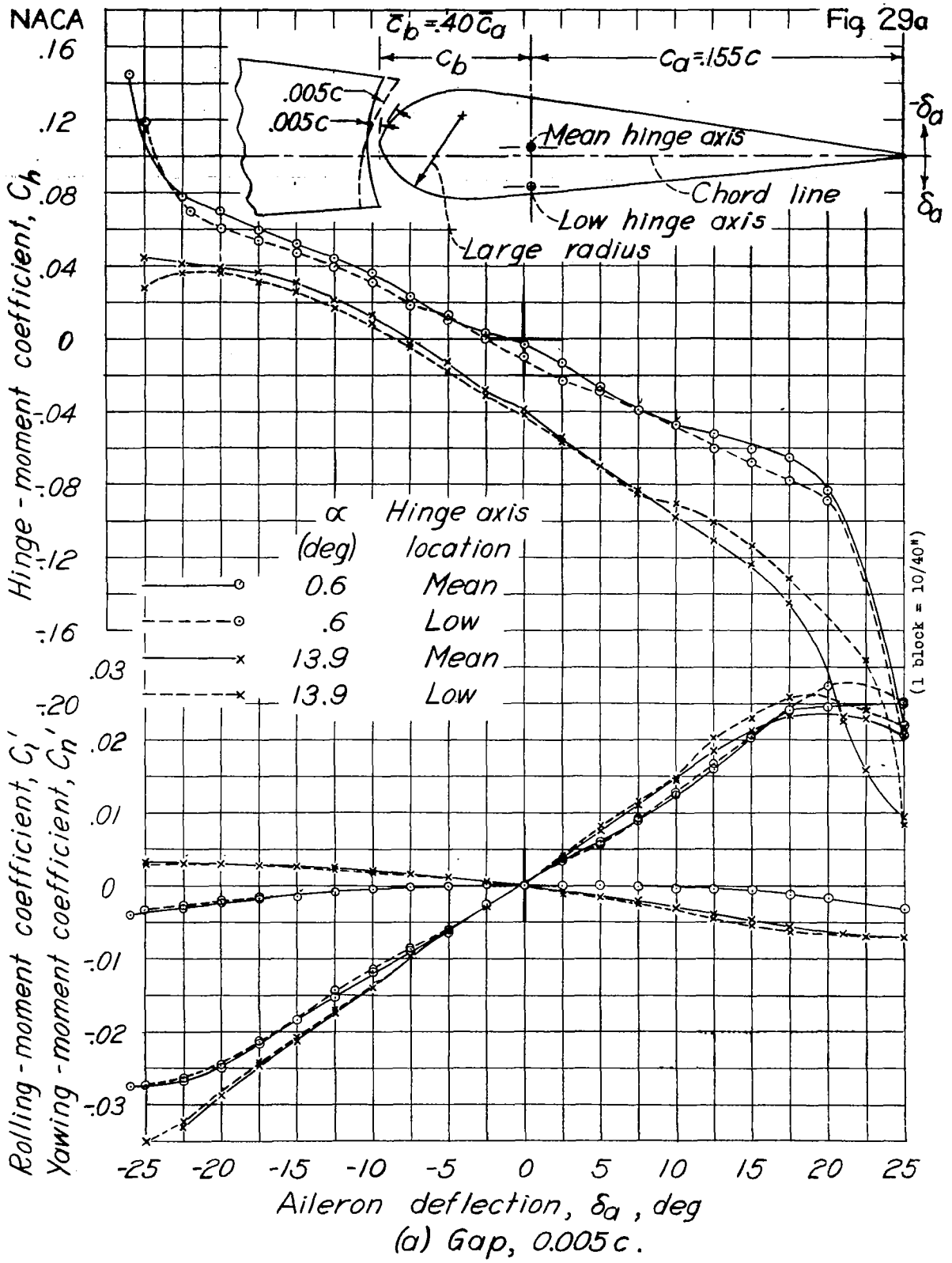

(a) Gap, 0.005 c.

Figure 29.- Effect of hinge-axis location on the characteristics of a 0.40 $\bar{c}_a$-balance blunt-nose aileron on the tapered-wing model. Nose radii, large; δ_f, 50°.

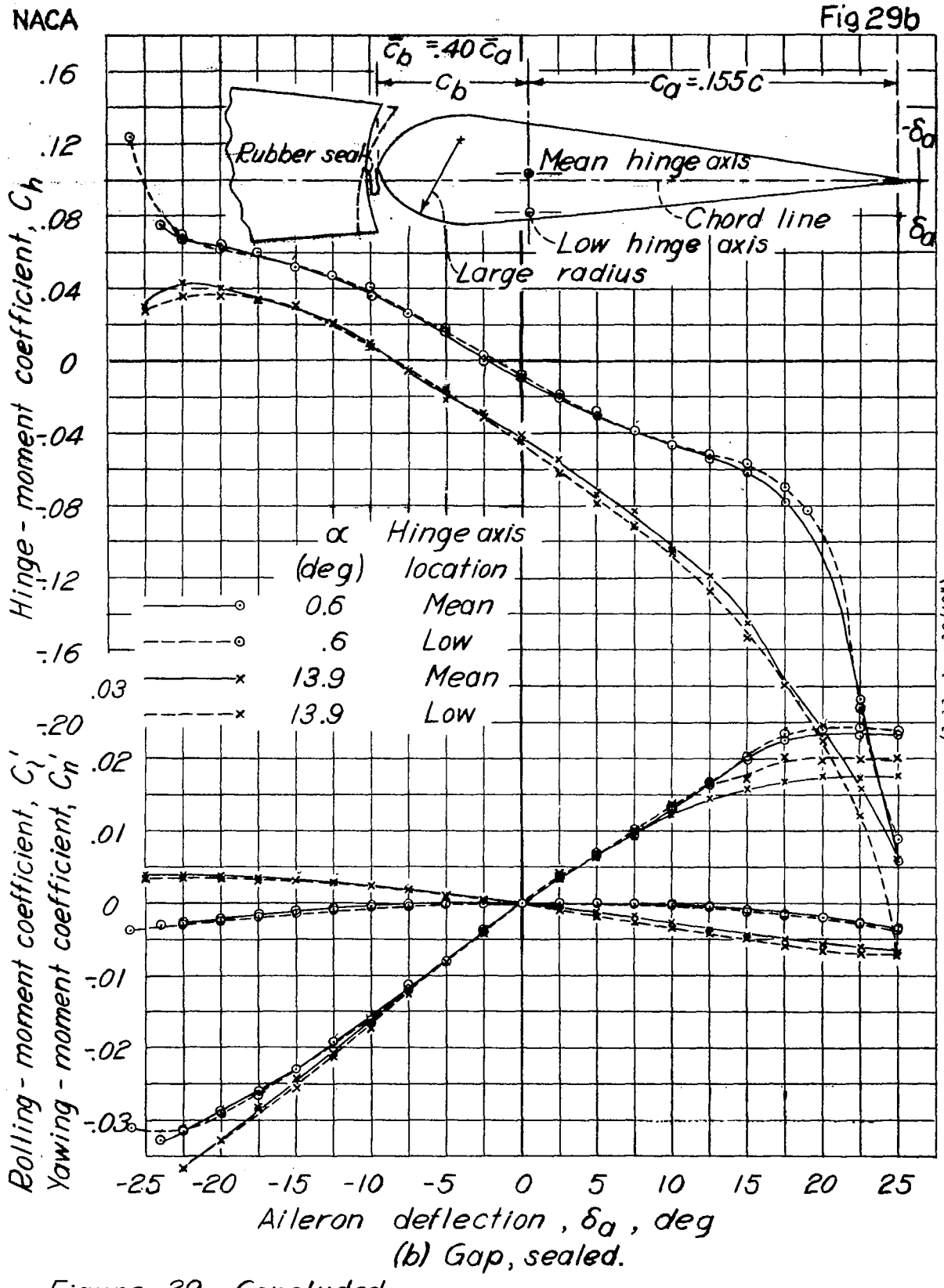

(b) Gap, sealed.

Figure 29.- Concluded.

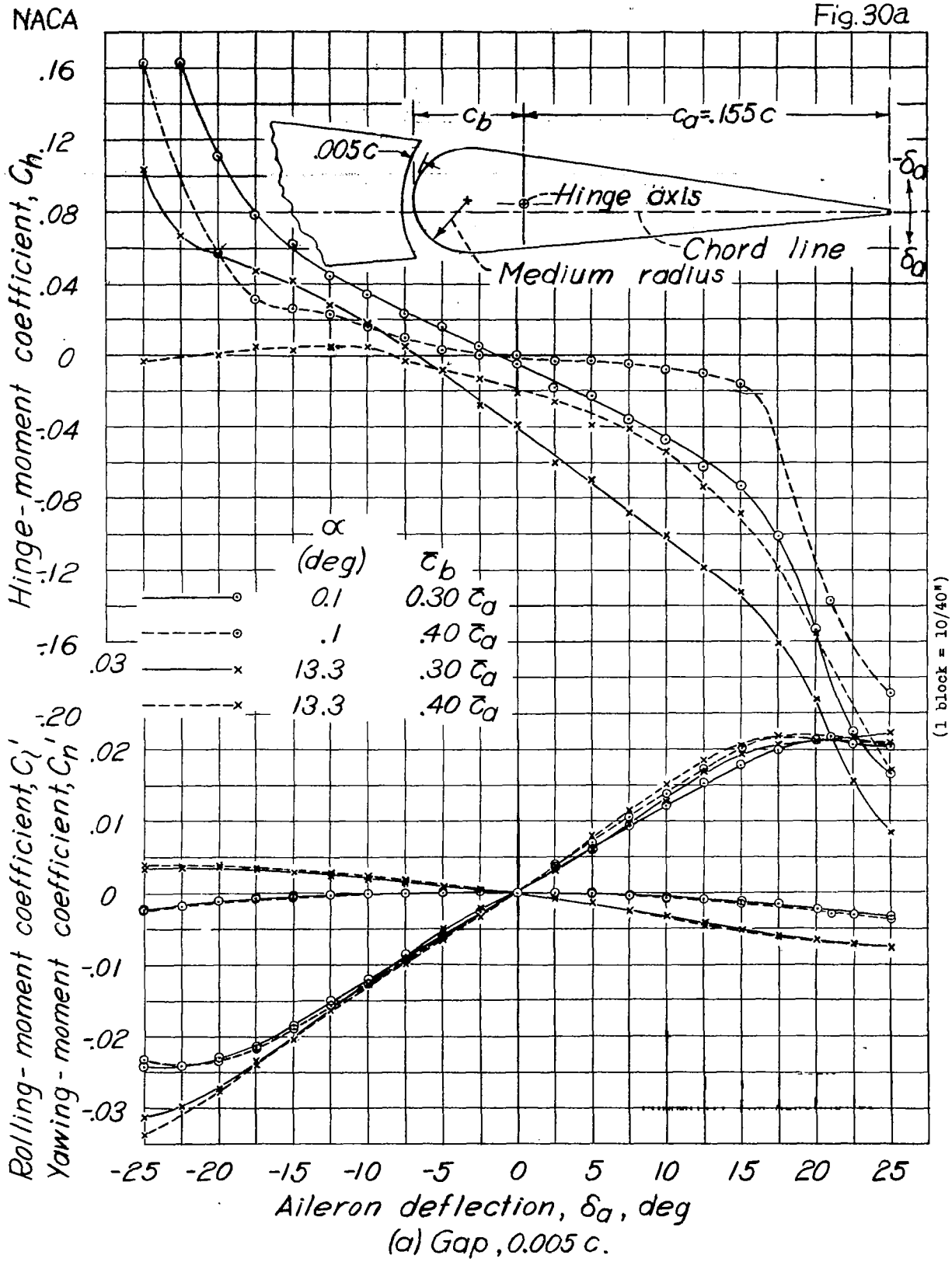

(a) Gap, 0.005 c.

Figure 30.- Effect of balance chord on the characteristics of blunt-nose ailerons on the tapered-wing model. Hinge-axis location, mean; nose radii, medium; δ_f, 0°.

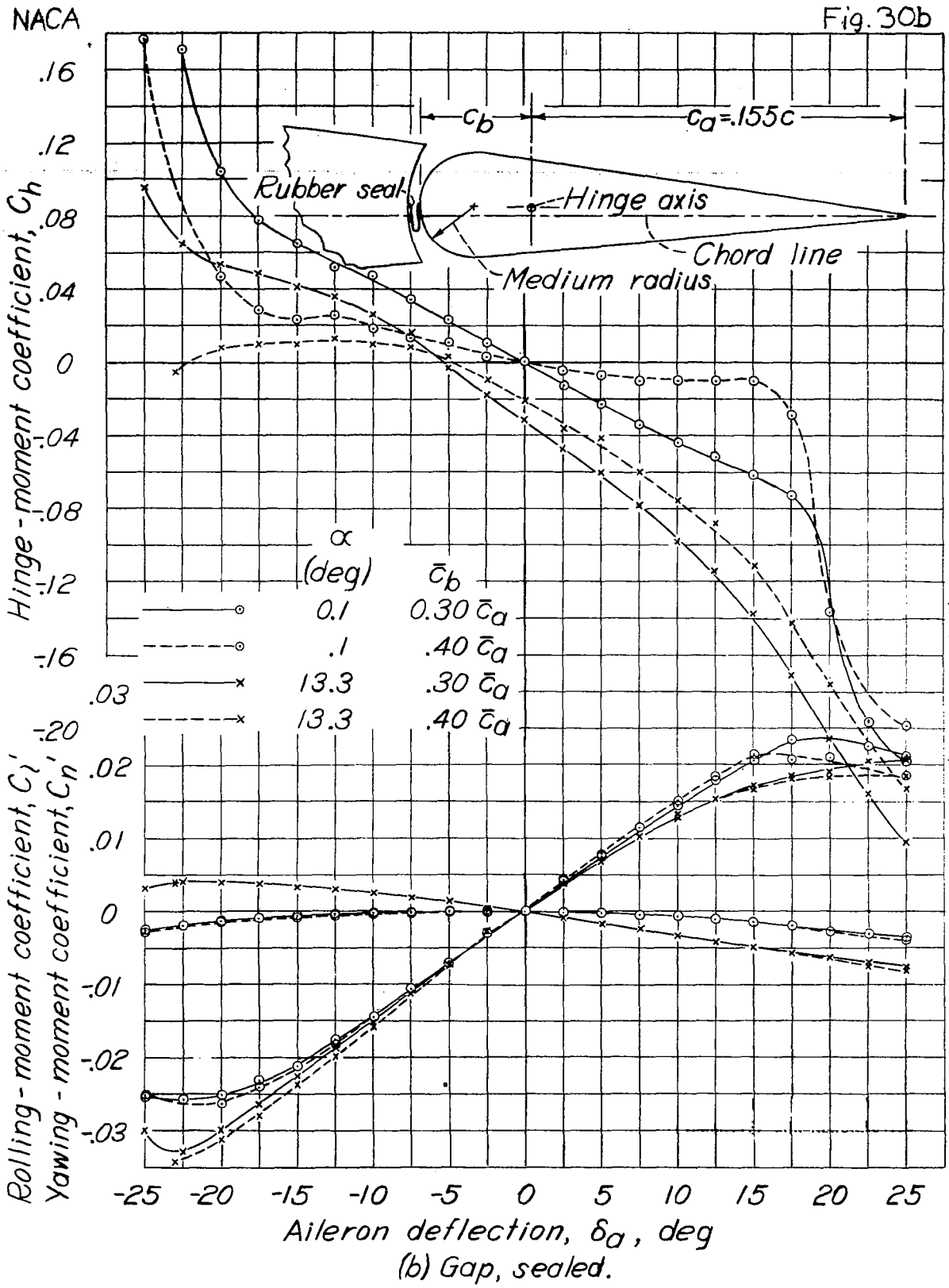

(b) Gap, sealed.

Figure 30.- Concluded.

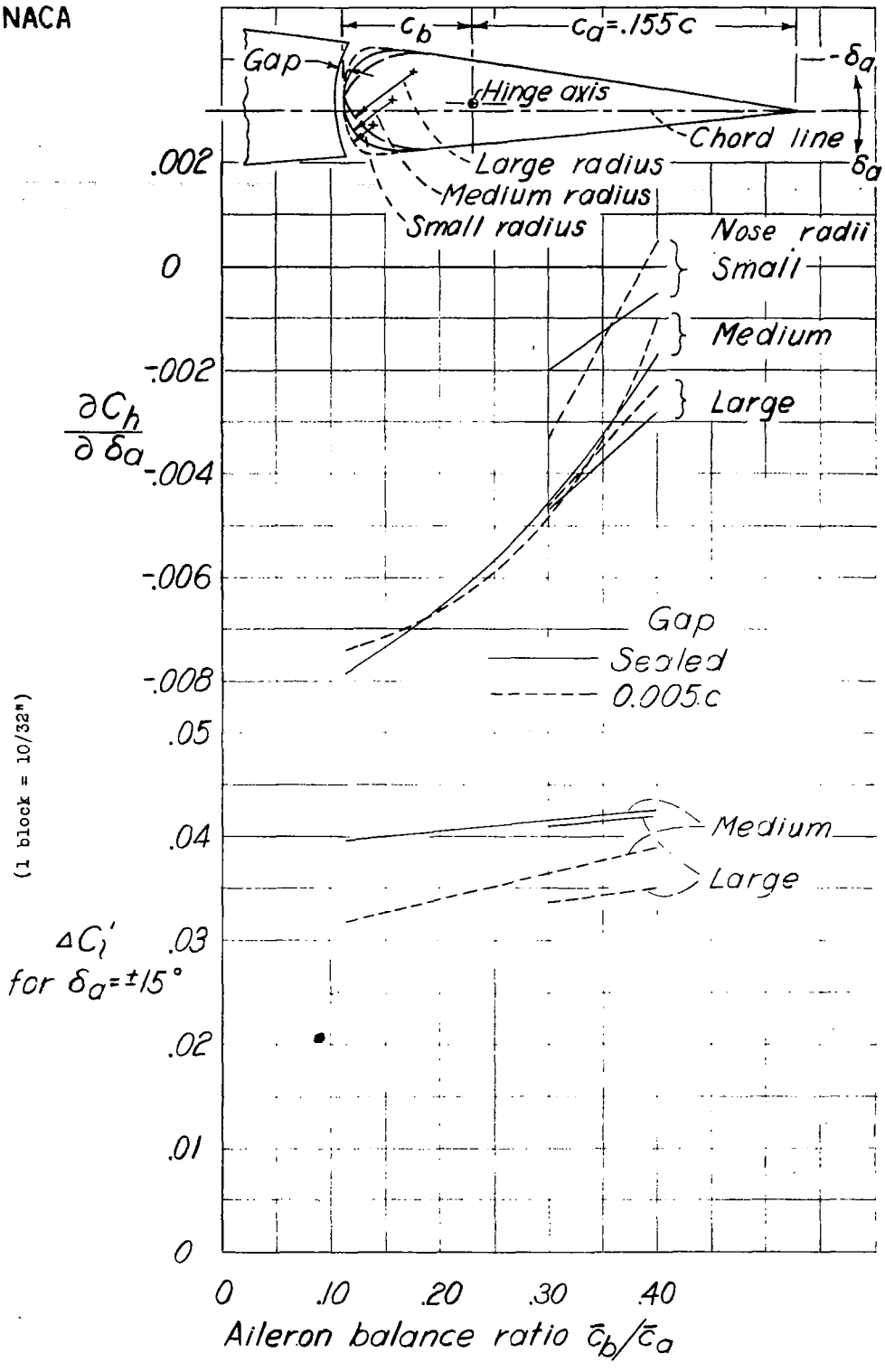

Figure 31.- Effect of balance chord and nose radius on the hinge-moment and effectiveness parameters for blunt-nose ailerons on the tapered-wing model. Hinge-axis location, mean; δ_f, 0°; α, 0.1°.

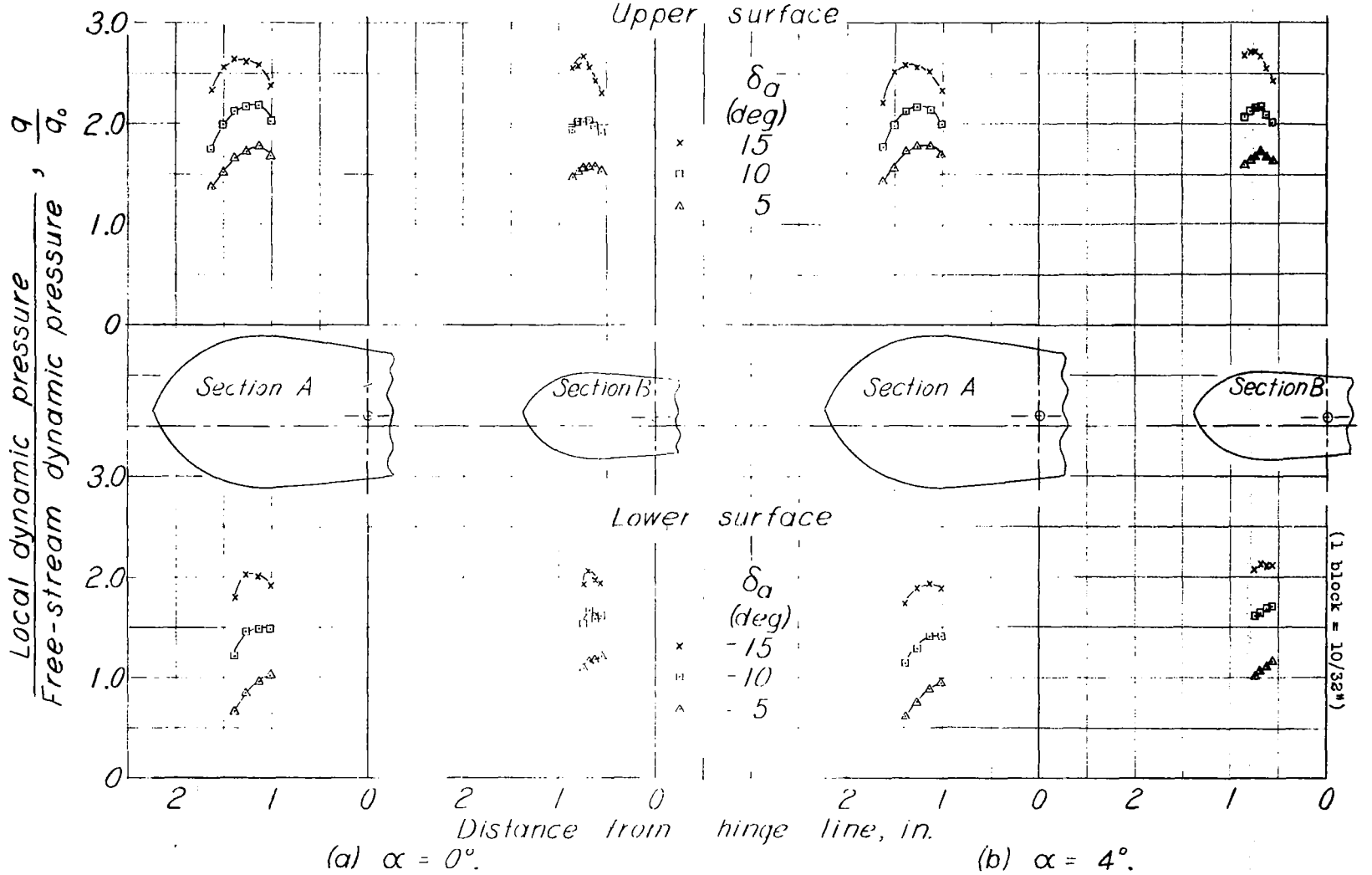

Figure 32.- Effect of aileron deflection on the dynamic pressures over the nose of a $0.40\bar{c}_a$-balance blunt nose aileron on the tapered-wing model. Hinge-axis location, mean; nose radii, large; gap, 0.005c; δ_f, 0°.

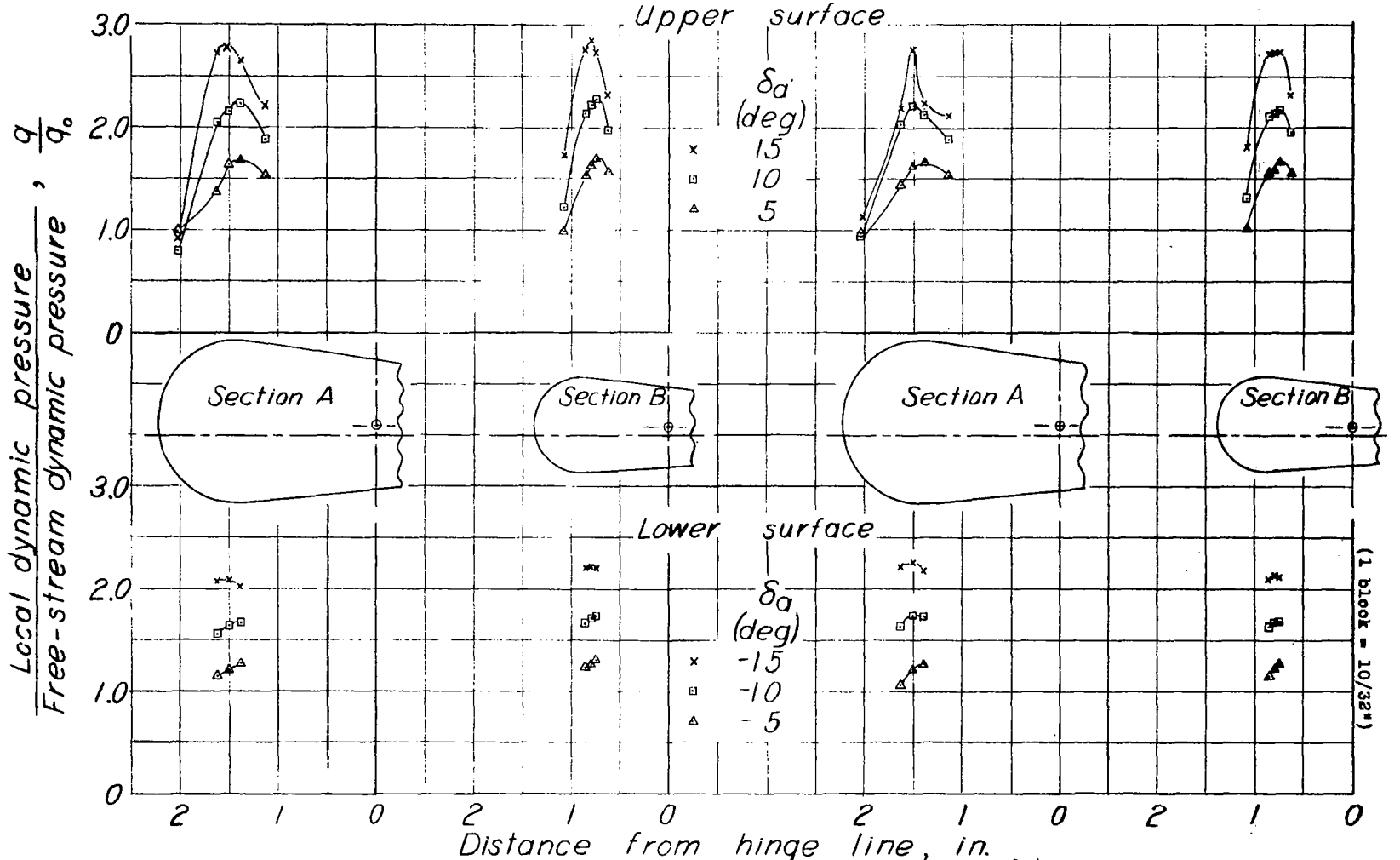

(a) $\alpha = -4°$. (b) $\alpha = 0°$.

Figure 33.- Effect of aileron deflection on the dynamic pressures over the nose of a $0.40\bar{c}_a$-balance blunt-nose aileron on the tapered-wing model. Hinge-axis location, mean; nose radii, medium; gap, 0.005c; δ_f, 0°.

NACA

Fig. 33a,b

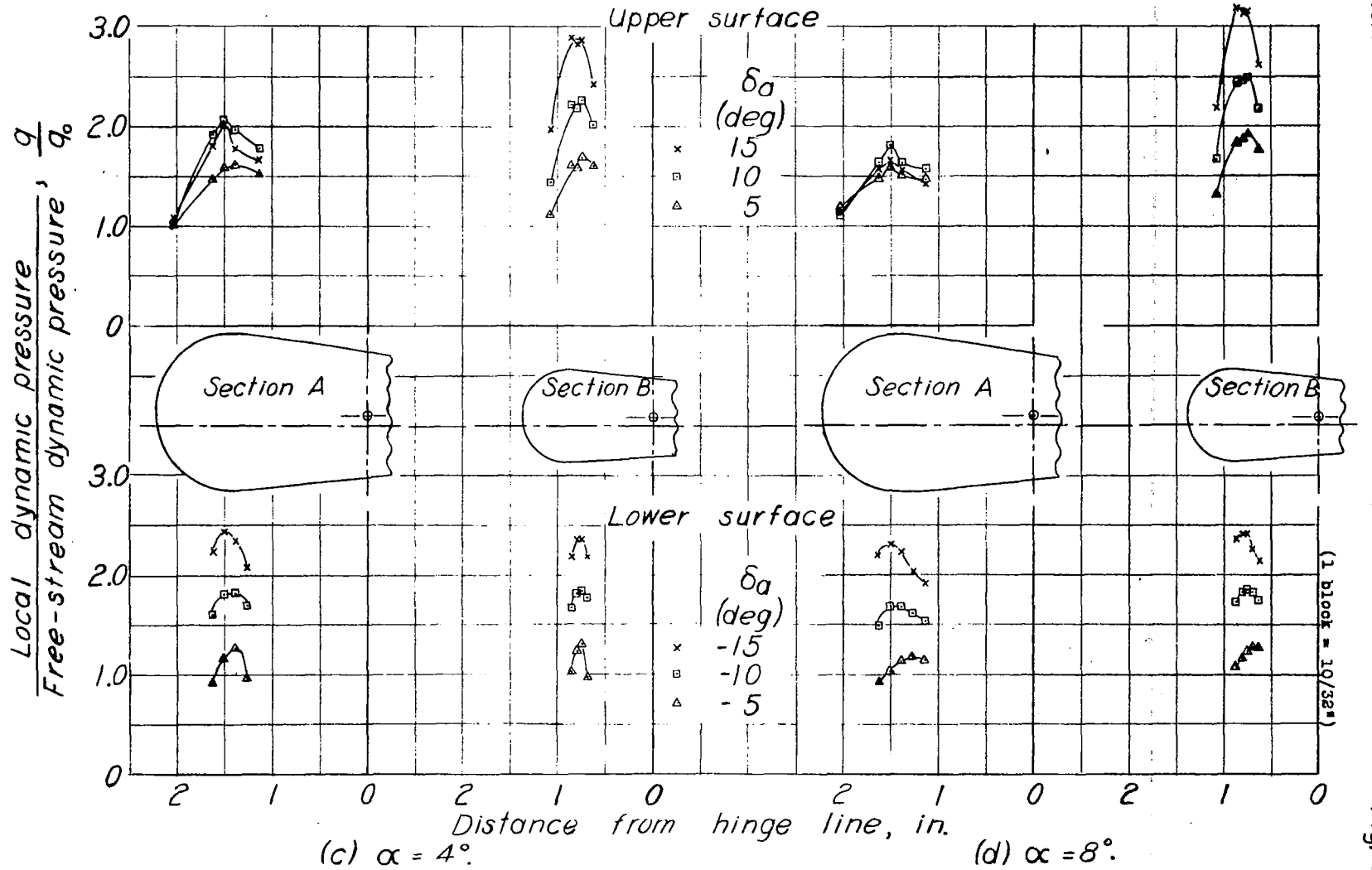

(c) $\alpha = 4°$.

(d) $\alpha = 8°$.

Figure 33.- Concluded.

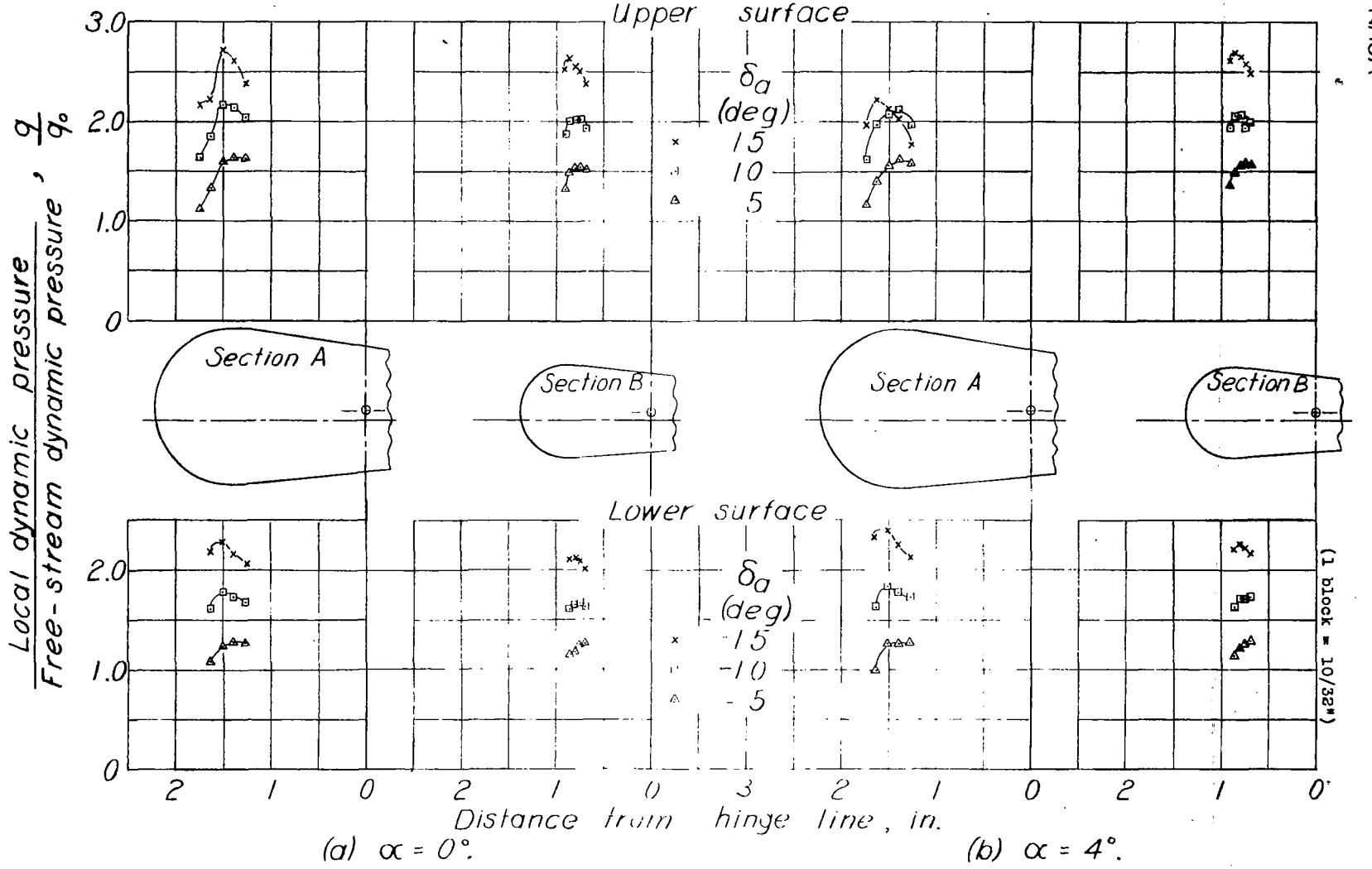

(a) $\alpha = 0°$. (b) $\alpha = 4°$.

Figure 34.- Effect of aileron deflection on the dynamic pressures over the nose of a $0.40\bar{c}_a$-balance blunt nose aileron on the tapered-wing model. Hinge-axis location, mean; nose radii, medium; gap, sealed; δ_f, 0°.

Fig. 34

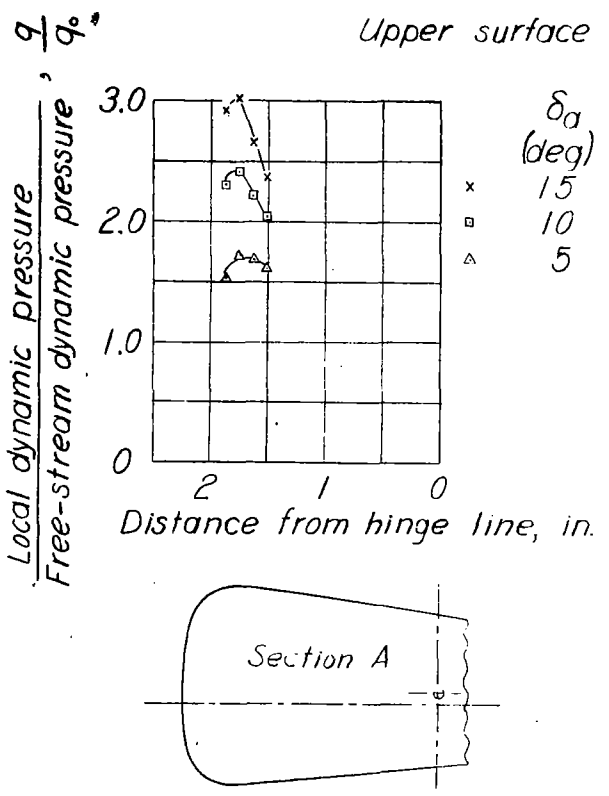

Figure 35.- Effect of aileron deflection on the dynamic pressures over the nose of a $0.40\bar{c}_a$ balance blunt-nose aileron on the tapered-wing model. Hinge-axis location, mean; nose radii, small; gap, 0.005c; δ_f, 0°; α, 0°.

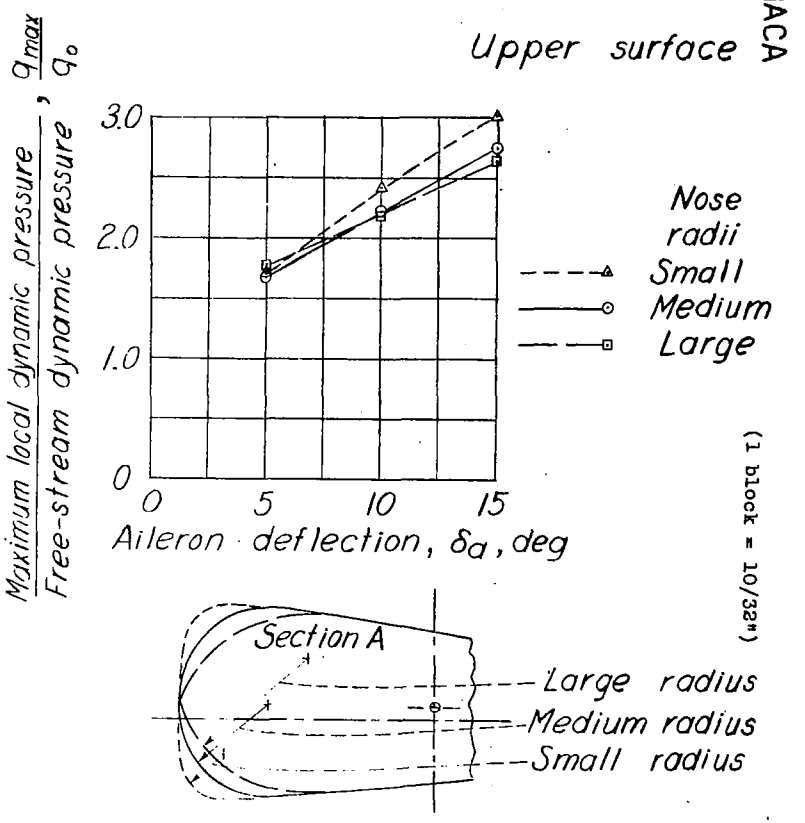

Figure 36.- Effect of nose radius on the peak dynamic pressures over the nose of a $0.40\bar{c}_a$ balance blunt-nose aileron on the tapered-wing model. Hinge-axis location, mean; gap, 0.005c; δ_f, 0°; α, 0°.

NACA

(1 block = 10/32")

Figs. 35, 36

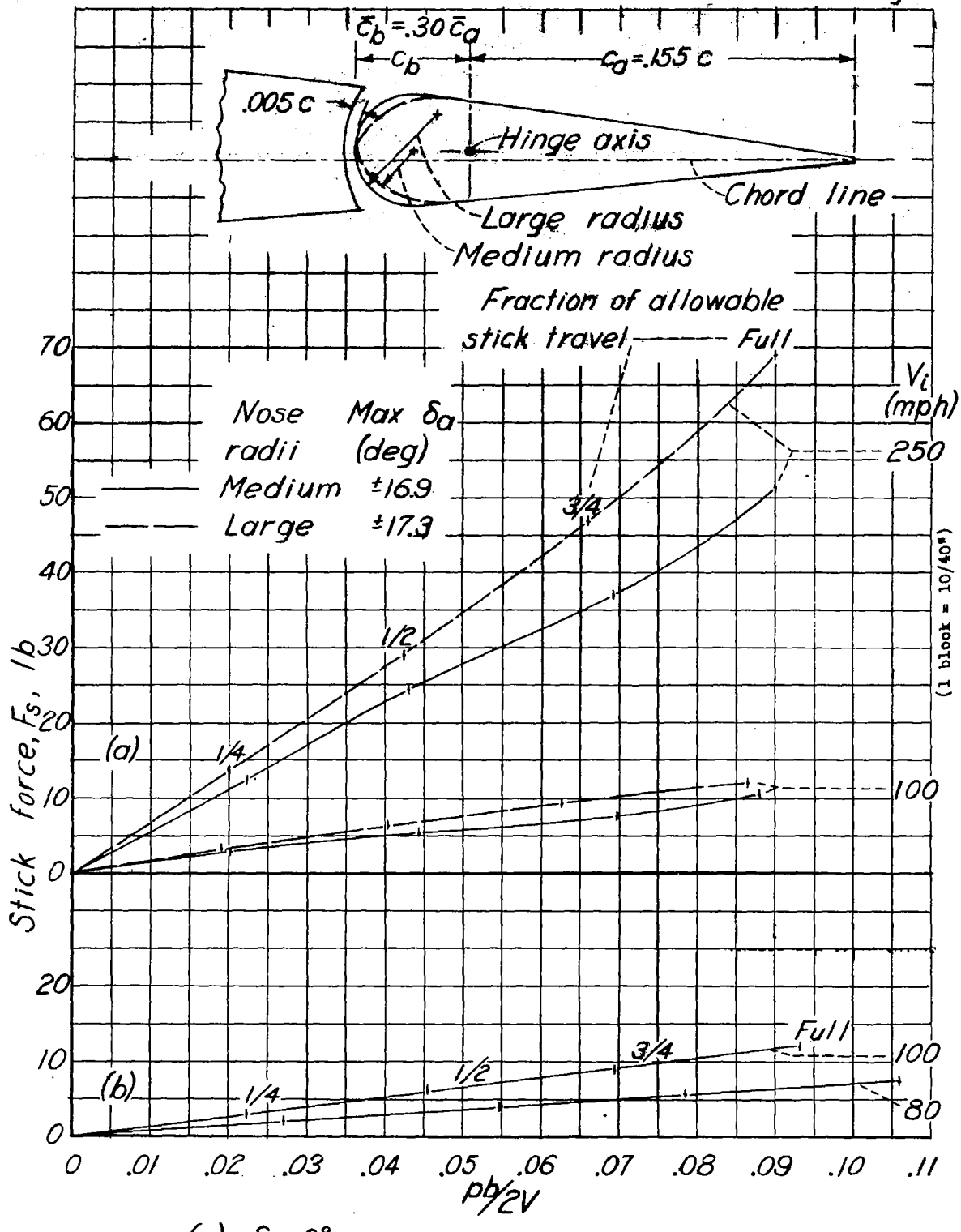

(a) δ_f, 0°.

(b) δ_f, 50°; nose radii, medium; maximum δ_a, ± 16.9°.

Figure 37.- Stick-force characteristics of $0.30\bar{c}_a$ -- balance blunt-nose ailerons on the tapered wing. Gap, 0.005c.

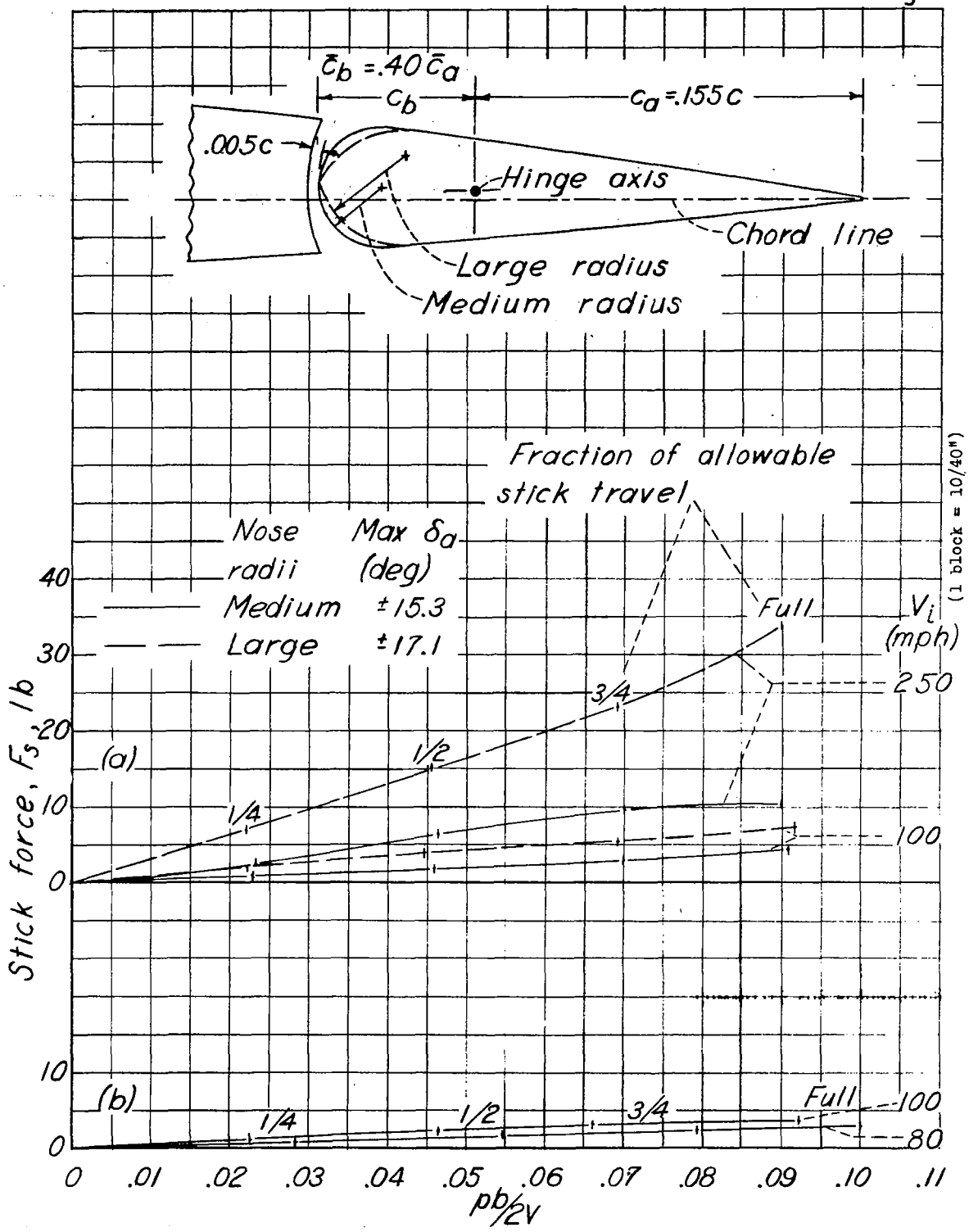

(a) δ_f, 0°

(b) δ_f, 50°; nose radii, medium; maximum δ_a, ±15.3°.

Figure 38.- Stick-force characteristics of 0.40 $\bar{c}_a$-balance blunt-nose ailerons on the tapered wing. Hinge-axis location, mean; gap, 0.005c.

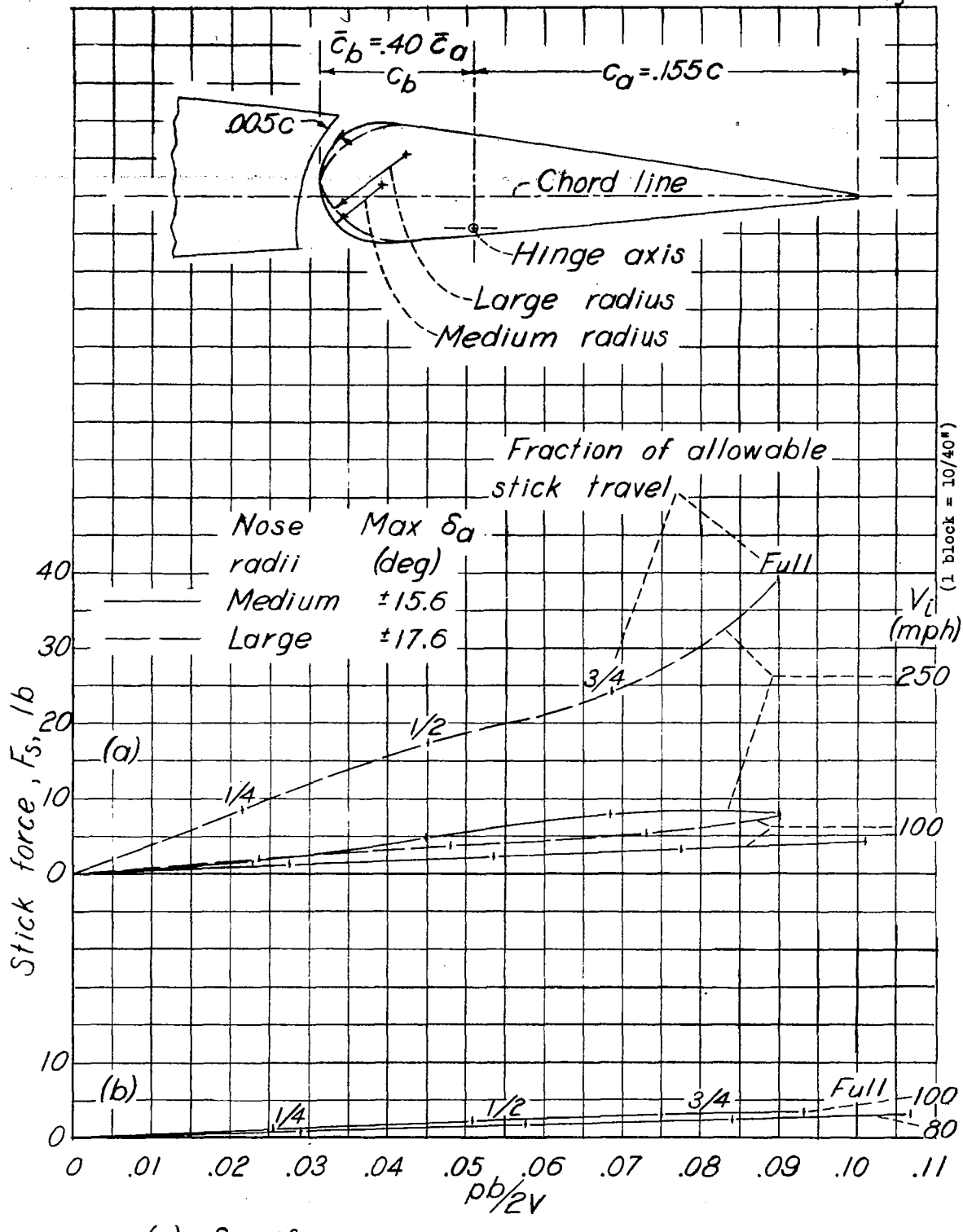

(a) δ_f, 0°.

(b) δ_f, 50°; nose radii, medium; maximum δ_a, ± 15.6°.

Figure 39.- Stick-force characteristics of a 0.40 $\bar{c}_a$-balance blunt-nose ailerons on the tapered wing. Hinge-axis location, low; gap, 0.005c.

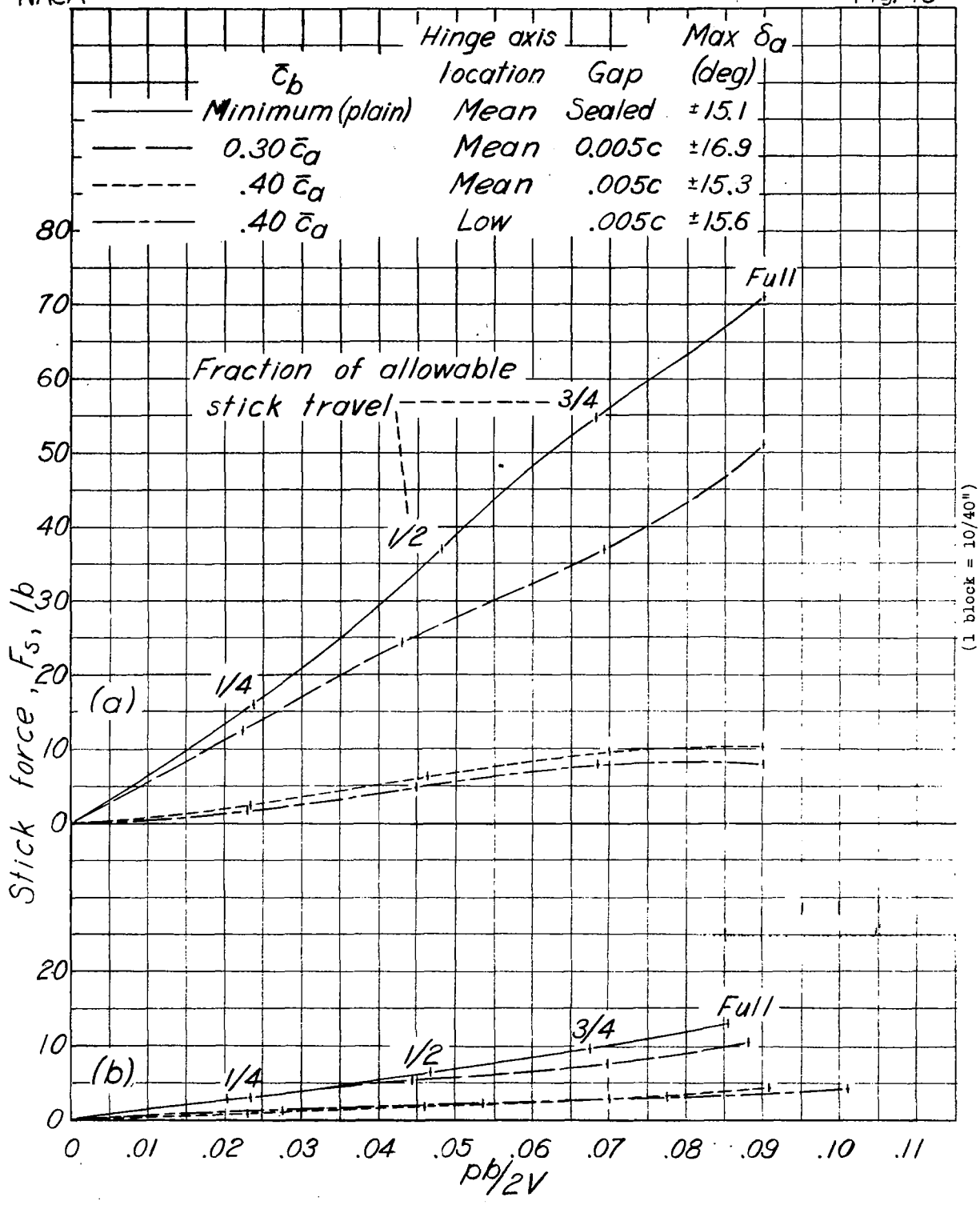

(a) V_i = 250 miles per hour.

(b) V_i = 100 miles per hour.

Figure 40.- Comparison of the stick-force characteristics of the various blunt-nose ailerons on the tapered wing. Nose radii, medium; δ_f, 0°.